FORMATION OF PROTON TRANSLOCATING WATER CHANNELS IN ATP SYNTHASE

A Dissertation Presented to

the Faculty of the Department of Physics

University of Houston

In Partial Fulfillment

of the Requirements for the Degree

Doctor of Philosophy

By

Sladjana Maric

August 2019

FORMATION OF PROTON TRANSLOCATING WATER CHANNELS IN ATP SYNTHASE

_____

Sladjana Maric

APPROVED:

_____

Dr. John H. Miller, Jr., Chairman
Department of Physics

_____

Dr. James M. Briggs, Co-Chairman
Department of Biology and Biochemistry

_____

Dr. Kevin E. Bassler
Department of Physics

_____

Dr. Gemunu H. Gunaratne
Department of Physics

_____

Dr. Donna W. Stokes
Department of Physics

_____

Dr. Dan E. Wells, Dean
College of Natural Sciences and Mathematics

Acknowledgments

There are no words that can express the gratitude I feel for every single one of you who has played a role, directly or indirectly, in the fulfillment of this incredible journey.

First and foremost, I would like to thank my advisors, Dr. John Miller and Dr. James Briggs. Dr. Miller, thank you for all the words of encouragement through all these years. We worked together on many different projects, and I can truthfully say that I learned a lot from you. Dr. Briggs, you adopted me into your group and treated me equally as your student. Without you, I would still be sitting in front of my computer, wondering what to do next. Our weekly meetings taught me how to be a better scientist in the academic world and a better person overall. The imprint of your influence on me will always be visible in my approach to research and teaching. I sincerely hope that one day, I can be half as good a mentor to another student as you were to me. Together with Dr. Miller, you guided me through my scientific career, always showing care for my personal and professional success.

To the members of my committee, Dr. Bassler, Dr. Gunaratne, and Dr. Stokes, thank you for the time you spent to help me and for the interest shown in my research. I will never forget what you did for me when I was ready to call it quits. Not many students can say that their committee did for them what you did for me. For that, I will indeed be grateful for the rest of my life and will do everything in my power to pay it forward.

My walking companions, Dr. Forrest, Dr. Stokes, and Dr. Wood, thank you for all the help and support. You encouraged me to believe in myself, kept me accountable, and have given me so much academic and life-related advice. Dr. Wood, you are closest to a father

figure I have ever had in my life. Thank you for the opportunity to work closely with you, I have learned a lot and hopefully will continue to learn from you for many years to come. You taught me how to be a better teacher, supervisor, and above everything, a better person; you never held back on advice and always showed interest in my academic and personal endeavors.

I have been very fortunate to have met some people here during my academic career that I consider very close friends. I know that wherever we are some years from now, we will always remember our lives during grad school, the ups and downs, and how we all stood by each other when someone was in need. To all my TAs, thank you for being so supportive and understanding, especially during the last two months.

So much of the good in a person's life comes from his or her family. Now that I have spent years apart from mine, I can really appreciate how true this is. I want to thank my mom Mirjana, sister Suzana, and brother Sladjan, for the values they taught me and the support they always showed for what I do. I am proud to be your daughter and sister.

Finally, I want to say thank you to my daughter Petra and husband Nebojsa. Nebojsa, you have been my rock, my strength, shoulder to cry on, my companion, and my love. My dear Petra, you are the light of my day, the air that I breathe, my world, my everything. If it weren't for you two, I would never know what it was like to be able to look at someone and smile for no reason. I am privileged to be called your wife and mom, love you the most in the whole world.

FORMATION OF PROTON TRANSLOCATING WATER CHANNELS IN ATP SYNTHASE

An Abstract of a Dissertation

Presented to

the Faculty of the Department of Physics

University of Houston

In Partial Fulfillment

of the Requirements for the Degree

Doctor of Philosophy

By

Sladjana Maric

August 2019

Abstract

The F_1F_O – ATP synthase has been the object of study in the scientific community both from theory and experiment over the past couple of decades. The ATP synthase is a protein complex in the mitochondrial membrane that efficiently converts the cell's transmembrane proton gradient into chemical energy stored as adenosine triphosphate (ATP). The protein is made of two molecular motors, F_1 and F_O, coupled by the central stalk. The free energy used for the synthesis of ATP is in the form of protons moving down the electrochemical gradient from the inner-membrane space to the mitochondrial matrix via the two offset half-channels. The membrane bound part of ATP synthase, F_O, converts the transmembrane electrochemical potential into mechanical rotation of the rotor in F_O and the stalk physically connected to it. Mutations in a gene encoding ATP synthase are proven to affect its function and cause severe syndromes related to energy deficiency.

In this dissertation, we study, using molecular dynamics (MD) simulations, the formation of the half-channels within the stator part of F_O. These half-channels enable the proton translocation to and from the rotor portion, known as the *c*-ring. Combining MD with the protein structure network paths and hydrogen-bonding network analysis, we were able to observe clear evidence for proton pathways and compare our results with previous experimental results. We also report studies of leucine-arginine and leucine-proline amino acid replacements, encoded by the T-G and T-C point mutations at locus 8993 of mtDNA. Our results suggest, for the first time, that these mutations adversely affect water half-channels, and consequently impair the ability of the ATP synthase to produce ATP.

Table of Contents

List of Figures

List of Tables

Chapter 1 Introduction

1.1 Motivation

ATP synthase is a unique enzyme complex embedded in the inner mitochondrial membrane that embodies two of the primary cellular energy transduction mechanisms [1]. Also known as the F_1F_O-ATPase, this complex catalyzes the formation of adenosine triphosphate (ATP) from adenosine diphosphate (ADP) and inorganic phosphate. This molecular machine can also work in reverse and hydrolyze ATP. The energy necessary to catalyze the creation of ATP is derived from a transmembrane proton motive gradient. The structure of the ATP synthase complex is represented in Figure 1.1.

ATP is the core of all organisms energetics; it stores the energy in high energy second (beta) and third (gamma) phosphodiester bonds. The human body contains approximately 50 grams of ATP at any time which is continuously recycled. Food is the source for the synthetic precursors of ATP. For example, a daily intake of 2500 food calories will result in 160 kg of ATP produced per day [2]. The human body roughly uses all of ATP produced in a day [3-7].

The free energy used for the synthesis of ATP is in the form of protons moving down the electrochemical gradient from the inner-membrane space to the mitochondrial matrix. During the last step of the metabolic cycle, oxidative phosphorylation results in electron buildup pushing protons across the inner mitochondrial membrane to the inner-membrane space. Accumulation of this charge provides an electrochemical potential.

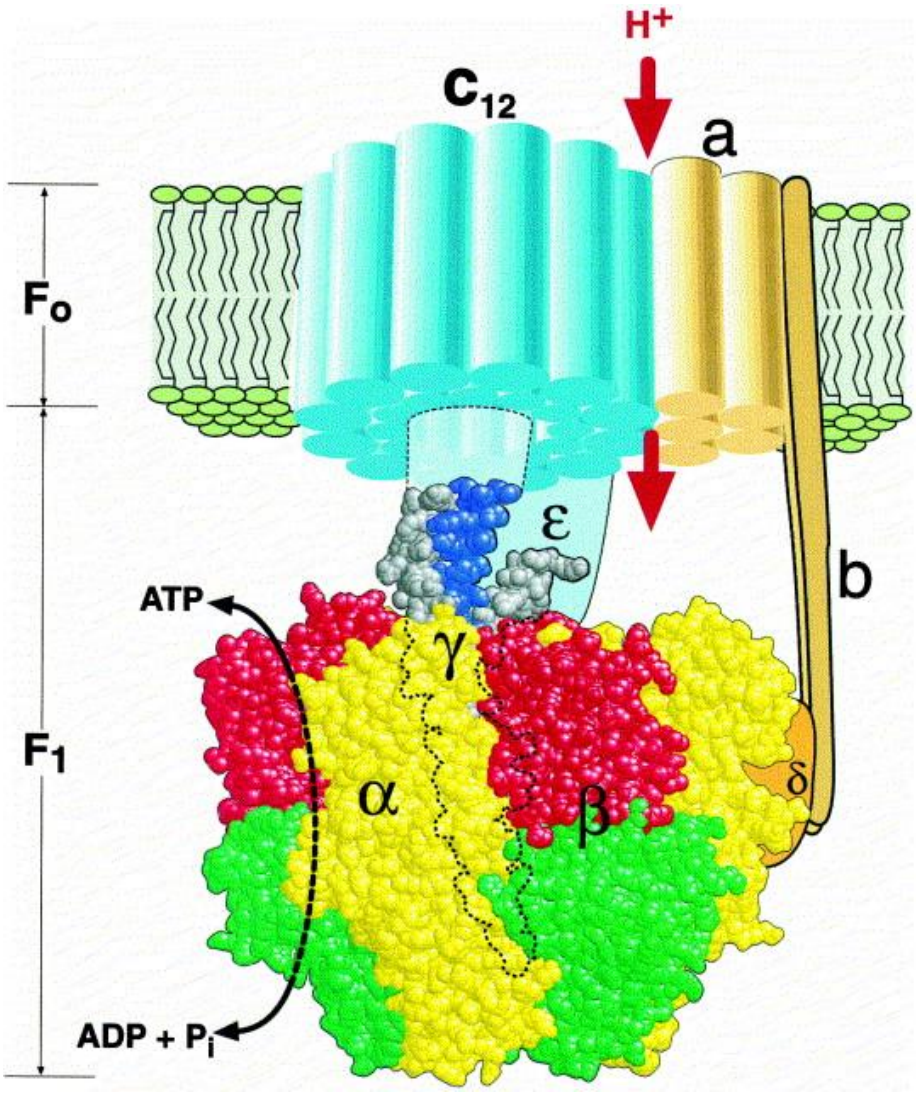

Figure 1.1 Structure of the ATP synthase from *E. coli*. The F_O portion of the motor is embedded in the inner mitochondrial membrane, while the F_1 portion lies in the mitochondrial matrix. The main components of the F_O portion are the $\boldsymbol{c}$-ring, consisting of 8-15 identical helices, and the $\boldsymbol{a}$-subunit, composed of four membrane-spanning helices. The proton-translocating half-channels are located at the interface between the $\boldsymbol{a}$-subunit and the $\boldsymbol{c}$-ring. Protons flowing through these channels are generating torque on the F_O by converting the energy stored in the electrochemical proton gradient into mechanical energy. The rotational energy is transmitted, via the $\boldsymbol{\gamma}$-shaft and $\boldsymbol{\varepsilon}$ subunit, to F_1 which catalyzes the formation of ATP. The $\boldsymbol{a}$-subunit is connected to F_1 by the $\boldsymbol{b}$ and $\boldsymbol{\delta}$ subunits. The catalytic complex, F_1, is a hexamer composed of three $\boldsymbol{\alpha}$ and three $\boldsymbol{\beta}$ subunits alternately packed where only $\boldsymbol{\beta}$ subunits are capable of catalyzing the phosphorylation of ADP to produce ATP. This molecular machine is usually called F_1F_O-ATP synthase and has the general formula $\boldsymbol{c_{(8-15)}a_1b_2\delta_1\gamma_1\varepsilon_1\alpha_3\beta_3}$. (Reprinted from *BBA-Bioenergetics, 2000* with kind permission from Elsevier) [1]

During the synthesis of ATP molecules, this electrochemical gradient drives the membrane-bound portion of the ATP complex, F_O, to rotate, producing a torque on F_O. F_1 will generate torque during the hydrolysis of ATP molecules. These two torques are applied in opposite directions [8], and correctly functioning ATP synthase has a high value of torque generated by the electrochemical gradient. This is the torque that rotates F_O toward the synthesis of ATP molecules.

Based on current models [9-13], protons enter the half-channel at the interface between the a-subunit and c-ring and are redirected to the binding sites on the c-ring. Each proton is then translocated to the opposite side of the inner mitochondrial membrane after completing nearly one full revolution. The rotating c-ring drives the rotation of the F_1 part of the complex, through the connecting γ-shaft, enabling ATP phosphorylation. This process brings to mind a molecular water wheel that couples the flow of protons to the production of ATP molecules. Each revolution of ATP synthase requires the energy of nine to fourteen protons returning to the mitochondrial matrix. This number depends on the organism; in this project, the *Escherichia Coli* NMR solution model, which contains 12 helices in the c-ring, was used. Within the F_1 portion of the ATP synthase molecule are three active sites. Each site converts ADP to ATP with every revolution of the ATP synthase. Under optimal conditions, ATP synthase rotates at the rate of up to 200 revolutions per second, resulting in 600 ATP molecules produced [14].

Approximately 14 nuclear DNA (nDNA) and two mitochondrial DNA (mtDNA) genes are responsible for making the ATP synthase enzyme. Subunit a is encoded by the

mitochondrial mtAtp6 and mtAtp8 genes [15, 16]. Mutations in these genes lead to maternally inherited Leigh syndrome (MILS), a disease that affects babies resulting in a shortening of their life span to between one and five years. MILS is a severe neurological disorder that typically arises in the first year of life and is represented by the progressive loss of mental and movement ability. Children affected by MILS are unable to grow and gain weight. MtAtp6 and mtAtp8 gene mutations decrease the ability of ATP synthase to extract energy from proton translocation.

Understanding the mechanism of proton translocation and proton pathways through the F_O part of the ATP synthase will play a critical role in understanding this disease and its treatment.

1.2 Hypothesis

Insights into the molecular mechanism behind the operation of the F_O sector of ATP synthase [1, 12, 13, 17-25] will provide a platform for detailed analysis of proton translocation. Details about protonation of the binding sites at the c-ring are well known. Hydrogen-bonding networks at the binding sites are extensively explained, but the path protons take to reach this site is not completely clear. From previously published experimental work, we know that, in the case of MILS, the efficiency of ATP synthase is decreased [26-29].

In this study, we focus on answering the question ‘How are the protons mediated along the half-channels?’. Understanding proton translocation through half-channels will elucidate pathways protons take before binding to the binding sites and clarify the difference between healthy and mutated ATP synthase. In addition, we focus on understanding how specific mutations on genes encoding the a subunit affect the proton translocation.

The main idea behind our work is that half-channels are ‘water wires’ that translocate protons via hydrogen-bond networks, and that channels can be adversely affected by specific mitochondrial mutations. It is our hope that the results from this study will help in improved diagnostic and therapeutic approaches to treating mitochondrial diseases related to ATP synthase energy deficiency.

1.3 Bioenergetics

1.3.1 Mitochondrial Structure and Function

The mitochondrion is a peanut-shaped cellular organelle made of an outer membrane, inner membrane, and two internal compartments named the inner-membrane space (located between the membranes) and matrix (located at the center of the organelle). Dimensions of a mitochondrion are 0.5 – 10 μm in diameter and about 7 μm in length. For a very small organelle, mitochondria are perfectly shaped to maximize the surface area of their inner

membrane which is convoluted into folds called cristae, see Figure 1.2. The inner membrane represents the principal site of energy production inside the mitochondrion. Basically, inside this membrane, the majority of energy necessary for cellular survival is produced. The matrix contains the enzymes of the citric acid cycle and the molecules produced by the citric acid cycle are fed to the electron transport chain (ETC) complexes located inside the mitochondrial inner membrane.

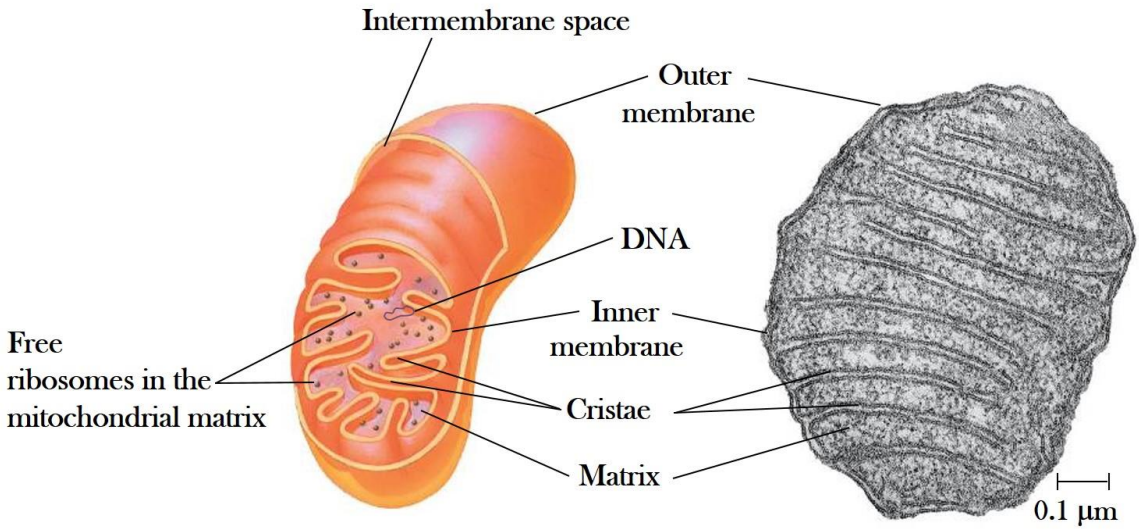

Figure 1.2 Mitochondrion. On the left side is the schematic diagram showing the structure of a mitochondrion. On the right is the transmission electron microscopy image of the mitochondrion. (Reprinted from *Campbell Biology (9th Edition), 2010* with kind permission from Pearson Education, Inc.) [30]

The mitochondrion is mostly protein, but it also contains some lipid, mitochondrial DNA, and RNA. Metabolic activity of the cell is related to the number of mitochondria in a way that cells with high metabolic activity (*e.g.*, heart cells) contain many well-developed mitochondria [31], up to 25% to 30% of the cell volume. The number of mitochondria inside the cell depends on the cellular function. For example, skeletal cells which require

large amounts of energy for mechanical work contain a large number of well-developed mitochondria. Biosynthesis of the insulin, detoxification, and nerve cells require remarkable amounts of energy, which is why pancreas, liver, and brain cells also contain large numbers of mitochondria. Mitochondria are usually called cellular power plants. They use energy from the food we eat and the oxygen we breathe to phosphorylate adenosine diphosphate (ADP), thus creating energetic ATP molecules. This process of creating cellular energy in mitochondria is known as cellular respiration [32].

The cellular functions driven by the ATP include force generation (muscle contraction and cell division for example), the biosynthesis, folding and degradation of proteins, and the generation and maintenance of membrane potentials [33]. The outer membrane is less restrictive than the inner membrane, allowing for the smooth movement of larger macromolecules in and out of the space between the two membranes and thus resembles the cytosolic environment. The inner membrane, pivotal in ATP production, is more restrictive and possibly the only biological bilayer which has the highest protein to lipid mass ratio, with an almost a 60% protein make up [34, 35]. Although the primary role attributed to mitochondria is the synthesis of ATP from ADP and inorganic phosphate, it is far from the only one. Mitochondria are involved in additional processes such as apoptosis or programmed cell death [36].

Mitochondria have their own set of DNA (mitochondrial DNA, mtDNA) that is more similar to bacterial DNA [37]. Human mtDNA contains only 37 genes with just 13 of these genes encoding the polypeptides, which are all the components of the respiratory chain-

oxidative phosphorylation system [15]. The oxidative phosphorylation system, in addition, contains approximately 70 nuclear-encoded structural protein subunits.

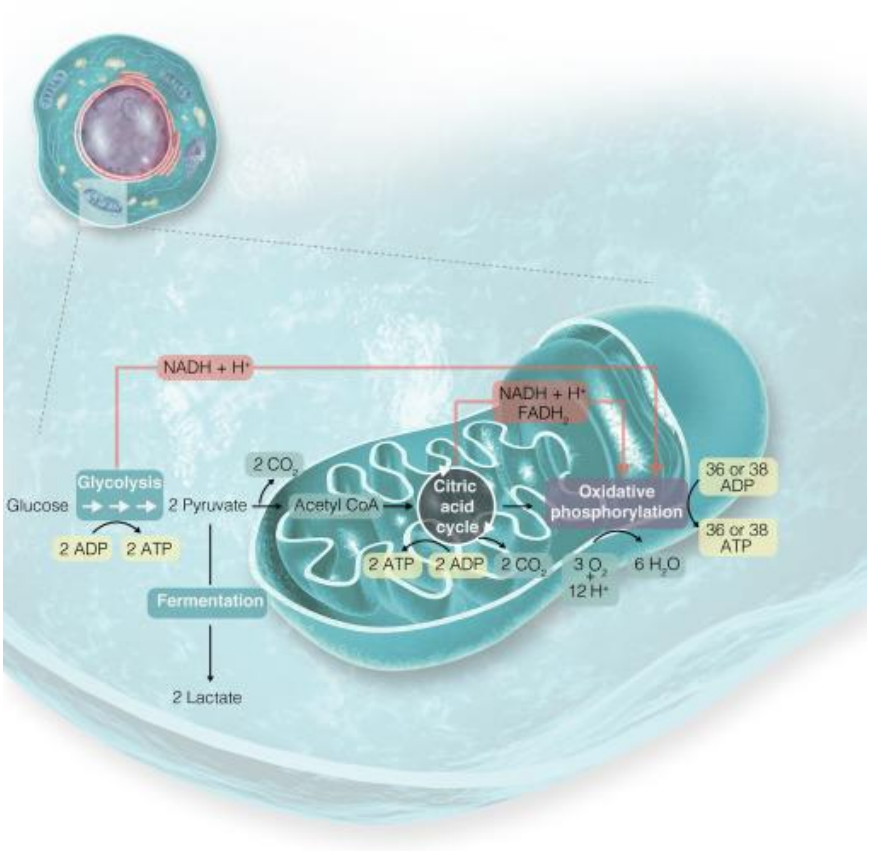

Figure 1.3 Cellular ATP production pathways. Adenosine triphosphate (ATP) is a high-energy compound that provides energy for a wide range of cellular processes. ATP is produced through the breakdown of glucose via two pathways. Via glycolysis in the cytoplasm, one molecule of glucose is converted to two molecules of pyruvate, NADH, and two ATP. Pyruvate can either be fermented or translocated to the mitochondria, where it is converted to Acetyl-CoA and metabolized to CO_2 and H_2 O in the Krebs cycle or citric acid cycle. The Krebs cycle provides substrates for the electron transport chain (ETC) and oxidative phosphorylation. If glucose is metabolized via the latter pathway, it yields an additional two molecules of ATP in the Krebs cycle and 32 more by oxidative phosphorylation, resulting in a total of 36 molecules of ATP from the breakdown of 1 molecule of glucose. Therefore, mitochondrial energy production is responsible for the bulk of the production of cellular energy. The ETC is at the core of this process since it reduces O_2 and generates the proton motive force that drives the production of 32 molecules of ATP. The processes in the Krebs cycle, the ETC, and oxidative phosphorylation thus act in concert during cellular respiration, consuming O_2 and producing CO_2. (Reprinted from *Parkinson's Disease, 2017* with kind permission from Elsevier) [38]

The last step of the metabolic cycle happens inside the mitochondrion. During the last steps in the breakdown of glucose, mediated by the citric acid cycle, the energy necessary for oxidative phosphorylation is released. This energy is in the form of the two important high-energy molecules, NADH and $FADH_2$, which are fed into the ETC. Oxidation of NADH and $FADH_2$ produces free energy necessary for pumping protons across the mitochondrial inner membrane. The potential difference created by proton buildup in the inner mitochondrial membrane is used to drive ATP synthase, which results in ATP production (Figure 1.3).

1.3.2 The Electron Transport Chain

The ETC is a series of four multi-subunit mitochondrial complexes [36-38]. These complexes participate in the electron transport coupled with the translocation of protons across the inner mitochondrial membrane. The process of proton translocation across the inner mitochondrial membrane generates the electrochemical gradient (proton motive force) in the mitochondrial inner-membrane space, which drives the production of ATP molecules by the ATP synthase protein. These complexes are designated by Roman numerals I through IV. Three of these complexes, complex I, II, and IV, are called the proton pumps; they participate in pumping the protons across the membrane, while complex II is an additional entry point for electrons into the chain. The ATP synthase is sometimes referred to as complex V of the ETC even though it does not take part in electron transport, but instead, it serves as the ion channel through which the protons are transported

back to the mitochondrial matrix. The ETC and APT synthase together constitute the oxidative phosphorylation system (Figure 1.4).

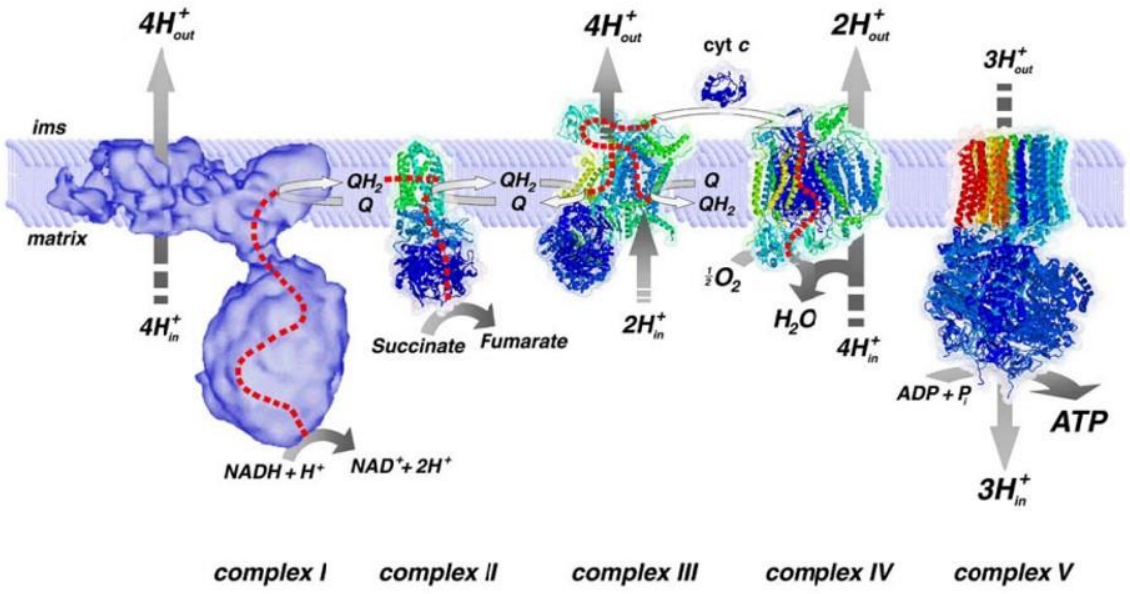

Figure 1.4 Schematic representation of the oxidative phosphorylation. Complexes I, II, III, IV, V are indicated. Dotted lines indicate the direction of the electron flow and solid arrows indicate the direction of proton translocation. All complexes are represented as a monomer. cyt *c* – cytochrome *c*; Q – ubiquinone; QH_2 – ubiquinol; ims – inner-membrane space. (Reprinted from *Mitochondrial Function and Biogenesis, 2004* with kind permission from Springer) [39]

NADH enters the ETC through complex I, the largest enzyme-complex of the ETC and oxidative phosphorylation. The energy released from the oxidation of NADH is used to pump four protons across the mitochondrial inner membrane.

While complex II is made of only four protein subunits, it plays a vital role in producing the substrate for complex III. In addition, it is involved in both the TCA cycle and electron transfer but does not have proton pumping ability.

Complex III is also known as *cytochrome bc1 complex* – it translocates four protons to the mitochondrial inner-membrane space to contribute to the proton gradient.

Complex IV is unique, since it not only pumps the protons, it also produces water. The contribution to the proton gradient from this complex is equal to 2 protons. This complex is the last enzyme of the respiratory chain.

The last and fifth complex of oxidative phosphorylation is the ATP synthase. It is an essential enzyme that connects the proton gradient to phosphorylation, the process of adding a phosphate to ADP to create ATP. The potential energy in the form of an electrochemical gradient is harnessed to create chemical energy in the form of ATP [32].

The energy released from the oxidation of one NADH molecule will result in pumping 10 protons across the mitochondrial inner membrane, which contributes to the proton gradient.

Sometimes, electrons will leak from ETC to react with oxygen and form superoxide free radicals. These highly reactive molecules have been implicated in a number of diseases, aging being one of them [40, 41]. The two sites within ETC where electrons can leak are Complexes I and III.

1.3.3 The ATP Synthase

ATP is the vital energy source used by aerobic cells. A number of enzymes couple the energetically favorable hydrolysis of ATP to energetically unfavorable chemical reactions in order to carry out necessary life functions [42]. The energy released by the transmembrane proton translocation is used to power the ATP synthase molecular motor to synthesize the ATP from ADP and inorganic phosphate [43]. This molecular machine is found in plasma membranes of bacteria, the thylakoid membranes of chloroplast, and the inner mitochondrial membranes of mitochondria.

The ATP synthase is a multiprotein complex consisting of a soluble F_1 part that synthesizes the ATP and a membrane-embedded F_O part that allows the proton translocation across the lipid membrane having the function of a proton channel. The F_O portion of ATP synthase is named this way because of its ability to bind the inhibitor oligomycin [44-46]. (Oligomycin is an antibiotic that obstructs the synthesis of ATP by blocking the translocating channel within the membrane-embedded portion of the molecular motor, binds to subunit c [47].) As a consequence, it would also stop the electron transport chain, because if the high proton concentration buildup in the inner-membrane space is not dissipated, the free energy released by the electron transport is not enough to pump any more protons against the steep electrochemical gradient. The geometrical structure of ATP synthase is represented in Figure 1.1.

The F_1 region includes the subunits α, β, γ, δ, and ε, while the a, b, and c subunits are identified to comprise the F_O portion of the molecular motor. The c subunits comprise the

rotor of the F_O part. Subunits α and β are packed alternatively, forming the six-fold pseudo-symmetric ring [43, 48], where only the β subunits have the capability of catalyzing the phosphorylation of ADP to produce ATP [43, 49-52]. Subunits γ, δ, and ε comprise the central stalk [53] of mitochondrial ATP synthase (γ and ε for bacterial) which acts as an axle and connects the rotation of electric motor (F_O) to the rotation of the chemical motor (F_1) [9, 10, 21, 54-57]. The central stalk connects F_O and F_1 and transmits the rotation from one to the other, while the stator, subunit b, links the two portions of the enzyme at the periphery. When F_O is turned, it rotates the central stalk (axle), and the chemical part of the motor becomes the generator creating ATP as it rotates. One can think of ATP synthase as two motors, F_O and F_1, connected by an axle, the central stalk.

The beauty of this complex is that one motor is forcing the other motor to turn and to change into a generator. In human cells, F_O uses the power from the proton gradient to force F_1 to generate ATP. As the food is broken down and used as a fuel to pump protons across the mitochondrial inner membrane, F_O allows these ions to return to the mitochondrial matrix turning the rotor in the process. The rotation from the rotor is transmitted via the axle to F_1, which becomes a generator. Remarkably, F_1 can operate as a motor and generator. In generator mode, the power of rotation is used to synthesize ATP, and when operating as a motor, it breaks down ATP and spins the axle in the opposite direction. Several steps are necessary for the synthesis of an ATP molecule: (1) binding of phosphate and ADP, (2) the creation of the new phosphate-phosphate (phosphodiester) bond, and (3) release of the newly formed ATP. Assisting these three complicated steps are three conformational changes in F_1 forced by the central stalk turning. The general

shape of the F_1 portion is conserved across organisms [42], while the F_O region has a lot of variation in composition from organism to organism.

Bacterial ATP synthase has the simplest structure of the F_O region with general formula ab_2c_{8-15} [58-64]. ATP synthases from other organisms have very similar structures with the exception of that from mitochondria, which is more complex and possesses additional subunits [40, 43, 49, 54, 65-69]. The functions of these additional subunits are generally still unclear [40]. Table 1.1 represents the subunit composition, genetic specification, and stoichiometry of mitochondrial ATP synthase from yeast and mammalian cells in comparison to the bacterial (*E. coli*) ATP synthase [54]. Often, F_1 is called a molecular machine, while F_O is called a proton turbine [70].

The focus of this study is the F_O part of the ATP synthase, and the Molecular Dynamics (MD) simulations are performed on the *Escherichia coli* model reported in the Protein Data Bank (PDB, http://www.rcsb.org/pdb). It is comprised of three subunits in a $a_1b_2c_{12}$ stoichiometry [57, 71]. F_O is often referred to as the electrochemical motor of the ATP synthase.

The rotor part of F_O plays a direct role in pairing proton translocation to conformational changes in F_1 driving ATP synthesis [56]. It is composed of 12 identical antiparallel hydrophobic α-helices connected by a polar loop. These α-helices, comprising 79 amino acids, fold through the membrane as a hairpin. The hairpin α-helices are arranged in an annular ring creating a cylindrical shape referred to as the c-ring. Subunits a and b_2 are at the periphery of the cylinder that represents the c-ring [72-76].

Table 1.1 Subunit composition, genetic specification, and stoichiometry of mtATPase from yeast and mammalian cells

	Bacteria (*E. Coli*)	Mitochondria			
		Yeast		Mammalian	Stoichiometry[c]
Sector	Subunit	Subunit	Gene[a]	Subunit[b]	
F_1	α	α	*ATP1*	α	3
	β	β	*ATP2*	β	3
	γ	γ	*ATP3*	γ	1
	δ	OSCP		OSCP	
	ε	δ	*ATP16*	δ	1
		ε	*ATP16*	ε	1
F_O	a	Su6	$ATP6_m$ *(oli2)*	$Su6_m$	1
	b	B	*ATP4*	b	1
	c	Su9	$ATP9_m$ *(olil)*	Su9	10
		Su8	$ATP8_m$ *(aap1)*	$A6L_m$	1
		OSCP	*ATP5*	OSCP	1
		D	*ATP7*	d	1
		E	*ATP21*	e	1 (2^d)
		F	*ATP17*	f	1
		G	*ATP20*	g	1
		H	*ATP14*	F_6	1
		i/j	*ATP18*		1
		K	*ATP19*		?
		INH	*INH1*	IF1	1
		STF1 (9 kDa)	*STF1*		1
		STF2 (15 kDa)	*STF2*		1
		STF3	*STF3*		?

Subunits are aligned horizontally based on the sequence of functional homology. The bacterial (*E. coli*) are shown for comparison with mtATPase subunits. [a] Genes are in nuclear DNA of *Saccharomyces cerevisiae*, except those marked with *m*, which are in mitochondrial DNA. References for individual subunits are *ATP1* [77]; *ATP2* [78]; *ATP3* [79]; *ATP16* [80]; *ATP15* [81]; *ATP6 (oli2)* [82]; *ATP4* [83]; *ATP9 (oli1)* [84, 85]; *ATP8 (aap1)* [86]; *ATP5 [87]*; *ATP7* [88]; *ATP21* [89]; *ATP17* [90]; *ATP20* [91]; *ATP14* [92]; *ATP18* [93, 94]; *ATP19* [95]; *INH1* [96]; *STF1* [97]; *STF2* [98]; *STF3* [99]. [b] $\alpha, \beta, \gamma, \delta, \varepsilon$ [100]; Su6, A6L [101]; Su9 [102]; b,d [103]; OSCP, F6, INH [104]; e [105]; f,g [53]. [c] Compilation of data for both yeast and bovine systems represented in the following references [95, 100, 106-114]. A question mark indicates subunits for which no reliable stoichiometric data are available. [d] [115] (Reprinted from *International Review of Cell and Molecular Biology, 2008* with kind permission from Elsevier)[54]

At the center of the membrane is an essential carboxyl group that serves as the proton binding site [55, 56, 116]; in a case of the model used (*E. coli*), this is aspartate at a position 61 (cAsp61), while for mammalian cells it is glutamate at a position 65 (cGlu65) [10, 57, 117]. Each cAsp61can assume either a protonated (neutral) or deprotonated (negatively charged) state. Proton binding and dissociation at this amino acid, and a resultant conformational change in the loop region initiate the rotation of the γ-subunit and release of ATP from F_1. The side chain of the carboxyl group acts as a proton donor and acceptor in the proton translocation. Fillingame postulated the existence of two half-channels formed by the a-subunit, which provide the access to the essential carboxylate on the c-subunit from the mitochondrial inner-membrane space and matrix [55, 118-122]. The c-ring rotates within the membrane in steps determined by the number of the c-subunits in a ring. For the model used in this study, 12 protons are used to rotate the c-ring 360° driving the synthesis of three ATP molecules.

Glutamate and aspartate contain carboxylic acid functionalities in their sidechains. The carboxylic acid can easily dissociate into carboxylate ion and proton. The negative charge that is left on the carboxylate ion after the deprotonation is stabilized by resonance; the electron is delocalized between two electronegative oxygen atoms. Energy delocalization lowers the potential energy of, in this case, the amino acid and in that way makes it more stable.

The essential aspartate (*E. coli*) is located at the center of the second helix of the c-subunit. This position is in the middle of the lipid bilayer. The laws of thermodynamics strongly suggest that only the protonated form of aspartate can exist in the center of the

lipid membrane and that the protonation/deprotonation reaction must occur in a hydrophilic environment. One can ask how it is possible to have a hydrophilic environment in a strongly hydrophobic region of lipid bilayer. The two half-channels will create this small hydrophilic region at the interface between the c-ring and the a-subunit; the first half-channel spans between the mitochondrial inner-membrane space and the middle of the lipid bilayer. The second one spans between the mitochondrial matrix and the middle of the membrane. It is essential to state that these two half-channels are offset. This widely accepted model on proton translocation is called a two-channel model [11, 123, 124]. The model suggests that these two half-channels are within the a-subunit, and the proton binding site is at the interface between the c-ring and the a-subunit at the middle of the lipid bilayer.

The principal component of the proton pathway is a strictly conserved amino acid, which is part of the a-subunit [70]. It is arginine at position 210 (aArg210) for *E. coli* and at position 159 (aArg159) for human mitochondria [125, 126]. Subunit a plays a key role in coupling proton transport to the rotations of the c-ring [118]. It folds in the mitochondrial inner membrane with five transmembrane helices (TMH), and it provides access channels to the proton binding cAsp61 [119, 127-129]. Based upon cross-linking experiments [76], aTMH4 and cTMH2, the helix to which cAsp61 is anchored [76], pack in parallel to each other. The interaction of conserved aArg210 in aTMH4 with cTMH2 is considered to be critical during the protonation and deprotonation of cAsp61 [130-133]; it is postulated to facilitate the protonation/deprotonation of cAsp61 and cause the rotation of the c-ring past the stationary subunit a [119, 122]. The a-c interface is formed by TMHs four and five of

the a-subunit and TMH2 from the c-ring [119, 121]. Two c-subunits are interacting with the a-subunit at all times; the first one is being protonated while the second one is releasing the proton. The proposed mechanism of proton transfer during the production of ATP is as follows [64, 134, 135]. A proton enters the half-channel from the intermembrane space (we will call it inlet half-channel) and then binds to the negatively charged cAsp61 transforming it to an ion-locked conformation. This proton neutralizes the negative charge on cAsp61 and allows the c-subunit to rotate towards the hydrophobic lipid layer. Simultaneously, the neighboring c-subunit returns from the lipid bilayer, and it is exposed to the second half-channel (we will call it outlet half-channel). The hydrophilic environment of the outlet half-channel will promote the deprotonation of cAsp61, and the released proton will enter the mitochondrial matrix region. The conserved arginine in the a-subunit is believed to prevent the proton shortcut from inlet half-channel to the mitochondrial matrix without c-ring rotation [136]. With its positive charge, it will block futile rotation of the c-ring without deprotonation.

The new insights into the molecular mechanism of rotation of F_O part of ATP synthase suggest the end positions of inlet and outlet half-channels. The membrane-spanning c-subunits are formed almost utterly comprised by hydrophobic amino acids (residues), and as a consequence, cannot mediate proton translocation. The binding site, cAsp61, can only change the protonation state when in contact with the a-subunit, which includes polar groups. The polar residues comprising a-subunit are thought to form two proton half-channels terminated by aSer206 (serine at a position 206, *E. coli* numbering) and aAsn214 (asparagine at a position 214, *E. coli* numbering) [10, 120, 133] (illustrated in Figure 1.5).

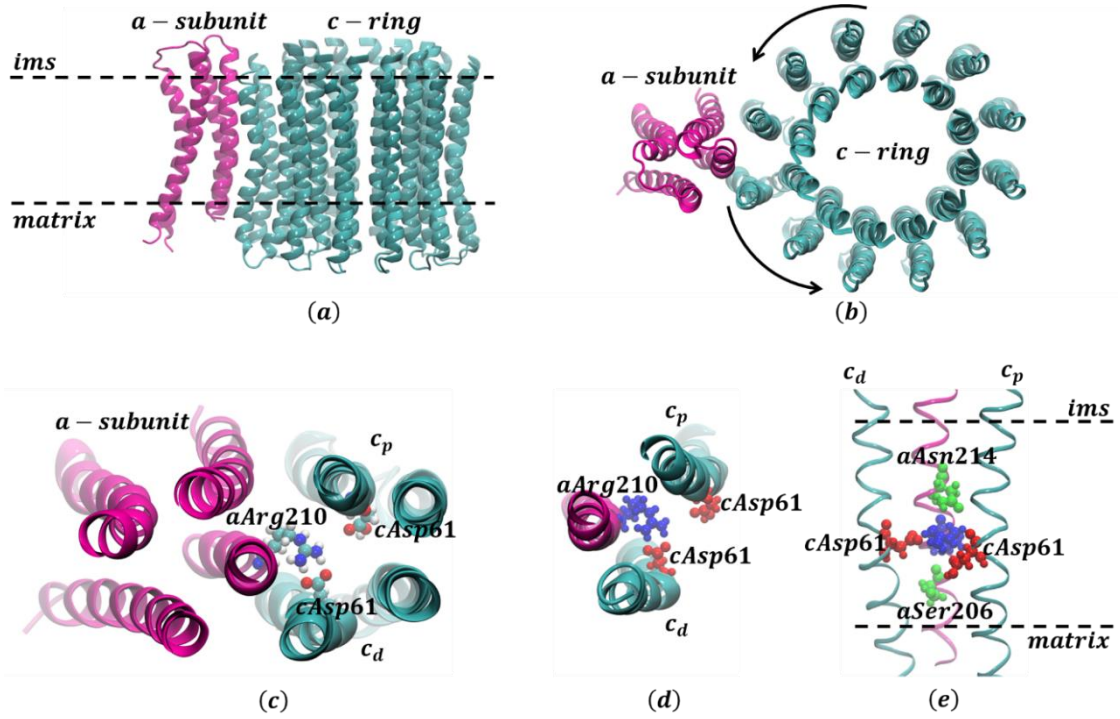

Figure 1.5 Ribbon representations of the membrane-bound FO portion of ATP synthase. (a) Side view of a-subunit (magenta) and c-ring (cyan) complex. (b) Top view of the a- c complex looking down from the mitochondrial inner-membrane space. The arrows point in the direction of rotation of the c-ring. (c) The top view from mitochondrial inner-membrane space at the a-subunit and two c-subunit at the a-c interface. The aArg210 and two cAsp61 residues are represented in CPK style (solid van der Waal spheres for atoms and cylinders for bonds). (d) The close view of the binding site at the a-c interface. Only transmembrane helices nesting the critical residues involved in proton transfer are represented. (e) The side view (looking from the inside of the c-ring) of the binding site at the a-c interface. Beside the aArg210 (blue) and cAsp61 (red), the two terminal residues of the inlet (aAsn214) and outlet (aSer206) half-channels are represented in lime color. All the images are rendered using the molecular visualization program, VMD [137]. ims – mitochondrial inner-membrane space, matrix – mitochondrial matrix, c_p – protonated c-subunit, c_d – deprotonated c-subunit.

The inlet half-channel, terminated at aAsn214, connects the proton-rich inner-membrane space to the proton binding region in the middle of the hydrophobic membrane bilayer. The outlet half-channel starts at aSer206 connecting the proton binding region to the mitochondrial matrix. Fillingame *et al.* [10, 55, 118, 119, 122, 133, 138, 139] proposed a mechanism where a proton travels from the inner-membrane space via the inlet half-

channel and protonates the cAsp61 binding site. The protonation of cAsp61 before leaving the a-c interface is needed to avoid energetically unfavorable exposure of a negatively charged residue to the hydrophobic membrane environment. The rotation of the c_{12}-ring, which is induced by the proton electrochemical gradient, will bring cAsp61 close to the a-subunit again after nearly a full revolution. This will cause the release of a proton, which then travels to the mitochondrial matrix via the outlet half-channel. Also, significant rotation of the outer TMH of a c-subunit around its axis is needed in order to bring the cAsp61 to the a-c interface where it will be protonated or it will release the proton; the side chain of cAsp61 is brought to either proton half-channel (Figure 1.6a).

After cAsp61 is deprotonated, it will form a stable hydrogen-bond with aSer206, the terminal residue of the outlet half-channel. Another stable hydrogen-bond will be formed between still-protonated cAsp61 and aAsn214 (the terminal residue of the inlet half-channel) while aArg210 is forming transient hydrogen-bonds with cAsp61 on both cTMH2 exposed to the a-c interface. This situation is represented in Figure 1.6b. At this point, the positively charged aArg210 will prevent protons from moving from one binding site to the other.

To summarize, the rotation of the c-ring is induced by cooperative interaction of two neighboring c-subunits with aTMH4. The cAsp61 of one of these two is always deprotonated. The rotation of the two c-subunits exposed to the aTMH4 brings the binding sites in contact with aArg210 and with the terminal residues of the proton half-channels (aSer206 and aAsn214). Furthermore, the direction of the c-ring rotation is controlled by the proton-motive force, and it will only continue rotating when one of the binding sites

exposed to the a-c interface is protonated. Although we know details about protonation/deprotonation of the c-subunits and terminal residues for half-channels, detailed explanations of proton pathways are somewhat unclear. The main focus of this study is to shed some light on proton mediation along the half-channels. Combining the hydrogen-bonding network with structural communication between residues within the c-subunits will elucidate the details about proton translocation.

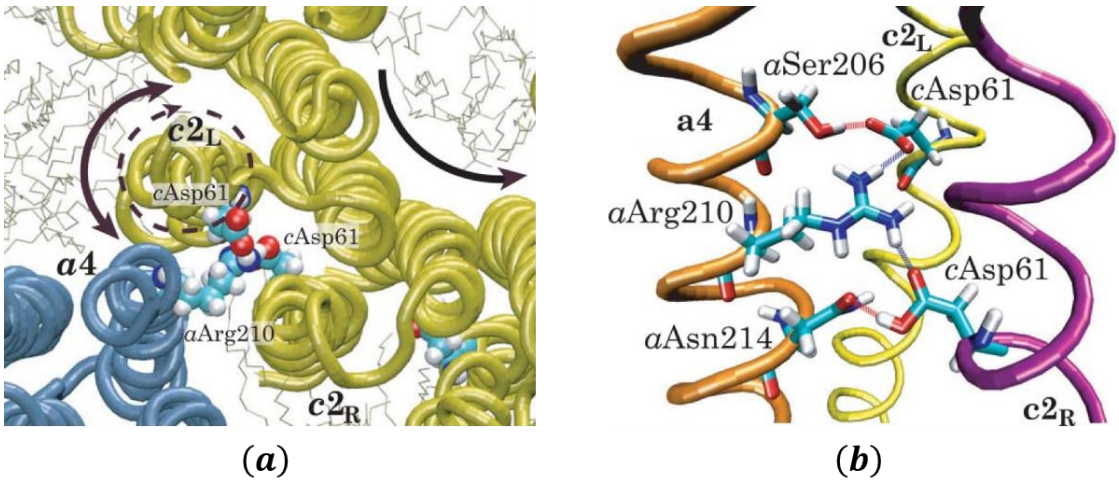

$(\boldsymbol{a})$ $(\boldsymbol{b})$

Figure 1.6 The protonation/deprotonation at the proton binding site. (a) Concerted rotation of the c-subunit outer helix and the c-ring in a lipid bilayer. The $c2_L$ helix has been forced to rotate clockwise by 180°. Shown in the instance when the salt bridge is transferred between two neighboring c-subunits, *i.e.*, when the conformation $cAsp61^{\ominus} - aArg210 - cAsp61^{\ominus}$ has been momentarily assumed. The view is from the inner-membrane space down to the mitochondrial matrix. (b) Hydrogen-bond network formed between the binding sites (cAsp61) and the terminal residues of the inlet (aAsn214) and outlet (aSer206) half-channels. The critical residue aArg210 forms transient hydrogen-bonds with both binding sites. The bottom is the inner-membrane space side, while the top is the matrix side. (Reprinted from *Biophysical Journal*, *2004* with kind permission from Elsevier) [10]

1.4 Mitochondrial Genetic Diseases

1.4.1 Mitochondrial Mutations

Human mitochondrial DNA is a circular DNA [140] that contains 37 genes where only 13 of them encode polypeptides. All 13 genes are components of the electron transport chain or ATP synthase (22 encode the transfer RNAs, tRNA, and other two ribosomal RNA). The electron transport chain complexes contain approximately 70 nuclear-encoded peptides imported into the mitochondrion by specific import pathways [15]. Two of the mitochondrial ATP synthase subunits are encoded by the mitochondrial human genome, $Su6_{m,}$ and $A6L_m$ (*cf.* Table 1.1). Subunit $Su6_m$ corresponds to the a-subunit where the $A6L_m$ subunit is the additional subunit present in human and yeast mitochondria. The genes encoding these two subunits are the mtAtp6 and mtAtp8 genes [15, 16, 70]. Figure 1.7 represents the architecture of the mitochondrial genome and the electron transport chain.

A single cell contains hundreds of mitochondria, and each mitochondria multiple copies of mitochondrial DNA (on average two to ten). The cells comprising the organs with high metabolic activity contain a high number of mitochondria. As a consequence, the severity of mutation in mtDNA differ between organs. Mitochondrial genetic diseases are maternally inherited. The majority of the mutations associated with the mitochondrial diseases are the mutations in the mtAtp6 gene. Since this is the gene that encodes the a-subunit, it only reflects the importance of the a-subunit in proton translocation.

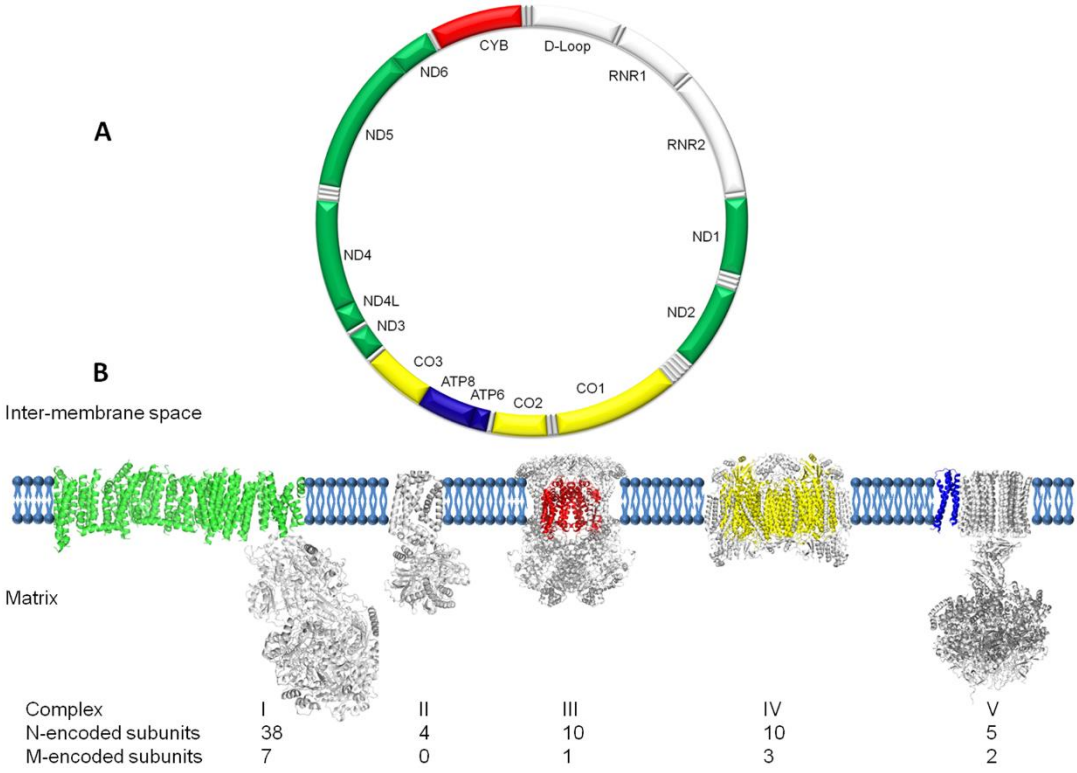

Figure 1.7 Architecture of the mitochondrial genome and respiratory chain. (A) Schematic representation of the 16,569 bp human mitochondrial genome (NC_012920), with the protein-coding genes colored according to the complexes to which they contribute subunits, two ribosomal RNAs, 22 tRNAs and non-coding D-loop in white. (B) Montage depicting the structural information currently available for the five complexes that together contribute to the mitochondrial oxidative phosphorylation machinery. Each complex (to scale) is embedded in a cartoon representation of the lipid bilayer with the mitochondrial (m)-encoded subunits colored corresponding to the genome diagram. The nuclear (n)-encoded subunits are shown in grey. (Reprinted from *PLOS ONE, 2013*, Open Access license) [141]

Disease-causing mutations in the genes encoded in the mtDNA were first identified in 1990 [142]. In Table 1.2 below, the primary mitochondrial DNA-related diseases are listed. A continuously updated list of mitochondrial diseases is reported on www.mitomap.org.

Table 1.2 Selected list of the primary mitochondrial DNA-related diseases

Disease	Locus	Allele	nt change	AA change
LHON	mtND1	G3460A	G-A	R340H
LHON	mtND4	G11778A	G-A	A52T
LHON	mtND6	T14484C	T-C	M64V
LS	mtND3	T10158C	T-C	S34P
LS	mtND4	C11777A	C-A	R340S
LS	mtND5	T12706C	T-C	F124L
MELAS	mtND5	A13514G	A-G	D393G
MELAS	mtTL1*	A342G	A-G	*
MERRF	mtTK**	A8344G	A-G	**
MERRF	mtTK**	T8356C	T-C	**
NARP/MILS	mtAtp6	T8993C	T-C	L156P
NARP/MILS	mtAtp6	T8993G	T-G	L156R
AD	mtND2	G5460A	G-A	A331T

AD – Alzheimer disease; LHON – Leber Hereditary Optic Neuropathy; LS – Leigh Syndrome; MELAS – Mitochondrial Encephalomyopathy, Lactic Acidosis, and Stroke-Like Episodes; MERRF – Myoclonic Epilepsy and Ragged Red Fiber Disease; MILS – Maternally Inherited Leigh Syndrome; NARP – Neurogenic Muscle Weakness, Ataxia, and Retinitis Pigmentosa; * mutation in $tRNA^{Leu\ (UUR)}$; ** mutation in $tRNA^{Lys}$; A – Adenine;C – Cytosine; G – Guanine; T – Thymine; G3460A – replacing Guanine at allele 3460 with Adenine; R340H – replacing the Arginine at the position 340 with Histidine; nt change – nucleotide change; AA change – amino acid change; A – Alanine; D – Aspartate; F – Phenylalanine; G – Glycine; H – Histidine; L – Leucine; M – Methionine; P – Proline; R – Arginine; S – Serine; T – Threonine; V – Valine.

To date, 36 disease or phenotype-causing mutations are reported. This number includes only mutations in the mtAtp6 gene (*cf.* www.mitomap.org). From the literature, we know that most of the mutations in the human subunit a are associated with diseases [26, 28, 29, 142-181]. Table 1.3 lists the confirmed mutations (two or more independent laboratories have published reports on the pathogenicity of a specific mutation) in the mtAtp6 gene with related diseases. Residues aLeu156, aLeu217, and aLeu220 (leucine at positions 156, 217, and 220 for human numbering) are characteristic since their position is at the location

of the outlet half-channel. The question is how these mutations will affect the existence of the outlet half-channel. The corresponding residues for the *E. coli* model are aLeu207, aLeu259, and aVal262 (valine at a position 262). The aLeu207 and aLeu259 are highly conserved residues located at aTHN4 and aTHN5 while aVal262 is adjacent to the aTHN5 and binds the highly conserved aIle261 (isoleucine) and aTyr263 (tyrosine) which are thought to be implicated in the proton translocation. The position of aLeu207 is only three residues away from the highly conserved aArg210 and one residue away from the terminal residue of the outlet half-channel. In this study, we will focus on mutations of the aLeu207 residue and investigate how this specific point mutation is affecting the outlet half-channel and consequently, the production of ATP.

Table 1.3 Up-to-date list of the confirmed mtAtp6 gene disease-causing mutations, as of July 2019

Disease	**Allele**	**nt change**	**AA change**
BSN/Leigh Syndrome	T8851C	T-C	W109R
MLASA/IgG nephropathy	G8969A	G-A	S148N
NARP/Leigh Disease/MILS	T8993C	T-C	L156P
NARP/Leigh Disease/MILS	T8993G	T-G	L156R
Ataxia syndromes	T9035C	T-C	L170P
FBSN/Leigh Disease	T9176C	T-C	L217P
Leigh Disease/Spastic Paraplegia	T9176G	T-G	L217R
Leigh Disease/Ataxia/NARP-like syndromes	T9185C	T-C	L220P

BSN – Bilateral striatal necrosis; NARP – Neurogenic muscle weakness, Ataxia, and Retinitis Pigmentosa; alternate phenotype at this locus is reported as Leigh Disease; MELAS – Mitochondrial Encephalomyopathy, Lactic Acidosis, and Stroke-like episodes; MILS – Maternally Inherited Leigh Syndrome; A – Adenine;C – Cytosine; G – Guanine; T – Thymine; G8851A – replacing Guanine at allele 8851 with Adenine; W109R – replacing the Tryptophan at the position 109 with Arginine; nt change – nucleotide change; AA change – amino acid change; L – Leucine; N – Asparagine; P – Proline; R – Arginine; S – Serine; W – Alanine;

1.4.2 Bioenergetics of Mitochondrial Diseases Associated with mtDNA Mutations

Mitochondrial DNA mutations cause diseases associated with defects in oxidative phosphorylation, which is the primary energy-producing system in cells. The production of ATP is catalyzed in the mitochondrial respiratory chain (comprised of four large protein complexes I – IV) and the ATP synthase. Complexes I – IV are parts of the electron transport chain, and the ATP synthase harnesses the energy generated by the electron transport chain. All five complexes together comprise nearly 90 different subunits, and 13 of them are encoded by mtDNA. To understand the underlying pathophysiology of any mtDNA mutation, one should examine multiple aspects of bioenergetics [182]. This test involves the analysis of checkpoints in energy metabolism (the end point of glycolysis, the final step of oxidative phosphorylation – production of ATP, and overall respiratory chain function – rates of oxygen consumption). In this section, we will discuss the bioenergetics for some of the mutations listed in Tables 1.2 and 1.3. A large number of mutations affecting human mtDNA are linked with disorders involving tissues that are characterized by a high-energy demand, including the central nervous system, skeletal, and cardiac muscles.

LHON (Leber Hereditary Optic Neuropathy) is an inherited form of central vision loss [183, 184]. The three most frequent mutations causing this disease are G3460A/ND1, G11778A/ND4, and T14484C/ND6. Biochemical investigations revealed that G3460A/ND1 mutation has a consistent reduction of 60-80% in complex I electron transfer activity [185-187], while the other two mutations had normal or slightly reduced activities

[188, 189]. The reduced activity of complex I leads to impaired electron flow, which will cause decreased respiratory activity. Furthermore, proton pumping through complex I is defective and affects energy conservation. Finally, an increase in reactive oxygen species (ROS) generation will occur as a consequence of disrupted electron transport.

The Neurogenic muscle weakness, Ataxia, and Retinitis Pigmentosa syndrome (NARP) and the maternally inherited Leigh syndrome (MILS) are rare genetic disorders caused by abnormalities affecting mitochondrial energy production. NARP is characterized by a disease affecting the nerves outside of the central nervous system (peripheral neuropathy), a diminished ability to coordinate voluntary movements (ataxia), an eye condition known as retinitis pigmentosa (RP), and a variety of additional abnormalities. MILS is a more severe mitochondrial disorder that often becomes apparent during infancy or childhood and is characterized by brain disease, elevated levels of lactic acid in the body, seizures, heart disease, respiratory abnormalities, and developmental delays. NARP and MILS are both caused by the mutations in the mtAtp6 gene, more specifically at the base pair 8993 (*cf.* Table 1.3) [142, 190].

The two mutations are associated with mitochondrial dysfunction and cause severe syndromes in energy deficiency. The T8993G mutant decreases the ability of ATP synthase to extract energy from proton translocation to only 5% of its full capacity. On the other hand, the T8993C mutant will slow down the synthesis of ATP by less than 25% and proton translocation by 30% [26, 27, 191]. It is safe to state that mutations in the mtAtp6 gene will cause diseases associated with energy deficiency. Additionally, it is important to stress that severity of the given disease will depend on the mutation load (percentage of the mutant

mtDNA), the nucleotide change (*e.g.*, T8993G point mutation will replace conserved Leucine with positively charged Arginine at the outlet half-channel), and the position of the mutated residue within the a-subunit. The mutations along the proposed inlet and outlet half-channels within the ATP synthase are expected to affect the proton translocation and production of ATP tremendously. In this study, the main focus will be on the T8993G and T8993C mutations and their effect on proton translocation.

1.4.3 Maternally Inherited Leigh Syndrome

MILS and NARP syndrome are mitochondrial conditions transmitted from the mother to the children. The specific mutations in the mitochondrial mtAtp6 gene, T8993G, and T8993C mutations, cause both MILS and NARP. When the mutation load, the percentage of mutant mtDNA within cells, is typically in a range between 75% and 90%, individuals are classified as having NARP syndrome [192]. In the case of MILS, the mutation load is higher than 90% [193]. When the mutation load is below 60%, patients carrying the mutation on base pair 8993 will remain asymptomatic [194]. Within the same family one individual may have NARP syndrome while another individual is diagnosed with MILS.

MILS is a fatal neurodegenerative disease with early childhood onset and is often apparent during the first three months to one year of life (onset can occur at any time from birth through adulthood). Later onset of this disease is often associated with a slower progression of symptoms. Many cases of MILS are first observed following a viral infection. The specific symptoms and severity can vary significantly from one individual

to the next. Generally, Leigh syndrome is a progressive neurodegenerative disorder. If the onset of the disease is during the first year of life, the initial signs may be weak sucking ability and loss of head control. Additional symptoms can include an intense loss of appetite, recurring vomiting, and possible seizure activity. Infants affected by Leigh syndrome will have delays in reaching developmental milestones. Affected children will experience the inability of an organ system to compensate for illness or deficiency (*e.g.*, loss of functions that require the coordination of mental and muscular activities). If the onset of the disorder is later during childhood, ataxia (affected children appear clumsy or unsteady) or difficulty articulating words will be the initial signs. Additionally, affected children will lose previously acquired intellectual skills, and intellectual disability will occur.

The symptoms that characterize the progressive neurological deterioration associated with MILS are: generalized muscle weakness; lack of muscle tone; tremors, seizures, infantile spasms; movement disorders such as rapid involuntary jerky movements; the stiff movement of the legs, and dystonia (involuntary muscle contractions that force the body into abnormal, painful movements, and positions).

Individuals with MILS will develop a range of respiratory abnormalities, including the temporary cessation of spontaneous breathing, difficulty in breathing, abnormally rapid breathing, and irregular breathing patterns. Some infants will additionally experience difficulty swallowing. Visual problems will include abnormally rapid eye movements, sluggish pupils, crossed eyes, paralysis of specific eye muscles, deterioration of the nerves of the eyes, and visual diminishing leading to blindness. MILS may also affect the heart.

Children with this disorder will have abnormal enlargement of the heart and overgrowth of the membrane that divides the chambers of the heart. In some cases of MILS, complications can develop by three years of age.

Previously in this section, we stated that the specific mutations in the mitochondrial mtAtp6 gene, T8993G, and T8993C, will result in NARP and MILS syndromes. The two mutations are on a base pair 8993 in mtDNA. The $T \rightarrow G$ point mutation changes Leucine at a position 156 with Arginine in the a-subunit, while the $T \rightarrow C$ mutation changes Leucine with Proline. These two mutations act differently on proton translocation through the ATP synthase [26]. Leucine at the position 156, aLeu156, (human numbering, *E. coli* analog is aLeu207) is a conserved residue of the a-subunit, and mutation in this residue causes an energy-deficient phenotype NARP in humans. aLeu156 occupies a critical position three residues away from the functionally essential aArg159 (*E. coli* analog is aArg210) and one residue away from the aAla155 (*E. coli* analog is aSer206), which is a terminal residue of the outlet half-channel. aLeu156 is not directly involved in proton translocation, but the position of this residue is essential for subunit function [142, 195].

Figure 1.8 illustrates the position of the mutated residue relative to the functionally essential Arginine at a position 159 (human numbering). Since aLeu156 is positioned on a helix turn directly above (looking from the mitochondrial inner-membrane space) the aArg159, it could influence the proton translocation [196], or the torque generation [10, 57] through the a-c interaction. Human ATP synthase carrying the Leu156Arg mutation is severely defective in the synthesis of ATP, but unlike the *E. coli* homolog, it is still fully assembled and sensitive to saturating oligomycin [27, 180, 195, 197-199].

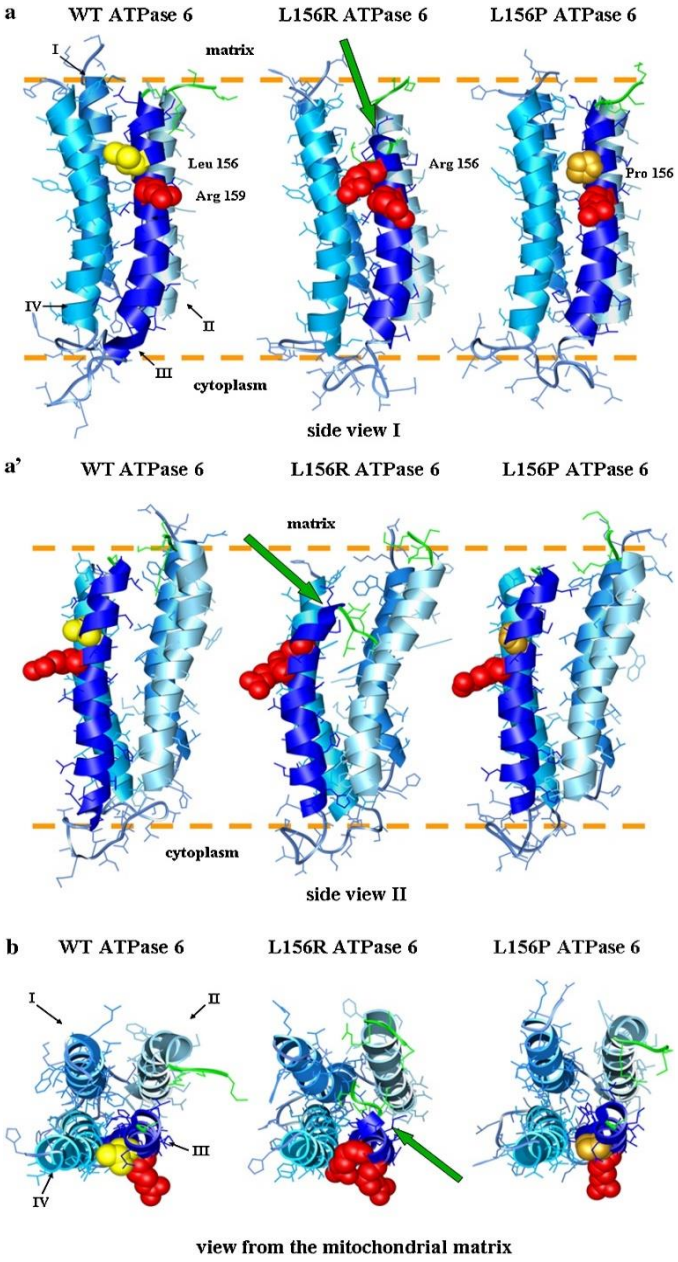

Figure 1.8 Ribbon models of the transmembrane α-helices of wild type and mutant human a-subunits (ATPase 6) of ATP synthase. The a-subunit membrane domain spans the lipid bilayer and, according to the *E. coli* model, consists of four α-helices. The essential Arg159 and Leu156 are shown with space-filling spheres in red and yellow, respectively, whereas the mutant amino acid is either red (Arg) or ochre (Pro). The green arrow indicates the position where helix III is interrupted in Leu156Arg mutant cells. (a and a') View perpendicular to the cell membrane, in two orientations at right angles to each other. (b) View in the plane of the membrane from the mitochondrial matrix. (Reprinted from *BBA-Bioenergetics, 2008* with kind permission from Elsevier) [26]

The severity of the Leu156Arg mutation at position 159 may be explained by replacing leucine with positively charged arginine. Leucine is a nonpolar, essential amino acid that is hydrophobic and generally buried in folded proteins, whereas arginine is a polar positively charged essential amino acid that maintains overall charge balance of the protein. The second mutation at this position (position 156 within α-subunit), Leu156Pro, has been reported and associated with much lower impairment of ATP synthesis than the Leu156Arg [29, 180]. Clinically this mutation exhibited less severe symptoms [26]. The main reason behind the lower severity of this mutation lies behind the characteristics of proline. It is an nonpolar imino acid (contains both, imine $= NH$, and carboxyl, $COOH$, functional groups) that when in a peptide bond, cannot donate the hydrogen-bond (amino acids contain amine $= NH_2$, and carboxyl, $COOH$, functional groups) to stabilize an α-helix or β-sheet. The α-helix containing proline will have a slight bend due to a very restricted phi/psi (backbone) torsional space, and it cannot accommodate the angles needed for alpha-helix or beta-strand.

Experimental studies have shown that the synthesis of ATP in cells carrying the Leu156Pro mutation is slowed by less than 25% [174, 180]. This impairment in the efficiency of ATP synthase corresponds closely with the 30% decrease in proton translocation rate. In the Leu156Arg mutation, the rate of ATP synthesis declines severely to only 5% of its standard rate [174, 180]. This observation indicates that the severe reduction in the rate of ATP synthesis is not only due to the decrease in proton pumping but rather in a decreased ability of ATP synthase to extract energy from proton translocation [192].

For this dissertation, the main focus is the study of the proton translocation mechanisms, more precisely the half-channel formation, utilizing the Molecular Dynamics (MD) calculations. Furthermore, the details on how specific mtDNA mutations will affect the half-channels will be investigated. Aside from the wild-type F_O portion of the ATP synthase, we will also complete the detailed calculations on the Leu156Arg mutation (T8993G). The model used for this work is the *E. coli* structure of the membrane-bound portion of the F_O. Figures 1.9 and 1.10 represent the primary amino acid sequence alignment of the *c*-subunit and *a*-subunit, respectively. Comparing the amino acid sequence between *E. coli* and human, it is clear that the structure of *E. coli* is a suitable candidate for MD calculations.

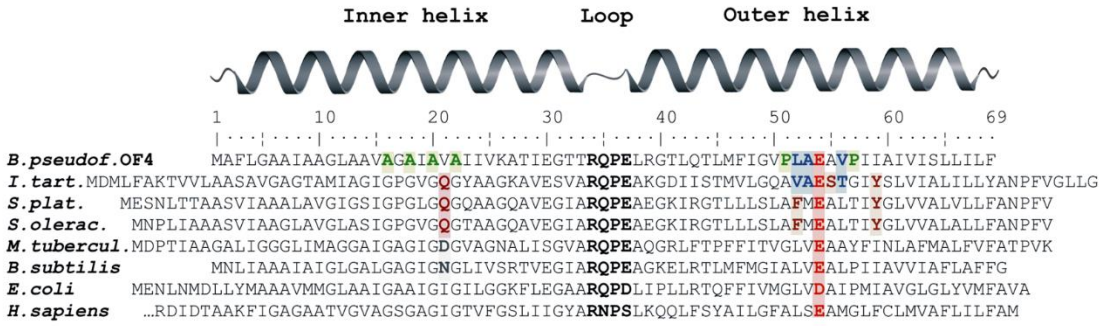

Figure 1.9 Amino acid sequence alignment of *c*-subunit. The *c*-subunits of selected species were aligned according to their cytoplasmic loop region (loop exposed to the mitochondrial matrix) (bold). Residues structurally proven to be involved in ion coordination are shown in dark red and blue. The conserved ion-binding glutamate/aspartate is highlighted in red for all species. (Reprinted from *PLOS Biology*, 2010, Open Access license) [200]

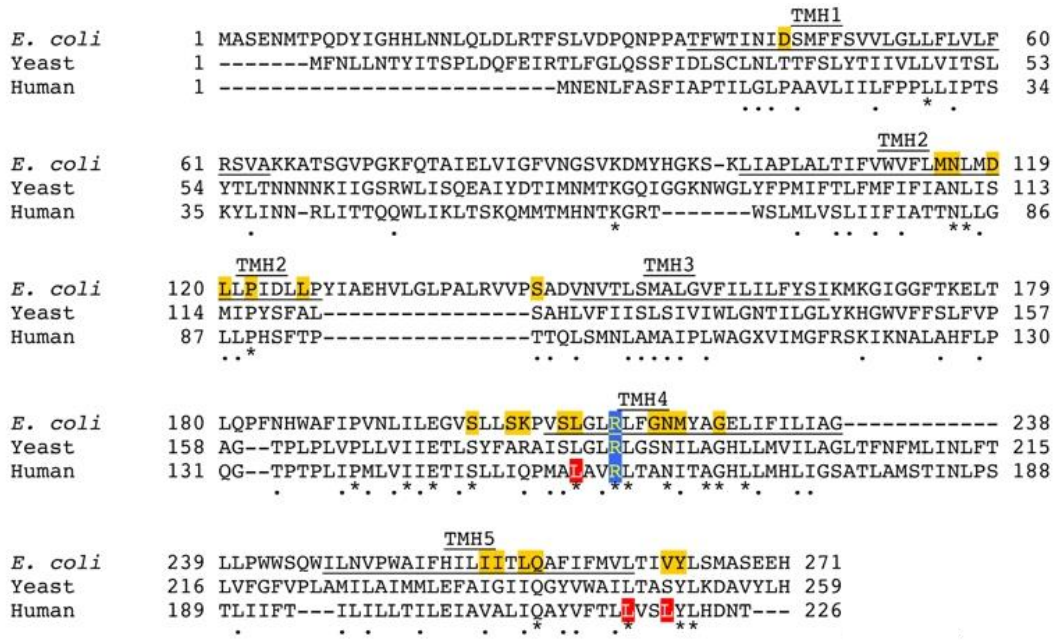

Figure 1.10 Primary sequence alignment of *a*-subunit. The partial primary sequence alignment of *a*-subunit from *E. coli*, yeast, and human. The residues predicted to form transmembrane helices 3-5 are underlined and labeled. The highly conserved and essential R210 (*E. coli* numbering – Arginine at position 210) is shaded blue. The residues shaded red are mutated in the discussed human diseases. The residues shaded gold are identified as important for proton movement. (Reprinted from *Microbial Cell*, 2015, Open Access license) [70]

1.4.3.1 MILS Statistics, Diagnosis, and Treatment

NARP syndrome and MILS affect both male and female children in equal numbers. NARP is estimated to occur in 1 in 12000 births, while Leigh disease, in general, is estimated to affect 1 in 36000-40000 newborns (*cf.* https://rarediseases.org/). Experimentally, it is estimated that 30% of Leigh disease patients have MILS. In the United States, mitochondrial disorders are estimated to occur in 1 in 4000 births. Most of the time, those disorders are unrecognized, which leads to the difficulty to determine the exact frequency of mitochondrial disorders in the general population. In specific populations,

MILS and Leigh syndrome are more common. For example, 1 in 2000 newborns is affected by Leigh syndrome in the Saguenay Lac-Saint-Jean region of Quebec, while on the Faroe Islands 1 in 1700 babies is affected (*cf.* https://ghr.nlm.nih.gov).

The diagnosis of mitochondrial disorders is difficult if one is not explicitly looking for it. Some of the cases of NARP and MILS can be confirmed through molecular genetic testing. The mtDNA mutations related to these disorders can be detected in white blood cells, but other tissue samples may be required, such as skin, skeletal muscle, hair follicles, or urinary sediment.

To date, there are no proven treatment regimens for Leigh syndrome and MILS. Most of the time, the treatment recommendations are based upon extensive experimental studies. Due to the complexity of this particular disease, the treatment may require the coordinated efforts of a team of specialists.

Remembering that MILS is a fatal disease affecting children, one would agree that it is imperative to understand mechanisms of proton translocation through the membrane-bound part of the ATP synthase. Once a detailed, clear picture of proton translocation and energy production is painted, we can focus on possible treatment mechanisms. In this dissertation, we will attempt to elucidate proton pathways and get closer to that 'clear picture.'

Chapter 2 Theory and Background

2.1 Molecular Motors

The molecular devices are classified into two groups – enzymes (biological catalysts) and molecular machines. Molecular machines include one-shot machines (*e.g.*, osmotic machine) and cyclic machines. Cyclic machines are furthermore classified into

- Motors – transduce free energy into directional motion,
- Pumps – transduce free energy to create concentration gradients, and
- Synthases – transduce free energy to drive a chemical reaction and then synthesize products.

According to the Merriam-Webster dictionary, '*a motor is a rotating machine that transforms any given form of energy into mechanical energy'* (https://www.merriam-webster.com). Biological molecular motors are protein complexes that convert chemical energy directly into mechanical work, thereby ensuring suitable energy storage, force production, and directional motion on both microscopic and macroscopic scales. These biological machines are the basis of life. Within cells, there are hundreds of different types of molecular motors; each of them is specialized for a particular function.

The wide range of functions, including chemical synthesis, organelle transport from one cell part to another, muscle contraction, protein folding, chromosomal segregation during the cell division, or the maintenance of a potential across the membrane all involve

directional movement and transport of chemical species. Additionally, cells must often move and orient in response to external chemical gradients and other signals.

The machine-like devices, molecular motors, help the cells overcome the randomizing effect of Brownian motion and carry out the directional processes mentioned above. Because of their dimension, these devices are unlike the macroscopic engines. Macroscopic motors, as well as their surroundings, are made of a large number of small molecules. Although these molecules move according to Newton's laws, on time scales relevant for the operation of macroscopic motors, information on their deterministic trajectories is lost, and their behavior can be described statistically. The most likely configurations of the system are very similar to each other, and on macroscopic scales, differences between these configurations, *i.e.*, thermodynamic fluctuations, are negligible. As a result, the collective behavior of a large number of molecules that the macroscopic motor and its surrounding are made of can be described through thermodynamic properties and laws of thermodynamics. The number of molecules in a microscopic motor is still significant, but microscopic motors are so small that they are subjected to sizeable thermodynamic fluctuations due to the significant number of small parts that must operate at energies marginally higher than the thermal bath. These fluctuations are an essential component of the molecular motor and must be taken into account. Although the forces generated by molecular motors are minimal on a macroscopic scale, they are substantial on a microscopic level (on the order of picoNewtons).

Table 2.1 lists some of the known biomolecular motors, including their functions and energy sources. It is likely that many more molecular motors exist and that all of the

functions of the ones known so far are not yet recognized. The malfunction of specific molecular motors can be a source of disease [201]. Detailed understanding of how biomolecular motors function and their role in the machinery of the cell may provide the guide for the treatment of certain diseases. The complexity and effectiveness of these motors as part of the cellular network are beyond impressive.

Table 2.1 Examples of some of the known biomolecular motors

Motor	**Occurrence**	**Function**	**Source of energy**
ATP synthase	Membranes of mitochondria, chloroplast, and bacteria	Synthesis of ATP and proton pump	PMF and ATP hydrolysis
DNA and RNA polymerase	Prokaryotic and eukaryotic cells	Catalyze DNA and RNA synthesis	ATP hydrolysis, nucleotide phosphorylation
DNA helicase	Prokaryotic and eukaryotic cells	Unwind double-stranded DNA	ATP hydrolysis
GroEL	Bacterial cell	Unfolding and refolding misfolded proteins	ATP hydrolysis
Myosin V and VI	Eukaryotic cells	Intracellular cargo transfer	ATP hydrolysis
Myosin II	Muscle cells	Muscle contraction	ATP hydrolysis
Dynein	Eukaryotic cells	Intracellular cargo transfer	ATP hydrolysis
Kinesin	Eukaryotic cells	Intracellular cargo transfer	ATP hydrolysis
Bacterial flagellar motor	Bacterial cell membrane	Bacterial motion	Ion gradient

PMF – proton motive force.

2.2 The Physics of Molecular Motors

The basic physics principle that governs the operation of molecular motors is not quite as simple as it seems. Molecular motors generate mechanical forces using intermolecular binding energy to capture favorable Brownian motions. They achieve this in two ways: (1) bias against unfavorable Brownian motions by a sequence of small free-energy drops, making the backward steps slightly less likely than the forward ones; or (2) rectify a long run of favorable thermal fluctuations via a significant free-energy drop, making backward steps extremely unlikely in comparison to forward steps [19]. The latter is generally called a Brownian ratchet and the former a power stroke. These two mechanisms are two extreme cases of using random thermal fluctuations to drive a load. The mechanism that is intermediate between these two is more likely to be observed within the cell.

Some of the biological motors operate cyclically where the steps of the mechanical cycle are coupled to the state of a chemical cycle that generates energy that fuels the movement. Cyclic biological motors undergo the number of steps that correspond to changes in conformation and chemical states and eventually reset to their initial conformation. The chemical steps providing fuel for cyclic motors typically involve catalytic turnover of a high-energy molecule (*cf.* Table 2.1). The one-shot motors (enzymes) release previously stored elastic energy and then are disassembled.

Since molecular motors are small, the Brownian motion dominates their operation. As a consequence, thermal fluctuations are an essential component of the molecular mechanisms related to the operation of molecular motors. To describe the way molecular

motors work, one needs to define the bath and system variables [202]. Bath variables represent the extra degrees of freedom in the molecular motor and surrounding molecules in solution when in the cell environment. Most of these fluctuate rapidly enough on the experimental time scale to be approximately at equilibrium. System variables define an n-dimensional space in which the molecular motor moves. Each point in that space characterizes a unique configuration of the motor with a corresponding free energy value (the potential of mean force). This potential of mean force defines the potential energy surface spanning an n-dimensional state space in which the motor moves. The potential energy surface arises primarily from three sources: (1) interactions within the molecular motor, including the interactions with the track along which the motor moves (if one is present), (2) interactions with the motor molecules and molecules that serve as fuel (source of chemical energy), and (3) interactions of all of the above with the solvent environment. Knowing that a molecular motor must have a source of chemical energy, at least one of the variables will be called the chemical variable (measures the progress of chemical reaction) or reaction coordinate. The rest of the variables are called the mechanical variables. Finally, at least one of the mechanical variables must describe the progress of the molecular motor along the track it takes (if one is present) or, in a case of rotary molecular motors, the angle of rotation along its rotating axis.

Figure 2.1a represents the potential energy surface of the most straightforward case when the molecular motor is described by only one chemical and one mechanical variable. Since the motor is microscopic, its motion is not given as a deterministic trajectory defined by the energy surface, but it is better described by the Smoluchowski equation as the diffusion of the system along the potential energy surface.

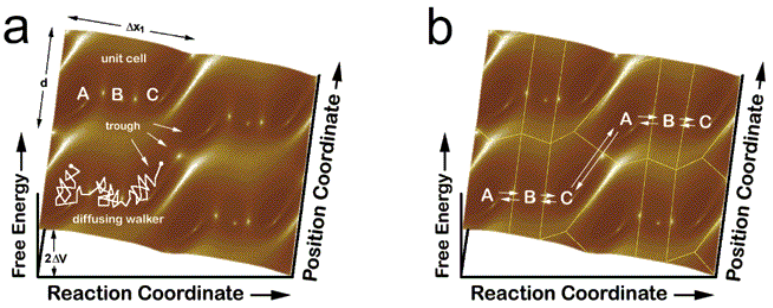

Figure 2.1 Potential energy surface for a molecular motor. (a) Minimal potential energy surface for a molecular motor. The surface is periodic in both the reaction coordinate and position coordinate, reflecting the cyclic nature of both enzymatic turnovers and motor cycles. The surface has three local minima (labeled A, B, C) connected by low-energy passes and is tilted along the chemical axis, representing the driving force for the motor, *i.e.*, the free energy of the reaction. An externally applied load force would appear as a tilt of the surface along the position coordinate. The long through in the center couples the chemical energy to mechanical motion. The system point moves by random walk over this surface. (b) Correspondence between the potential energy surface and the kinetic mechanism of the motor. The regions around the local minima represent intermediate species. Diffusion between minima is equivalent to chemical transitions, which can be described by kinetic rate constants. Reprinted with permission from [202]. Copyright 2001 American Chemical Society.

The Smoluchowski equation for the probability distribution $\omega(x_1, x_2, t)$, where x_1 and x_2 represent chemical and mechanical coordinates respectively, is given by

Equation 2.1

$$\frac{\partial \omega}{\partial t} + \left[\sum_{i=1}^{2}\left(-\frac{k_B T}{\gamma_i}\frac{\partial^2}{\partial x_i^2} + \frac{1}{\gamma_i}\frac{\partial}{\partial x_i} f_i\right)\right] = 0$$

where i is the number of system variables (one mechanical and one chemical), f_i represent the external mechanical forces acting on the i^{th} component of the space state due to the potential and external forces (excludes the stochastic force), the γ_i are friction coefficients, k_B – the Boltzmann constant, and T represents the temperature of the system [202].

The standard kinetic view is represented in Figure 2.1b. Minima in the energy surface, around which a system tends to fluctuate for long periods, are recognized as intermediate states (A, B, C). Kinetic rate constants give the statistical rate at which the transition between minima will occur. The external forces acting on the spatial positions of the molecular motor, probability densities, and diffusion currents are determining factors for the kinetic rate constants. It is important to note that all the mechanical motions in this approximation are thermally excited transitions and the kinetic rate constants have the form $exp(-fL/k_BT)$. Here L is the mechanical transition distance.

In the discrete case, the Smoluchowski equation becomes a set of first-order or pseudo-first-order equations governing the populations of the discrete states. The set of these equations can be written in the form

Equation 2.2

$$\frac{\partial \rho}{\partial t} = \boldsymbol{K}\rho \,,$$

where $\rho = (\rho_1, \rho_2, \ldots, \rho_n)$ represents the vector of populations, one for each discrete state, and $\boldsymbol{K}$ is a matrix of rate constants or step transition probabilities defined as

$$\boldsymbol{K} = \begin{pmatrix} k_{11} & k_{12} & \cdots & k_{1n} \\ k_{21} & k_{22} & & \\ \vdots & \vdots & \ddots & \\ k_{n1} & k_{n2} & \cdots & k_{nn} \end{pmatrix}.$$

The continuous description of a molecular motor is given by the Smoluchowski equation (Equation 2.1), while the kinetic equation (Equation 2.2) provides a fully discrete

description. Both of these equations govern all Markov processes (the future processes depend only on the current state instead of on the processes that occurred in the past) [202]. A ‘mixed’ description, in which the chemistry is discrete, but the mechanics are continuous is also probable. The best example for ‘mixed’ description is the F_O rotary motor model presented in the next section. All three approaches outlined represent the reliable basic methods to describe molecular motors.

The two general mechanisms by which the chemical energy can be converted into mechanical motion are identified as the power stroke and the Brownian ratchet. The F_O motor is a perfect example of a motor that includes both a power stroke and a Brownian ratchet within the motor mechanism. The molecular motors that resemble the macroscopic engine involve power stroke mechanism, where the free energy supplied by the, *e.g.*, proton influx or ATP molecules, is directly coupled to the force and/or torque generation. The power stroke is a large, rapid structural change in a protein that can be used to do mechanical work. In a Brownian ratchet, the chemical fuel is used in a way that forward fluctuations on the load are selected rather than the application of the direct mechanical force.

2.2.1 The F_o Motor

The F_O portion of the ATP synthase is referred to as a Brownian ratchet with a power stroke. It draws the energy from the chemical energy stored in a transmembrane proton motive force. The energy released in the process of transferring electrons laterally via the ETC is used to translocate protons across the mitochondrial inner membrane into the inner-membrane space generating the transmembrane electrochemical gradient, $\Delta\mu_{H^+}$. This electrochemical gradient is used to power the ATP synthase by providing the energy reservoir that the motor will convert into a rotary torque. The electrochemical gradient is defined by [203, 204]

Equation 2.3

$$\Delta\mu_{H^+} = -F\Delta\psi + 2.3\,RT\Delta pH\,,$$

where

Equation 2.4

$$RT = \frac{k_B T}{e}.$$

ΔpH is the difference between inner-membrane space and mitochondrial matrix pHvalues. Note that in respiring mitochondria, this value is less than 0. $\Delta\psi$ represents the transmembrane electrochemical potential, and it is usually positive. F is the Faraday constant while R and T are the universal gas constant and temperature, respectively. k_B is the Boltzmann constant and e is the charge of the electron.

Using the electrochemical gradient, Mitchell defined the term protonmotive force (pmf or Δp, in units of voltage) [40] which it has the form

Equation 2.5

$$\Delta p\ (mV) = -\frac{\Delta \mu_{H^+}}{F}.$$

Protonmotive force defined in this way facilitates the comparison with redox potential differences in the ETC complexes where the proton gradient is generated and emphasizes that we are dealing with a potential driving a proton circuit [40]. At a standard temperature of 25°C, Equation 2.5 has the final form

Equation 2.6

$$\Delta p\ (mV) = \Delta \psi - 59 \Delta pH\ .$$

The first term in Equation 2.6 is an electrical term, while the last term is chemical. The inner-membrane space represents the acidic reservoir, the protons are being concentrated in between the outer and inner mitochondrial membranes, and the mitochondrial matrix is the basic reservoir.

Protons flow from the acidic region down to the basic reservoir through the rotor-stator interface. The rotor, c-ring, carries twelve negatively charged proton binding sites equally spaced around its periphery. The ion binding sites, cAsp61, are positioned in a hydrophobic region of a lipid bilayer at the middle of the c-subunits comprising the rotor. In this configuration, the sites outside of the rotor-stator interface are in equilibrium with the acidic reservoir. The stator, a-subunit, is responsible for a hydrophobic seal that prevents protons from leaking across the inner mitochondrial membrane. An aqueous inlet half-channel allows protons to access and bind to the binding site on c-ring. Positively charged aArg210, positioned below the inlet half-channel and right across from cAsp61, repels protons and forces them to bind to the binding site. In this way, it prevents the protons from

leaking from inlet half-channel to the mitochondrial matrix. After a proton binds to cAsp61, it neutralizes it so that the rotor can rotate through the hydrophobic region of the lipid bilayer. After the nearly full revolution, the neutralized cAsp61 is exposed to the low proton concentration at the outlet half-channel, and the proton will easily dissociate. The critical question one can ask is how the electrochemical gradient is converted to a rotary torque at the a-c interface. The structure of the a-c complex allows only one c-subunit at the a-c interface, and during the proton translocation, only one reaction take place at atime, either proton binding or proton dissociation. The torque produced at the a-c interface drives the rotary motion of the c-ring. This torque originates from three interactions: [202]

- The Coulomb interaction between c-ring and a-subunit $\phi_Q(\theta, s)$, (depends on the c-ring occupancy, $s = (0,1)$ where 0 – unoccupied and 1 – occupied).
- The dielectric barrier, $\phi_{\Delta\varepsilon}(\theta, s)$, that prevents rotation of empty sites and exposure of the negatively charged residue to the highly hydrophobic region of the lipid bilayer. The height of the hydrophobic barrier is approximately $45k_BT$.
- The membrane potential, $\phi_M(\theta, s)$, that tilts the Coulomb interaction potential.

Taking all of these into account, one can write the equation for torque in terms of a potential function, Φ, as follows

Equation 2.7

$$\tau_M(\theta, s) = -\frac{\partial \Phi(\theta, s)}{\partial \theta} = -\frac{\partial}{\partial \theta}\Big(\phi_Q(\theta, s) + \phi_{\Delta\varepsilon}(\theta, s) + \phi_M(\theta, s)\Big).$$

From here the Langevin equation governing the rotational motion of the c-ring is given by

Equation 2.8

$$\xi \frac{d\theta}{dt} = \tau_M(\theta, s) - \tau_L(\theta) + \tau_B(\theta), \qquad s = (0,1)$$

where ξ is the frictional drag, τ_M is the motor torque, τ_L is the load torque, and τ_B is the Brownian torque [202]. Without the membrane potential, the motion of the rotor would be driven only by its diffusion (pure Brownian ratchet). When a significant membrane potential is present, the F_O takes on a hybrid quality with characteristics of both a Brownian ratchet and a power stroke [1]. The main assumption behind this theory is that membrane potential spans the half-channels in the direction perpendicular to rotor motion [17]. Finally, the F_O motor could be driven in reverse to function as an ion pump.

2.2.2 Stochastic Model of F_o Function

Schulten's group combined mathematical modeling with all-atom MD simulations of the *E. coli* F_O in the lipid-solvent environment (its native environment) [10]. The stochastic model proposed by this group is directly related to the atomistic structure and dynamics of the F_O portion of ATP synthase. Even though this model is based on the c-ring comprised of 10 subunits, the same principle can apply to our model (12 subunits comprising the c-ring). The geometry of the model is defined in Figure 2.2.

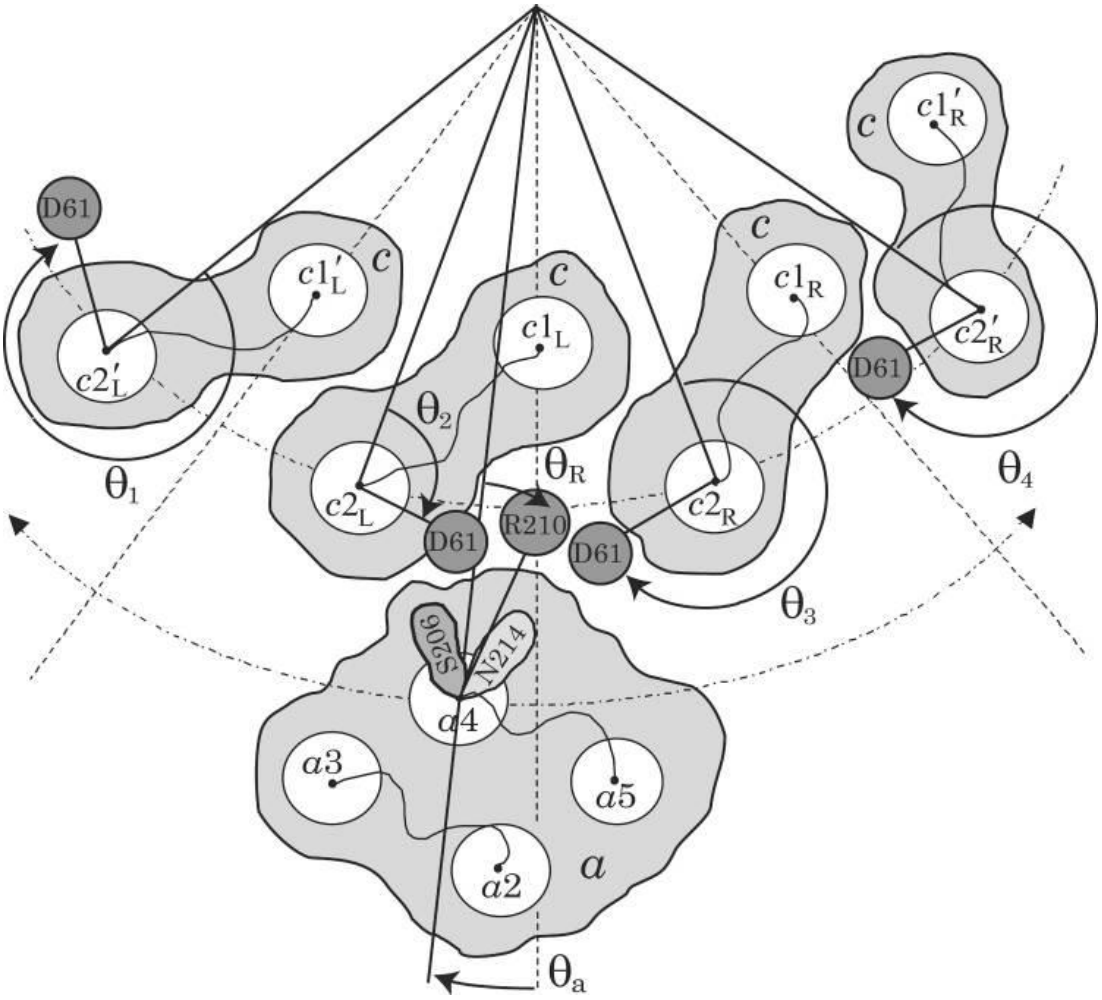

Figure 2.2 Stochastic model for F_O (view from the cytoplasm – mitochondrial matrix). Four c-subunits and the a-subunit are shown. The c-ring is fixed, and the a-subunit can move in either direction (angle θ_a). This is equivalent to the more natural choice of a fixed a-subunit and a moving c-ring. The second transmembrane helix ($c2$) of each c-subunit can rotate independently (described by angles θ_1, θ_2, θ_3, and θ_4), thereby moving the key cAsp61 residues, which are the proton binding sites. The $c1$ helices do not rotate. Similarly, only the fourth helix of the a-subunit ($a4$) can rotate (angle θ_R) moving the aArg210 residue; helices $a2$, $a3$, and $a5$ do not rotate. Proton transfer occurs between the terminal residue of the inlet half-channel (aAsn214) and the cAsp61 binding site on the helix $c2_R$, and between the terminal residue of the outlet half-channel (aSer206) and the aAsp61 binding site on the $c2_L$. Motions are confined to the plane of the figure. The system is fully described by helix orientations θ_1, θ_2, θ_3, and θ_4 (c-subunits), θ_R ($a4$), rotor angle θ_a, and protonation state for two aspartates (cAsp61) on helices $c2_L$ and $c2_R$. (Reprinted from *Biophysical Journal, 2004* with kind permission from Elsevier)[10]

When $a4$ is at equal distance from the two $c2$ helices, $\theta_{\mathrm{a}} = 0$. The protonation or deprotonation will occur only when the proton binding site (cAsp61) is in close proximity to the terminal residue of either the inlet or outlet half-channel. Once cAsp61 approaches the terminal residue of the inlet half-channel (aAsn214), it will get protonated, whereas when it approaches aSer2016 (the terminal residue of the outlet half-channel), it will get deprotonated. The periodicity of the system is assumed by

Equation 2.9

$$f\left(\theta_{\mathrm{a}} \pm \frac{2\pi}{10}\right) = f(\theta_{\mathrm{a}}),$$

where f is any function dependent on θ_{a}, and, in the case of 12 c-subunits, the left-hand side term becomes $f(\theta_{\mathrm{a}} \pm 2\pi/12)$.

The system of Langevin equations below represents the equations of motion for this part of the protein complex,

Equation 2.10

$$\xi_i \frac{d\theta_i}{dt} = -\frac{\partial \Psi(\theta_{\mathrm{a}}, \theta_R, \theta_1, \theta_2, \theta_3, \theta_4)}{\partial \theta_i} + \eta_i(t), \qquad i = a, R, 1, \ldots, 4.$$

The fluctuation-dissipation theorem relates ξ_i (friction coefficients) to the η_i (average magnitudes of the corresponding random forces) in the following way

Equation 2.11

$$\langle \eta_i(t)\eta_j(t')\rangle = 2\xi_i k_B T \delta_{ij}\delta(t - t').$$

The friction coefficients, ξ_i, in Equation 2.10 determine the time scale for the rotary motion of the c-ring and c-subunits. Additionally, the potential function, Ψ, is comprised of the following potential energy terms:

- nonbonded interactions between the proton binding sites and aArg210, U_{NB},

Equation 2.12

$$U_{NB} = U_{EL}(\vec{R}_{61L} - \vec{R}_{210}) + U_{EL}(\vec{R}_{61R} - \vec{R}_{210}) + U_{EL}(\vec{R}_{61L} - \vec{R}_{61R}) + U_{REP}(\vec{R}_{61L} - \vec{R}_{210}) + U_{REP}(\vec{R}_{61R} - \vec{R}_{210}) + U_{REP}(\vec{R}_{61L} - \vec{R}_{61R})$$

- hydrophobic interaction of the proton binding sites and the lipid bilayer, U_H,

Equation 2.13

$$U_H = H(|\vec{R}_{61L} - \vec{R}_{a4}|) + H(|\vec{R}_{61R} - \vec{R}_{a4}|)$$

- the proton-motive force that acts on the individual helices, U_{PMF},

Equation 2.14

$$U_{PMF} = \sum_{i=1}^{4} W_{c2}(\theta_i) + W_{a4}(\theta_R)$$

- and the torque, τ, generated by F_1 that acts on θ_a (F_O works against this load torque, and as a result, the ATP is synthesized).

Equation 2.15

$$\Psi = U_{NB} + U_H + U_{PMF} - \tau\theta_a ,$$

where, $\vec{R}_{61L}$, $\vec{R}_{61R}$, and $\vec{R}_{210}$ designate the positions of the critical residues on the helices hosting them, while $\vec{R}_{a4}$ represents the position of the $a4$ helix. W_{c2} and W_{a4} represent the proton-motive force for $c2$ and $a4$, respectively (the proton-motive force for each helix depends only on the orientation of that particular helix).

Finally, we have to define $U_{EL}(\vec{r})$, $U_{REP}(\vec{r})$, and $H(|\vec{r}|)$. $U_{EL}(\vec{r})$ represents the screened electrostatic potential explaining the interaction between charged residues, $U_{REP}(\vec{r})$ – the repulsive part of the Lennard-Jones potential (prevents the residues from getting too close

one to another), $H(|\vec{r}|)$ – smooth step function allowing the precise definition of range, d, and magnitude, S, of the interaction. The range and magnitude definitions are in place to prevent protons from binding to the binding sites which are away from the a-c interface.

Equation 2.16

$$U_{EL}(\vec{r}) = \frac{e^2}{4\pi\varepsilon_0\varepsilon}\frac{q_1 q_2}{|\vec{r}|}exp(-\lambda|\vec{r}|),$$

where q_1 and q_2 – charges of the residues; ε – dielectric constant of the protein environment; $1/\lambda$ – Debye screening length.

Equation 2.17

$$U_{REP}(\vec{r}) = \varepsilon_{vdW}\left(\frac{R_{min}}{|\vec{r}|}\right)^{12}.$$

Values for parameters R_{min} and ε_{vdW} in Equation 2.17 are based on the CHARRM (Chemistry at Harvard Molecular Mechanics) force field [205] and R_{min} is the size of the particle which represents the residue.

Equation 2.18

$$H(|\vec{r}|) = -q\frac{1}{2}\Delta G_H\left[tanh\left(S(|\vec{r}| - d)\right) + 1\right],$$

where ΔG_H specifies the free energy penalty (dielectric barrier) discussed in the previous section. If the deprotonated aspartate is exposed to the hydrophobic region of a lipid membrane, it will cause a free energy penalty of $\sim 45 k_B T$.

Note: *Equations 2.9 through 2.18 are reprinted from Biophysical Journal, 2004 with kind permission from Elsevier* [10].

The model described above directly relates the atomistic structure and dynamics of the F_O to the stochastic model. All geometrical parameters are determined after the analysis of the MD simulation of F_O.

Based on this model, the two c-subunits are exposed to the a-subunit at the same time (two cAsp61 residues participate in proton transfer at a time). One of the cAsp61 residues is in contact with the inlet half-channel (protonation of cAsp61), while the second one is in contact with the outlet half-channel (a proton dissociates to the mitochondrial matrix). To relate this to Figure 2.2, the binding site at $c2_R$ is exposed to the inlet half-channel, connecting aAsn214 and the mitochondrial inner-membrane space, and, at the same time, $c2_L$ is exposed to the aSer206, which is connected with the mitochondrial matrix by the outlet half-channel. The primary function of positively charged aArg210, which is located between aSer206 and aAsn214, is to act as a gate and prevent the direct proton transfer between the inlet and outlet half-channel. It is in the perfect position to lead the protons to and from the proton binding sites. It is clear from here that any point mutation on residues in close vicinity of three critical residues on a-subunit (aSer206, aAsn214, and aArg210) will disrupt the proton transfer patterns.

Finally, Figure 2.3 represents the sequence of events proposed by this model. The detailed explanation of events during protonation/deprotonation of cAsp61 are given, but we still have to investigate the proton pathways to and from the proton binding sites.

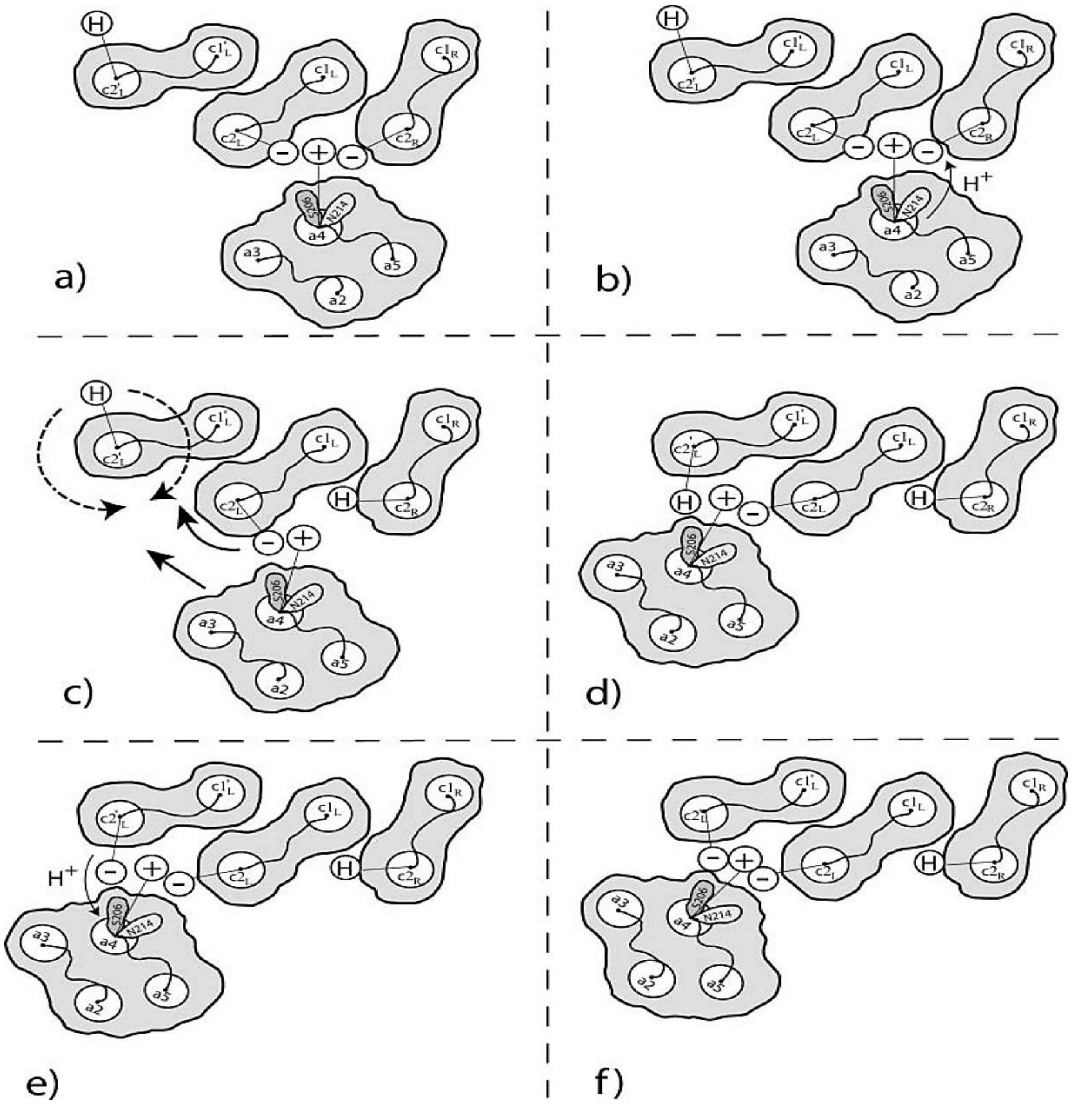

Figure 2.3 Schematic representation of the sequence of events suggested by Schulten *et al*. These events, labeled a-f occur during the rotation of c-ring by a $2\pi/10$ degrees in the synthesis direction, viewed from the mitochondrial matrix (the exact same events will occur in a case of 12 c-ring helices). (a) In the starting configuration, two residues cAsp61 are deprotonated and form a bidentate salt bridge with aArg210, $cAsp61^{\ominus} - aArg210 - cAsp61^{\ominus}$.(b) A proton is transferred from the terminal residue of the inlet half-channel, aAsn214, to cAsp61 on the helix $c2_R$. (c) Subunit a rotates clockwise with respect to the c-ring in concert with a clockwise rotation of the helix $c2_L$. When subunit a approaches helix $c2_L{}'$, cAsp61 on that helix rotates by 180°. The latter rotation may proceed in either clockwise or counterclockwise direction. (d) The concerted rotation of subunit a and helix $c2_L$ are completed: cAsp61 on the helix $c2_L{}'$ has rotated by 180° toward subunit a. (e) A proton is transferred to the terminal residue of the outlet half-channel, aSer206. (f) The system returns to the starting conformation (a), but with the c-ring advanced by an angle $2\pi/10$. We note that the processes depicted are of stochastic nature, and, hence, do not necessarily obey the strict sequence shown. (Reprinted from *Biophysical Journal, 2004* with kind permission from Elsevier) [10]

2.3 Aqueous Proton Access Pathways in F_o Motor

Over the past decade, the scientific community has investigated the physical mechanism of ATP synthase, with a primary focus on either MD calculations and mathematical models, or purely experimental work. Fillingame *et al.* performed extensive experimental investigations on the topography and function of a-subunit [55, 76, 118, 119, 121, 122, 127, 132, 133, 138, 139, 206].

To date, the complete three-dimensional structure of subunit a does not exist, but rather only fragmentary information is available. From the literature, we know that five transmembrane helices are spanning the membrane in the case of *E. coli*. The four helices (aTMH2, aTMH3, aTMH4, and aTMH5) pack tightly in a four-helix bundle on the periphery of the c-ring and host the critical residues involved in proton transfer and consequently the synthesis of ATP. The critical residues involved in proton transfer are aArg210 (regulates the proton flow from the inlet half-channel to the proton binding site and from the proton binding site to the outlet half-channel), aAsn216 (the terminal residue of the inlet half-channel), and aSer206 (the terminal residue of the outlet half-channel). All three are part of the aTMH4 that is directly exposed to the cTMH2, which hosts the proton binding site cAsp61. The presence of the polar residues within the a-subunit suggests the possible position of the two half-channels involved in proton translocation.

Rastogi and Girvin [57] reported via NMR spectroscopy (nuclear magnetic resonance), a solution structure of ac_{12} complex, the same model we used in this study. They reported a set of polar residues within the a-subunit – the list includes aGln252, aAsn214, aAsn148,

aAsp119, aHis245, aGlu219, aSer144, and aAsn238 (Gln – glutamine; His – histidine; Glu – glutamate). All listed residues are positioned between the critical aArg210 and the mitochondrial inner-membrane space. Since the inner-membrane space represents the basic reservoir, one can argue that these residues are involved in proton transfer via the inlet half-channel. The list of the polar residues between aArg210 and the mitochondrial matrix is reported as well and includes aSer206, aLys203, and aSer 159 (Lys-lysine). Additionally, in this same region (oriented towards the a-subunit), c-subunits host the following polar residues, cGln52 and cThr51 (threonine) on one subunit, and cArg50 on another c-subunit. The position of listed residues indicates that they may be involved in proton transfer via the outlet half-channel.

Fillingame and his group created cysteine carrying strains of the a-subunit by mutating the polar residues (previously identified as well as neighboring ones) [119, 120, 133]. Cysteine was substituted in a continuous stretch of residues at position 206 through 224 on aTMH4. N-ethyl-maleimide (NEM) and Ag^+ were used as probes of aqueous accessibility of cysteine substituted aTMH4 mutants. NEM reacts with the ionized thiol group, and residues reactive to NEM are assumed to reside in a polar aqueous accessible environment. The thiol group ($R-SH$) is a side chain in cysteine. Ag^+ is believed to react with the thiol group as a Lewis acid (it can accept a pair of electrons) and form a covalent bond. Ag^+ has an ionic radius resembling the ionic radius of the H_3O^+ and Na^+, making it an ideal probe for proton or sodium access channels.

The experimental results show that aSer206, aArg210, and aAsn214 are highly reactive to NEM, while the Ag^+ sensitive cysteine substitutions are also found in aTMHs

2, 3, and 5. Aside from aSer206 and aAsn214, aMet215 (methionine) and aGly218 (glycine) exhibited a high sensitivity to the Ag^+ probe. Considerably less sensitive residues to the Ag^+ probe include aTyr216, aAla217, aGlu219, aLeu220, and the continuous stretch of residues extending from position 214 through 220. Figure 2.4 lists all residues within the a-subunit that are sensitive to the Ag^+ probe.

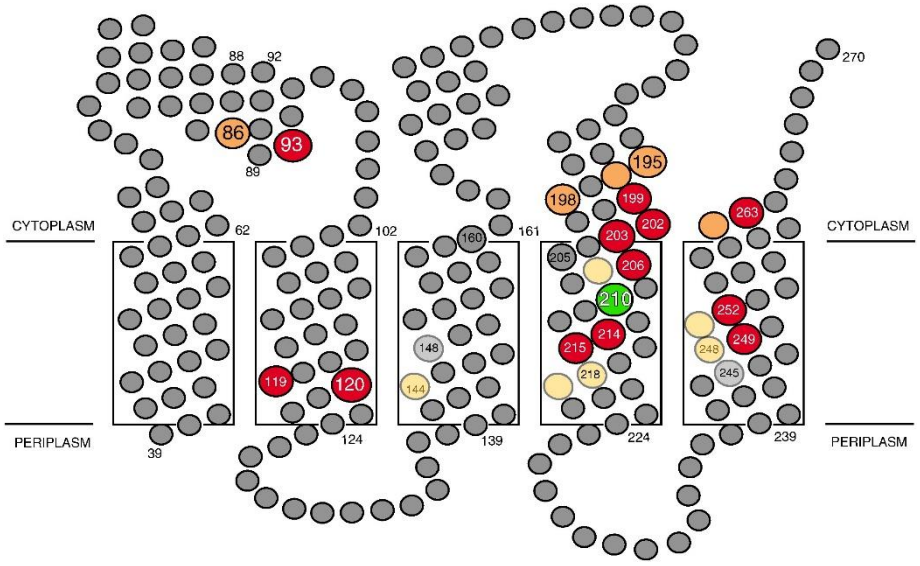

Figure 2.4 The experimental results with locations of the Ag^+ sensitive cysteine substitutions. The most sensitive residues are highlighted in red (>85% inhibition) and some of the more moderate sensitive residues are highlighted in orange (66-85% inhibition). The predicted topology of a-subunit (*E. coli*) transmembrane helices 1-5 are shown in boxes within the lipid bilayer. (Reprinted from *BBA-Bioenergetics, 2014* with kind permission from Elsevier) [207]

The most Ag^+ sensitive residues constitute an Ag^+ accessible pocket within the a-subunit bridging the space between aTMH4 and aTMH5. This aqueous pocket, referred to as the 'Fillingame pocket', is located close to the inner-membrane space. Utilizing MD, we examined if indeed this aqueous pocket exists.

2.3.1 Role of Subunit a in Proton Translocation

Detailed experimental and theoretical studies agree on the importance of the a-subunit within the F_O portion of the ATP synthase. As we previously discussed, it is positioned on the periphery of the c-ring and represents the stator, while the c-ring is the rotor of the F_O motor. The three residues to play a critical role in proton transfer are hosted in transmembrane helix four of the a-subunit. Two of them are terminal residues of the inlet and outlet half-channels, aAsn214 and aSer206, respectively. The third one is the conserved arginine at position 210 that acts as a gate regulating the transfer of protons to and from the proton binding sites on the c-ring. It is safe to state that, not only that the a-subunit is providing the pathways for protons to take while being translocated from the inner-membrane space to the mitochondrial matrix, but it also prevents protons from traveling through the membrane without protonating the critical residues on the c-ring.

In the previous three sections of this dissertation, we provided a detailed analysis of the a-subunit's function. The polar residues comprising the a-subunit are suggested to play a crucial role in proton transfer and half-channel formation. The experimental results from the Fillingame group identify the amino acids within the stator comprising the aqueous paths that protons may take during translocation (*cf.* Figure 2.5). To date, we know the detailed mechanisms of protonation/deprotonation of the cAsp61 residues, but how the protons span the length of the half-channels is still somewhat unclear.

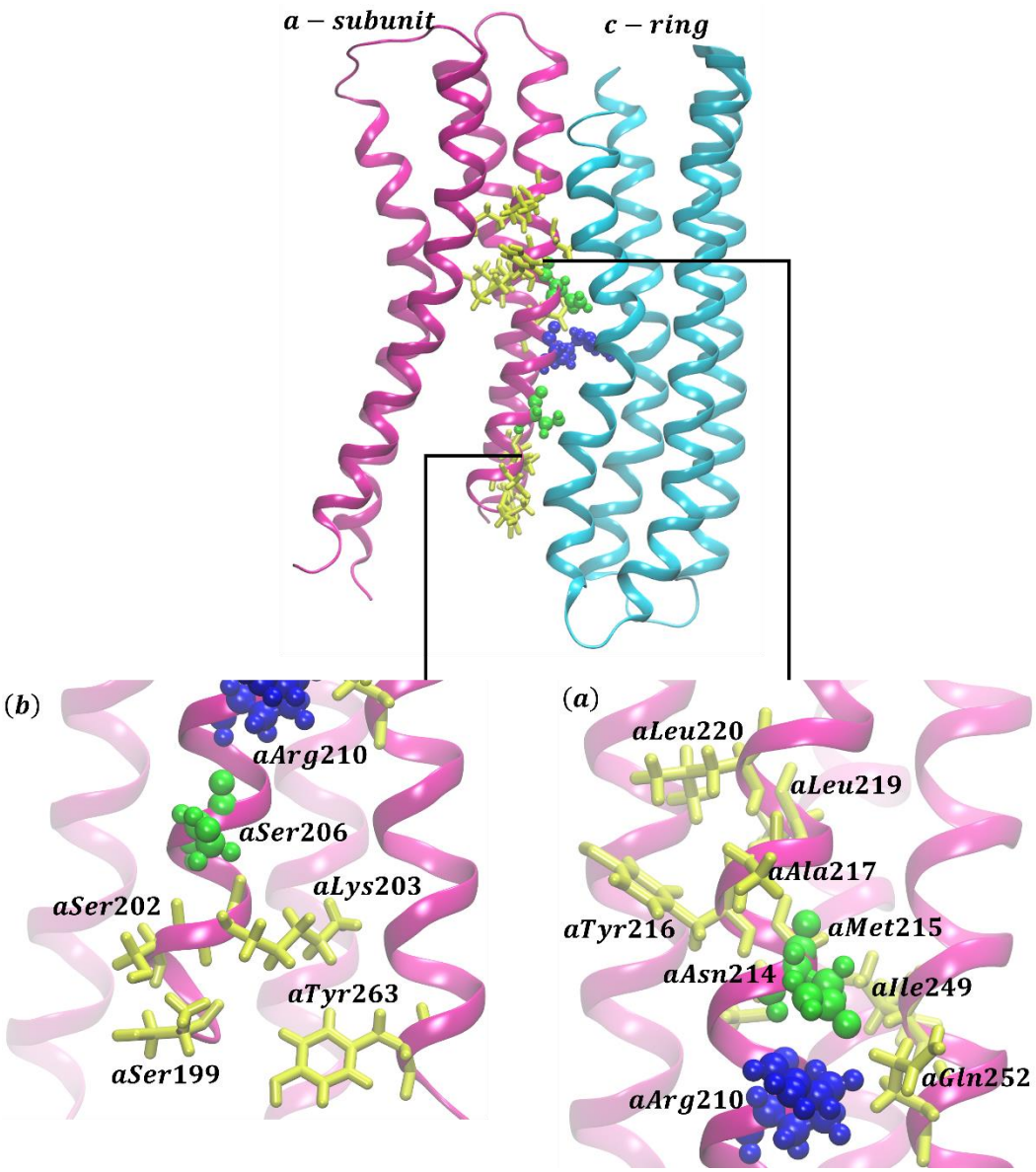

Figure 2.5 3D graphical representation of polar residues within the a-subunit that reported sensitivity to Ag^+ and NEM. The c-subunit is represented in cyan while the a-subunit is in magenta. Critical aArg210 (blue) and terminal residues of the inlet (aAsn214) and outlet (aSer206) half-channels (green) are represented in CPK style. These residues are sensitive to both the Ag^+ and NEM probes. Additional residues sensitive to the Ag^+ probe are represented in yellow color using Licorice style rendering (same as CPK but sphere radius the same as a bond). (a) Zoomed in (view from the center of the c-ring) on residues close to the inlet half-channel. Labeled residues are believed to create an aqueous pocket that spans aTMHs 4 and 5. aMet215 is located behind aAsn214. (b) Close view of Ag^+ sensitive residues in the outlet half-channel (view from the center of the c-ring).

2.3.2 Role of the Water in Proton Transfer

The proton translocation within the F_O requires protons to be moved over the distance of the inner mitochondrial membrane thickness. In order for this process to happen, the proton will have to take many elementary transfer steps, and the path it takes must structurally support this transfer. Based on experimental results, the polar residues involved in the structure of a-subunit, together with water, help facilitate this transfer. The proton is generally considered to be present in water as hydronium, H_3O^+, with size and solvent characteristics similar to the sodium ion. It exhibits the diffusive properties similar to the sodium ion with a diffusion coefficient in the range between the coefficients for sodium ion and water, $D_{Na} = 1.33 \times 10^{-5}\ cm^2 s^{-1}$ and $D_{H_2O} = 2.3 \times 10^{-5}\ cm^2 s^{-1}$ [208].

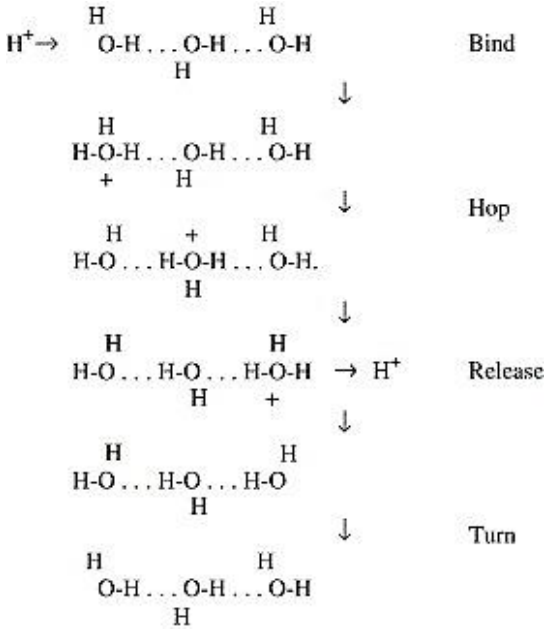

Figure 2.6 Grotthuss mechanism. Step-wise transfer of protons in bulk water. (Reprinted from *BBA-Bioenergetics, 2016* with kind permission from Elsevier) [208]

The Grotthuss mechanism (structural diffusion) explains the rapid transfer of protons between H_3O^+ and water, which transfers protonic charge without diffusive movement of H^+ or oxygen atom (*cf.* Figure 2.6). This process is fast and efficient, and is responsible for approximately 85% of the apparent ionic motility of protons in water. Additionally, this mechanism is only clear at an atomic level [209-214]. Based on this mechanism, the proton transfer in bulk water occurs in a step-wise manner, and it is an incoherent process.

Inside the low dielectric environment of the protein, a proton will travel a long distance, which requires reorganization of charge involving substantial electrostatic and reorganization cost at each step. The additional desolvation penalty (also primarily electrostatic) exists if the proton originates in the bulk phase. In this structured medium (solvated protein in a lipid membrane), the proton wires are an appropriate way of proton transfer (Figure 2.7). Proton translocation within the low dielectric medium of a protein must overcome the electrostatic cost of bringing the charge into the lower dielectric medium. Covalent association of the proton with carrier groups and the hydrogen-bonding between them will substantially diminish this electrostatic barrier.

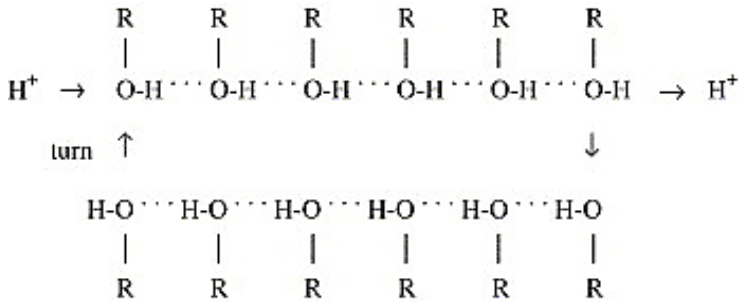

Figure 2.7 Proton wire. Step-wise transfer of protons inside the protein environment utilizing the hydrogen-bond chain. (Reprinted from *BBA-Bioenergetics, 2016* with kind permission from Elsevier) [208]

The rate of the proton wire transfer can be as fast as the structural diffusion in bulk water with transfer times of one picosecond between sites. The polar residues comprising the subunit a satisfy the structural requirement for proton transfer, and aqueous half-channels confined within the area of these residues provide the proton solvation medium. The speed of proton transfer depends on the proximity to the point of hydrogen-bond formation.

2.4 Hydrogen – Bond Network Formation

A hydrogen-bond is an attractive electrostatic (Coulombic) interaction between a hydrogen atom, which is a part of a molecule, and an atom (or group of atoms) in the same or a different molecule. In other words, when a partially positively charged hydrogen atom attached to a highly electronegative atom (nitrogen, oxygen, chlorine, or fluorine) is near another electronegative atom, the hydrogen-bond is created. The hydrogen-bond between two groups XH and Y is usually denoted by $X-H\cdots Y$. It is a type of dipole-dipole interaction and can occur between different parts of the same molecule (intramolecular) or between different molecules (intermolecular). Besides being reasonably strong, hydrogen-bonds are also somewhat directional, and this makes them appear like weak covalent bonds.

The length of the hydrogen-bond (in $X-H\cdots Y$, the distance between X and Y) ranges from 2.7 to 3.3 Å, with 3.0 Å being the most common value for protein and water hydrogen-bonds [215]. The energy of a hydrogen-bond is somewhat stronger than a van der Waals interaction ($\sim 1\ kJ/mol$) and weaker than fully covalent or ionic bonds ($\sim 500\ kJ/mol$).

The strengths of most of the hydrogen-bonds range between 10 and 40 kJ/mol, and they tend to follow a $1/r^2$ distance dependence [216]. Furthermore, the additional important determining factor for the strength of the bond is the angle the bond forms (the $X - H \cdots Y$ angle). The bond is stronger if closer to its correct geometry.

Hydrogen-bonds occur in inorganic molecules (*e.g.*, water) and organic molecules (*e.g.*, proteins and DNA) as well as in a nonpolar environment. Consequently, hydrogen-bonds are particularly crucial in macromolecular and biological assemblies (proteins, DNA). Hydrogen-bonds in biological systems are almost always weak, with bond energies below $20\ kJ/mol$. They are highly significant in terms of contribution to the stability of the protein. Most of the time, hydrogen-bonds within the protein occur in networks with water mediating. Water can be both an acceptor and a donor of hydrogen-bonds. These networks are essential in transporting protons within the proton-powered molecular motors. The hydrogen-bonding network formed between water and polar amino acids will allow the protons to transfer via a proton wire. Additionally, the network created between water molecules will allow the protons to transfer via the structural diffusion mechanism.

We believe that proton translocation within the F_O uses a combination of these two mechanisms utilizing the hydrogen-bonding network. The main reason behind this claim is that cavities are filled with water within the a-subunit.

2.5 Protein Structure Network – Elastic Network Model

The structural communication in biomacromolecules is investigated by borrowing concepts and methods from graph theory. This graph-based approach is defined as a protein structure network (PSN); it computes network features and shortest communication pathways on an ensemble of structures derived from the MD simulations. The concept of PSN has been explored with more care recently since it provides insights into the global properties of protein structure [217, 218]. The protein structures are represented as a network of interactions between residues within the protein and were proven to be extremely useful in studying the protein folding and prediction of functionally important residues in biomolecules. Therefore, PSN contributes to resolving the issue of intramolecular and intermolecular communications.

PSN is constructed based on the work of Vishveshwara *et al*. [219, 220], where each amino acid residue is represented as a node. Edges connect the nodes based on the strength of non-covalent interactions between amino acids. Two nodes, i and j, are connected by an edge and the strength of interaction (I_{ij}) between them is evaluated as a percentage given by

Equation 2.19

$$I_{ij} = \frac{n_{ij}}{\sqrt{N_i N_j}} 100,$$

where I_{ij} is the percentage interaction between residues i and j; n_{ij} – number of atom-atom pairs between the side chains of residues i and j within a distance cutoff (default value is

4.50 Å); N_i and N_j are normalization factors for residues i and j. The normalization factors account for the differences in the size of the amino acid side chains and their inclination to make the maximum amount of contacts with other amino acids within the protein structure.

The recently developed elastic network model (ENM), in combination with PSN, provides unique insights into the structural and dynamics of complex biological systems, and prediction of functional motions of the system. ENM gives the coarse-grained representation of protein structure. If one is interested in investigating the collective dynamics of complex systems, ENM should be combined with normal mode analysis (ENM-NMA). The NMA technique is also coarse-grained and additionally describes the vibrational dynamics of protein complexes around an energy minimum [221, 222]. The protein structure is described by a reduced subset of atoms (usually C_α atoms), whose coordinates can be derived either from structure determinations (crystallography, NMR) or from MD simulations. The interactions between particle pairs are given by a single term Hookean harmonic potential [223]. Therefore, the simple Hamiltonian describes the total energy of the system in the following way

Equation 2.20

$$E = \sum_{i \neq j} k_{ij}(d_i - d_{ij}^0)^2 ,$$

where d_i and d_{ij}^0 are instantaneous and equilibrium distances between C_α atoms i and j, respectively, and k_{ij} is a force constant.

As an extension of the PSN analysis, one can calculate the shortest non-covalently connected path between two residues of interest in a single structure or a trajectory. The

path is calculated by combining PSN interconnectivity and residue correlated motions, as described by Gosh and Vishveshwara [224]. The search for the shortest path for each frame of the MD trajectory between pairs of nodes relies on Dijkstra's algorithm [225]. By dividing the number of frames containing the selected path by the total number of frames in the MD trajectory, one can calculate the frequency of each communication path. The frequency of each communication path helps the selection of the most meaningful ones.

Seeber *et al.* developed Wordom [221, 222], a user-friendly program aimed at fast manipulation and analysis of individual molecular structures and molecular conformation ensembles utilizing the mixed PSN-ENM approach. A recent study demonstrated the advantages of this mixed PSN-ENM approach on a domain in its free state and together with a C-terminal peptide illustrating salient communication features within each system [226]. The benefits of this high-speed approach are well suited for high throughput investigation of the structural communication pathways including allosterism (change in the affinity for binding of a ligand or substrate that is instigated by the binding of another ligand away from the active site), in large biomolecular systems in different functional states [227].

Chapter 3 Computational Methods

3.1 Molecular Dynamics

Computational simulations are carried out in order to understand the properties of assemblies of molecules (structure and microscopic interactions). They serve as a complement to conventional experimental procedures. The two leading families of simulation techniques are molecular dynamics (MD) and Monte Carlo (MC). Moreover, a range of hybrid techniques, which combine features from both MD and MC, exists. Molecular dynamics provides a method to understand the static and dynamic properties of the molecular system and is one of the essential tools for modeling proteins, nucleic acids, and their complexes. It provides insight into the stability of a protein, folding of proteins, enzyme reactions, small and large scale conformational changes, and ion transport in biological systems. Additionally, MD is used for drug design, and determination and construction of three-dimensional structures of proteins. Most importantly, it allows one to gain insight into molecular mechanisms that are difficult or currently impossible to study experimentally.

MD simulates physical movements of atoms within the protein structure, using simplified models, and provides the individual trajectories. Numerical solutions of the classical equations of motion (Newton's equations) for a system of interacting particles determine the trajectory, and molecular mechanics force fields define the potential energy and forces between atoms.

There is a need to simulate large systems on the time scales relevant to those of natural processes, but they become more and more computationally expensive at longer timescales. For example, the size of the system and longer simulation timescales can require hundreds of CPU years. At this time, the typical length of an MD simulation is on the order of hundreds of nanoseconds and sometimes reaches microseconds. For a reference, Table 3.1 lists the timescales and associated ranges of biomolecular motions. The MD simulations presented in this dissertation were performed using the Nanoscale Molecular Dynamics (NAMD) program [228].

Table 3.1 Timescales and amplitudes of biomolecular motions

Timescale	Amplitude	Description
		Local Motions
$10^{-15} - 10^{-12}$ s	0.001 – 0.1 Å	• Atomic fluctuations (bond stretching, angle bending, dihedral motion) • Sidechain motions • Loop motions
		Rigid Body Motions
$10^{-12} - 10^{-9}$ s	0.01 – 10 Å	• Helix motions • Water relaxation • Collective subunit and domain motions (hinge bending, twisting)
		Large Scale Motions
$10^{-9} - 10^{-6}$ s	1 – 100 Å	• Folding in small peptides • Helix-coil transitions • Dissociation/association • Ion transport
		Very Large Scale Motions
$10^{-6} - 10^{-1}$ s	10 – 100 Å	• Folding and unfolding • Ribosome synthesis

3.1.1 Theory of Molecular Dynamics Simulations

In this section, we will outline the concepts of classical MD simulations. During the molecular dynamics simulation, the atoms of a protein structure move according to the Newtonian equations of motion

Equation 3.1

$$m_\alpha \overrightarrow{\ddot{r}_\alpha}(t) = -\frac{\partial}{\vec{r}_\alpha} U_{total}[\vec{r}_1(t), \vec{r}_2(t), \dots, \vec{r}_N(t)], \quad \alpha = 1, 2 \dots N,$$

where m_α is the mass of the atom α with a position $\vec{r}_\alpha$. U_{total} is the potential energy that depends on atomic positions and, thereby, couples the motion of atoms [228]. This potential energy is represented through the MD force field function and parameters, and it is the most crucial part of the simulation. It must realistically represent the interaction between each atom, and be in the form of a simple mathematical function that is quickly calculated. However, the evaluation of the forces, $U_{total}[\vec{r}_1(t), \vec{r}_2(t), \dots, \vec{r}_N(t)]$, is extremely time-consuming. To speed up calculations, NAMD uses scalable spatial parallelism, a fast multipole algorithm, along with multiple time steps.

One can use spatial decomposition to divide the simulation space into rectangular regions called patches. The dimensions of a patch must be greater than the cutoff radius for nonbonded interactions. This way, the need for communication between non-adjacent patches is eliminated. Each patch is responsible for updating the coordinates of the atoms contained in that space. During the computation, a cluster of adjacent patches is assigned to each processor, and the amount of interprocessor communication is reduced.

At a long length scale, the effect of a charged particle (long-range electrostatics) is pooled with other charges and represented by a multipole expansion. Furthermore, this effect is expressed as a Taylor expansion [229]. The sequence of impulses is used to approximate the forces by partitioning the potential energy in the following way

Equation 3.2

$$U_{total}[\vec{r}_1(t), \vec{r}_2(t), \ldots, \vec{r}_N(t)] = U^{fast} + U^{slow} \ ,$$

and Equation 3.1 becomes

Equation 3.3

$$m_\alpha \overrightarrow{\ddot{r}_\alpha}(t) = \sum_n \delta t \ \boldsymbol{\delta}(t - n\delta t) \left(-\frac{\partial}{\vec{r}_\alpha} U^{fast}\right) + \sum_n \Delta t \ \boldsymbol{\delta}(t - n\Delta t) \left(-\frac{\partial}{\vec{r}_\alpha} U^{slow}\right).$$

This algorithm allows the more numerous slow long-range interactions to be computed less frequently [230].

3.1.2 NAMD and Molecular Dynamics Simulations

NAMD was designed for simulating large biomolecules and alongside with its sister molecular graphics program, VMD (visual molecular dynamics) [137], delivers an easy-to-use tool for calculating and visualizing molecular all-atom trajectories. The force field used by this program incorporates local interaction terms consisting of bonded interactions between two, three, and four atoms and pairwise interactions (electrostatic and van der Waals forces). The electrostatic force evaluation is quite computationally complex, but the

incorporation of particle mesh Ewald (PME) allows to take the full electrostatic interactions into account beyond the pairwise electrostatic cutoff.

The velocity Verlet integration method [231] advances the velocities and positions of atoms in time to reduce the computational cost. Additionally, a multiple time step scheme is employed to reduce the cost of evaluation of long-range electrostatic forces [232-234]. Local interactions are calculated at each time step, while the longer range ones are computed less often. The quickly varying short-range portion of the electrostatic interaction can be separated from a slowly varying long-range component using a smooth splitting function. One can perform calculations including only bonded interactions every step by employing an intermediate timestep for a short-range nonbonded interaction.

The input and output files for NAMD are almost identical to those used by, *e.g.*, CHARMM or AMBER [228]. Input includes coordinate and structure files, as well as energy parameter files. The output provides a binary trajectory file that can be visualized in VMD when loaded into the protein structure file.

To date, NAMD simulations may be carried out using the following options:

- Constant energy dynamics,
- Constant temperature dynamics via
  - velocity rescaling,
  - velocity reassignment,
  - Langevin dynamics,
- Periodic boundary conditions,
- Constant pressure dynamics via

- Berendsen pressure coupling,
- Nosé-Hoover Langevin piston,

- Energy minimization,
- Fixed atoms,
- Rigid waters,
- Rigid bonds to hydrogen,
- Harmonic restraints,
- Spherical or cylindrical boundary restrains.

In the following section, we will give details about some of the listed dynamic parameters.

3.1.3 Force Fields and Standard Dynamics Parameters

For an all-atom MD simulation, we assume that every atom experiences a force that is specified by a model force field. The force field accounts for the interaction of that particular atom with the rest of the system and evaluating it is the most computationally demanding part of MD. The force is the negative gradient of the potential energy function

Equation 3.4

$$\vec{F}(\vec{r}) = -\nabla U_{total}(\vec{r}).$$

U_{total} sums over a large number of bonded and nonbonded terms. The bonded potential includes 2-, 3-, and 4-body interactions between covalently bonded atoms, while the nonbonded potential includes all-atom pair interactions (it usually excludes pairs of atoms already included in the bonded part)

Equation 3.5

$$U_{total}(\vec{r}) = \sum U_{bonded}(\vec{r}) + \sum U_{nonbonded}(\vec{r}).$$

The following equation gives the interactions between covalently bonded atoms

Equation 3.6

$$U_{bonded} = U_{bond} + U_{angle} + U_{dihedral}\,;$$

moreover, each part in Equation 3.6 describes the stretching, bending, and torsional bonded interaction.

Equation 3.7

$$U_{bond} = \sum_{bonds\ i} k_i^{bond}(r_i - r_{0i})^2,$$

Equation 3.8

$$U_{angle} = \sum_{angles\ i} k_i^{angle}(\theta_i - \theta_{0i})^2,$$

Equation 3.9

$$U_{dihedral} = \sum_{dihedral\ i} k_i^{dihedral}[1 + \cos(n_i\phi_i - \gamma_i)]\,, \quad n_i \neq 0,$$

where:

- $bonds$ count of each covalent bond in the system;
- $angles$ represent the angles between each pair of covalent bonds sharing a single atom at the vertex, and
- $dihedral$ represents the atom pairs separated by precisely three covalent bonds where the central bond is subject to the torsion angle ϕ (*cf.* Figure 3.1).

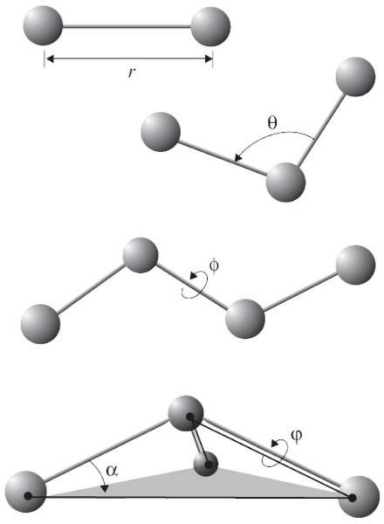

Figure 3.1 Internal coordinates for bonded interactions. r governs bond stretching; θ represents the bond angle term; ϕ gives the dihedral angle; the small out-of-plane angle α is governed by the so-called 'improper' dihedral angle φ. (Reprinted from *Journal of Computational Chemistry*, *2005* with kind permission from Wiley) [228]

The following equation represents the interactions between nonbonded atom pairs

Equation 3.10

$$U_{nonbonded} = U_{vdW} + U_{Coulomb},$$

where U_{vdW} corresponds to the van der Waal's forces approximated by a Lennard-Jones 6-12 potential

Equation 3.11

$$U_{vdW} = \sum_{i} \sum_{i>j} 4\varepsilon_{ij} \left[\left(\frac{\sigma_{ij}}{r_{ij}} \right)^{12} - \left(\frac{\sigma_{ij}}{r_{ij}} \right)^{6} \right].$$

The Lennard-Jones potential involves the weak dipole attraction between distant atoms and strong repulsion as the atoms come close one to another. It approaches zero rapidly as r_{ij} increases. Furthermore,

Equation 3.12

$$U_{Coulomb} = \sum_{i} \sum_{i>j} \frac{q_i q_j}{4\pi\varepsilon_0 r_{ij}}$$

represents the electrostatic, Coulomb, interactions.

Van der Waal's and Coulomb interactions exist between every nonbonded pair of atoms, and computing the long-range interaction precisely is unachievable since the space extends infinitely. In NAMD, the van der Waal's and electrostatic interactions are spatially truncated at a cutoff distance (specified by user); the particle mesh Ewald (PME) method is employed to account for long-range electrostatic interactions for simulation using periodic boundary conditions, and an analytical correction is used to account for truncated van der Waals interactions.

For a spatially limited system with periodic boundary conditions, Ewald summation accounts for the long-range electrostatic interactions [235]. The result of the summation depends on the order of Ewald summation; it is specified in the following way: sum over each periodic box first, and then sum over spheres of boxes of increasingly larger radii [232, 236-240]. NAMD uses smooth PME as a fast numerical method for full electrostatic computations. This feature of NAMD is used to compute the transmembrane electrostatic potentials from first principles averaged over an MD trajectory [241]. Besides, it replaces the previously used empirical potentials (*e.g.*, those derived from Poisson-Boltzmann theory).

Biological systems (*e.g.*, a solvated protein within the lipid bilayer) are chaotic and often require millions of time steps. The goal of biomolecular simulations is a proper

sampling of phase space. For constant energy simulation (NVE ensemble), NAMD utilizes the Verlet method [231]. The position and velocity at the next time step (r_{n+1}, v_{n+1}) are obtained from the current time step (r_n, v_n), assuming that the force, F_n, at that step is already computed. The following equations provide an order of computation using the velocity-Verlet method:

Equation 3.13

$$v_{n+\frac{1}{2}} = v_n + \frac{F_n}{M}\frac{\Delta t}{2},$$

$$r_{n+1} = r_n + v_{n+\frac{1}{2}}\Delta t,$$

$$F_{n+1} = F(r_n),$$

$$v_{n+1} = v_{n+\frac{1}{2}} + \frac{F_{n+1}}{M}\frac{\Delta t}{2},$$

where M is the mass. To conserve energy in the NVE ensemble, it is suggested to use $1fs$ to $3\ fs$ time steps. Usually, for NVT and NPT ensemble simulations, the time steps range from $2fs$ to $6fs$ for rigid bonds and $1fs$ to $4fs$ without rigid bonds [228]. The Langevin equation is used to generate the Boltzmann distribution for canonical (NVT) ensemble simulations, whereas for the NPT ensemble, constant pressure is simulated using a modified Nosé-Hoover method (Langevin dynamics is used to control fluctuations in barostat). This method is called the Nosé-Hoover Langevin piston [242].

In this section, we outlined the essential features of MD (and NAMD). We utilized these while simulating our protein system.

Chapter 4 Methods

4.1 Molecular Dynamics Simulation Setup

In this dissertation, we utilized NAMD to simulate half-channel formation in the membrane bound part (F_O) of ATP synthase. The starting coordinates of the ac_{12}-complex are reported in PDB by Rastogi and Girvin with the code 1c17.pdb [57]. The structure of one c-subunit was determined using triple resonance NMR experiments at the temperature of $300K$ and pH values 5 and 8 [56]. The 1c17.pdb is a model whose coordinates are calculated by NMR structure determination methods only using published biochemical data as constraints. The initial structure is deprotonated with one of the c-subunits at the ac-interface spatially positioned to accept the proton. We used the PSF generator (protein structure file generator) in VMD [137] to mutate the residue cAsp61 to its protonated form. According to the literature, one c-subunit is deprotonated while the rest of them are protonated (cAsp61 is neutralized to avoid exposure of charged particle to the hydrophobic membrane enviroment). Due to its spatial orientation, the c-subunit on the position L is the one whose cAsp61 is deprotonated (Figure 4.1). Visualizing the new, protonated, structure in VMD, we confirmed that indeed, oxygens on the side chains were protonated as shown in Figure 4.1. One of the possible problems during the protonation of the proton binding sites is that an improper definition of the dihedral angles for the protonated ASP can occur. In our case, during the first $100\ ps$ of energy minimization, the hydrogen swings back to

the carbon and creates new covalent bonds with both oxygens as well as with the C_γ. This problem is fixed by regenerating the dihedrals on the protonated form of ASP.

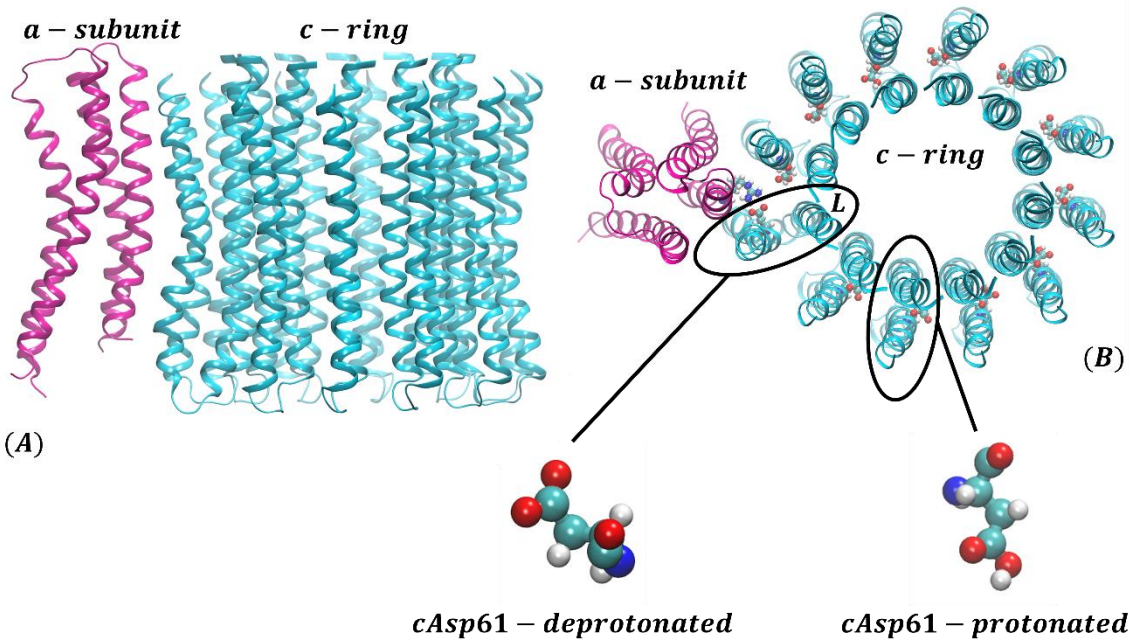

Figure 4.1 ac_{12} complex. (A) The new cartoon representation of the ac_{12} complex (side view). (B) The view from the mitochondrial inner-membrane space. Deprotonated (position L) and protonated (the remainder of the c-subunits) cAsp61 are in CPK representation.

The ac_{12} complex is placed in a $160 \times 120 \times 54$ Å^3 1-Palmitoyl-2-oleoyl-sn-glycero-3-phosphoethanolamine (POPE) membrane. The POPE membrane patch was built using the membrane builder extension in VMD. The polar headgroups of this lipid create viscous membranes, and this type of membrane is found in most of the biological membranes. The protein is aligned with the membrane, and overlapping lipid and water molecules within 0.6 Å and 0.3 Å, respectively, were removed. The lipid-protein system was then solvated by adding 2×30 Å of the TIP3P water patches on the planes of the membrane. During the

solvation of the system, water will be placed inside the lipid membrane and around the protein. The water molecules located in the membrane region must be removed. Finally, the protein-membrane-water system (Figure 4.2) is neutralized by adding sodium chloride in a concentration of $150\ mM/L$. The total size of the system was 196,939 atoms, and the simulation cell dimensions were set to $158 \times 120 \times 118\ \text{Å}^3$.

Aside from the wild-type F_O, we studied the two mutations, T8993C and T8993C. These two mutations correspond to replacing leucine at position 207 with proline and arginine, respectively. We used VMD to create mutated copies of the ac_{12} complex; we will refer to these two as L207P (T8993C mutation) and L207R (T8993G mutation). Both mutants were prepared for simulation in precisely the same way as the wild-type. The size of the each, L207R, and L207P mutant systems were 197,267, and 196,978 atoms, respectively. The same cell dimensions as for the ac_{12}-complex was used.

The all-atom MD simulations were performed using NAMD according to the described simulation protocol (details in the following section).

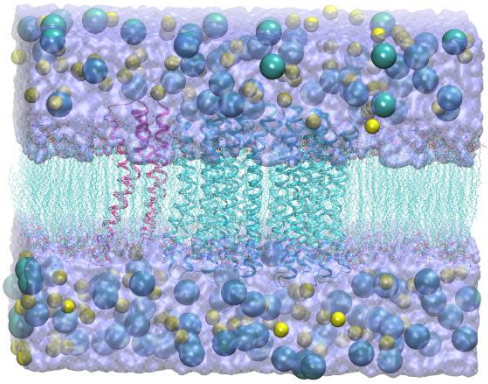

Figure 4.2. The final simulation system, including ac_{12}-complex, POPE membrane, water, and ions.

4.2 Simulation Protocol

All MD simulations were carried out in NAMD (version 2.10) with the CHARMM parameter file. Since we have put our system together by hand, it has many unnatural atomic positions. Before we were ready to run the system with full dynamics, we will performed a series of minimization and equilibration processes to bring the system to a more natural-like configuration.

4.2.1 Melting of Lipid Tails

Since we are using the membrane patch that had not been equilibrated, first we had to perform a simulation in which everything (water, ions, protein, lipid headgroups) except lipid tails are fixed. This process is known as melting lipid tails, and in this way, we induce the appropriate disorder of a fluid-like bilayer. The system is minimized for 10000 steps and gradually heated to $300\ K$ with increments of $10\ K$ and frequency of 10000-time steps. The time step we used throughout MD simulations is two femtoseconds. During the gradual heating process, while increasing temperature by ten Kelvin, we let the system equilibrate for 20 picoseconds between each increment. After reaching the desired temperature, the system is equilibrated for five nanoseconds in the canonical ensemble (NVT). The canonical ensemble is one in which the number of particles, volume, and temperature are conserved. The temperature was controlled by rescaling the velocities. The frequency of trajectory recording is two picoseconds.

4.2.2 Minimization and Equilibration with Protein Constrained

After the lipid tails relaxed to the more natural configuration (they will look disordered), minimization and equilibration with harmonic restraint only on protein are performed in the NPT ensemble. The minimization process guides the system to the nearest local minimum in the configuration space. Minimization is followed by equilibration with protein constrained to permit the environment to relax further. We want lipids to pack well around protein to achieve close to natural configuration. Minimization and equilibration differ from each other by the nature in which the MD force field is utilized. Energy minimization involves searching for a local minimum (the place in which the molecule is relaxed), by systematically varying the positions of atoms and calculating the energy. Equilibration involves MD whereby Newtonian equations of motion are solved for each atom in the system to dictate its trajectory. Judging how well, for example, velocities and pressure are distributed in the system throughout simulation time, we can deduce if the equilibration is successful. During this step of computation, the system is minimized and then equilibrated for another five nanoseconds.

The NPT ensemble is an isothermal-isobaric ensemble where the number of particles, temperature, and pressure are constant. For this type of simulation, aside from thermostat (Langevin), a barostat is needed. We used the Nosé-Hoover Langevin piston (Langevin dynamics to control fluctuations in the barostat). For the lipid bilayer, pressure control occurs under constant membrane area or constant surface tension. This step will produce conditions in which lipids are well packed around protein.

The harmonic restraint on the protein is achieved by setting the spring constant, k, to 1 $kcal/mol/\text{Å}^2$. Using the equipartition function and a given spring constant, one can estimate how much will atoms move around their constrained positions. In our case, each atom will move approximately 0.77Å.

4.2.3 Equilibration with Protein Released

The constraints on the protein were released, and the system was again equilibrated for another five nanoseconds in the NPT ensemble. During previous steps, and in this step of equilibration, we let the area fluctuation in the $x - y$ plane to permit packing of lipids against the protein. Each time we changed something in the system (protein restrained or released), the system is first minimized and then equilibrated.

4.2.4 Production Runs

Finally, production runs for 300 nanoseconds were computed in NpAT ensemble (pressure control occurs under constant membrane area). After a good packing of lipids against protein is observed, we kept the area in $x - y$ plane constant. The effective area of the lipid in the system is computed as a checkmark for constant membrane area. This is achieved by computing the area of the protein and subtracting it from the area of the simulation cell throughout MD simulation.

Throughout the simulations, the particle mesh Ewald method [243] was used to treat long-range electrostatic interactions. The bond lengths involving bonds to hydrogen atoms were constrained with the SHAKE algorithm for hydrogen atoms [244]. The time step for all MD simulations was two femtoseconds, with a local interaction distance common to both electrostatic and van der Waals calculations cutoff of 12 Å. The temperature was controlled using the Langevin dynamics parameters with a damping coefficient of $5/ps$, and the Langevin temperature set to $300K$. The Nosé-Hoover Langevin piston pressure control [245, 246] was used to control fluctuations in the barostat with a Langevin piston decay of 100 fs. All three proteins (wild type, L207R and L207P mutants) were simulated in three replicas using random numbers as seed for generating velocities, and average trajectories were analyzed. The trajectories were recorded every two picoseconds.

4.3 Analysis Protocol

The snapshots of the MD trajectory were recorded every two picoseconds. VMD with scripts developed in-house was used for the analysis of all trajectories. In the analysis of hydrogen-bonds, a hydrogen-bond was defined using the following geometric criteron, a donor (D) – acceptor (A) distance of ≤ 3.0 Å and the angle $D - H \cdots A$ less than 20 degrees (a perfect hydrogen-bond occurs at an angle of zero degrees). The protein network path analysis was done using the Wordom program [221, 222]. Wordom combines the PSN and dynamic cross-correlation method in a search for all shortest non-covalent communication pathways within the protein structure. The communication pathways are obtained by first,

calculating the extent of the correlation for amino acid – amino acid displacement along the trajectory, and then clustering. Molecular images were prepared using VMD.

4.4 Initial Analysis

One of the fastest initial analysis tools to check if the system is equilibrated is the root mean square deviation (RMSD). RMSD is a numerical measure of the distance between two structures (two snapshots of MD trajectory); it is defined as

Equation 4.1

$$RMSD_{\alpha}(t_j) = \sqrt{\frac{\sum_{\alpha=1}^{N_\alpha}\left(\overrightarrow{r_\alpha}(t_j) - \langle\overrightarrow{r_\alpha}\rangle\right)^2}{N_\alpha}},$$

where

Equation 4.2

$$\langle\overrightarrow{r_\alpha}\rangle = \frac{1}{N_t}\sum_{j=1}^{N_t}\overrightarrow{r_\alpha}(t_j)\ .$$

N_α is the number of atoms whose positions are compared, and N_t is the number of time steps over which atomic positions are being compared. $\overrightarrow{r_\alpha}(t_j)$ is the position of atom α at time t_j, $\langle\overrightarrow{r_\alpha}\rangle$ is the average value of the position of atom α to which the position $\overrightarrow{r_\alpha}(t_j)$ is being compared. The production phase of each simulation should be monitored by checking the system temperature and making sure it remains constant through the period of the MD simulation.

Chapter 5 Results

This chapter is organized in the following way. First, the results for each model are analyzed, and then they will be compared.

5.1 Wild Type ac_{12} Complex

The solvated protein/membrane systems were each simulated using NAMD for 300 nanoseconds. The all-atom MD simulations were performed on the Opuntia cluster at the Center for Advanced Computing and Data Science (CACDS) at the University of Houston.

'Opuntia contains 1,860 cores within 80 HP Proliant SL 230 compute blades (nodes), and 4 HP Proliant SL 250 Nvidia K40 GPGPU blades, 1 HP Proliant DL 380 login node. The system is also equipped with three large memory nodes – 1 HP Proliant DL 580 with 1 TB of main memory and 2 HP DL 560 each with 512 GB of main memory. Each compute node has 64 GB of memory, and the login/development node has 64 GB. The system storage includes a ~600 TB shared file system, and 85 TB of local compute-node disk space (~1 TB/node). Opuntia also provides access to eight nodes containing two NVIDIA GPU's, giving users access to high-throughput computing and remote visualization capabilities respectively. A 56 Gb/s Ethernet Mellanox switch fabric interconnects the nodes (I/O and compute). The cluster currently runs Rocks 6.1.1 and Red Hat Enterprise Linux 6.9.' (source https://www.uh.edu/cacds/resources/hpc/opuntia)

During the production runs, we used a two femtoseconds time step, and trajectories were recorded with a frequency of two picoseconds. As a consequence, each set of trajectories contained 150,000 frames (snapshots). The results were visualized in VMD, and the most representative member of all snapshots is shown in Figure 5.1.

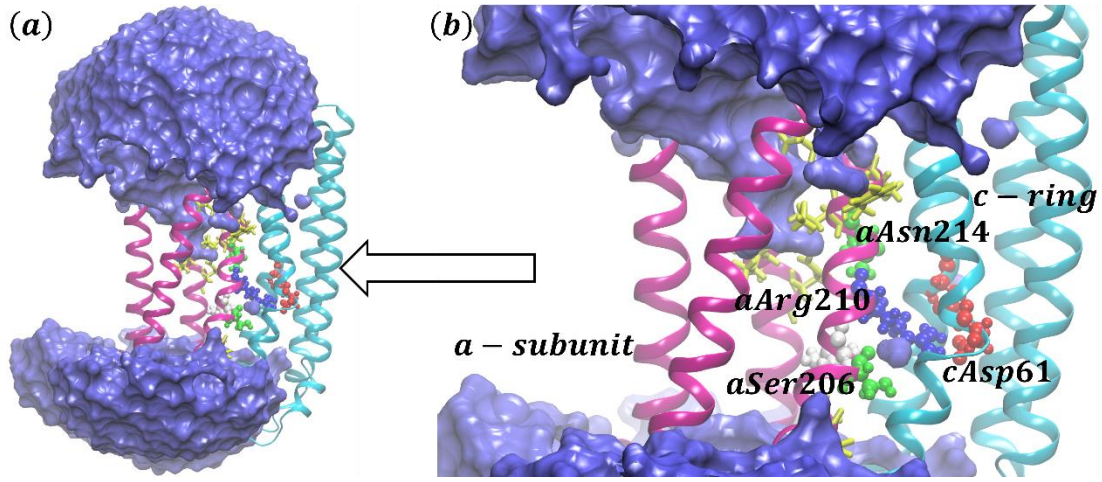

Figure 5.1 Wild-type ac_{12} after 300 nanoseconds MD simulation. (a) The representation of water accumulation within the a-subunit and ac-interface after MD simulation. Only the a-subunit and two of the c-subunits at the interface with the a-subunit are represented in order to simplify the figure. Water is shown in Surf representation and within 12 Å from the a-subunit. (b) The zoom in at the proton binding site. Critical residues directly involved in proton transfer are represented in CPK, and in addition, the residues identified by Fillingame and Steed [207] are shown in yellow licorice.

Since our system contains close to 200,000 atoms, we chose only to render molecular images depicting the a-subunit and the two c-subunits facing the subunit a. In this way, we will be able to render more detailed images. Additionally, this part of the protein plays a crucial role in proton transfer via the half-channels within the a-subunit. The a-subunit hosts the terminal residues of the inlet (aAsn214) and outlet (aSer206) half-channels, as well as aArg210, which plays an essential role in directing the protons to the outlet and

from inlet half-channel during the protonation and deprotonation of cAsp61. During the MD simulation, water accumulated within the a-subunit, submerging most of the residues experimentally identified by Fillingame's group as the ones positioned along the aqueous channels [55].

We believe that water spanning the distance between the inner-membrane space and terminal residue of inlet half-channel depicts one of the possible positions of the half-channel along which protons will move to the proton binding site. All of the polar residues that Fillingame and colleagues identified as sensitive to the Ag^+ probe in close proximity of mitochondrial matrix (aSer199, aSer202, aLys203, and aTyr263) are solvated. We believe that these amino acids indeed participate, together with water, in proton mediation to the mitochondrial matrix after it has been dissociated from the cAsp61.

Further, it is necessary to investigate the movement of the water molecules during the MD simulation period. We first investigated if the water molecules are moving from the upper side of the lipid bilayer to the lower side via the region that is considered to represent the proton binding site. The results showed that none of the water molecules traverse the inlet and outlet half-channels via the proton binding site. While visualizing trajectories of water around the a-subunit, we note one distinct pathway most of them take (*cf.* Figure 5.2). The black arrow is in the general direction of water movement and the proposed position of the inlet half-channel. Zooming into the proton binding region (Figure 5.2b), we note that some of the waters stay there for all 300 nanoseconds without moving across the lines in the plane of aAsn214 and aSer206. In Figure 5.2, we showed trajectories of some of the water molecules to keep the rendering image as clear as possible.

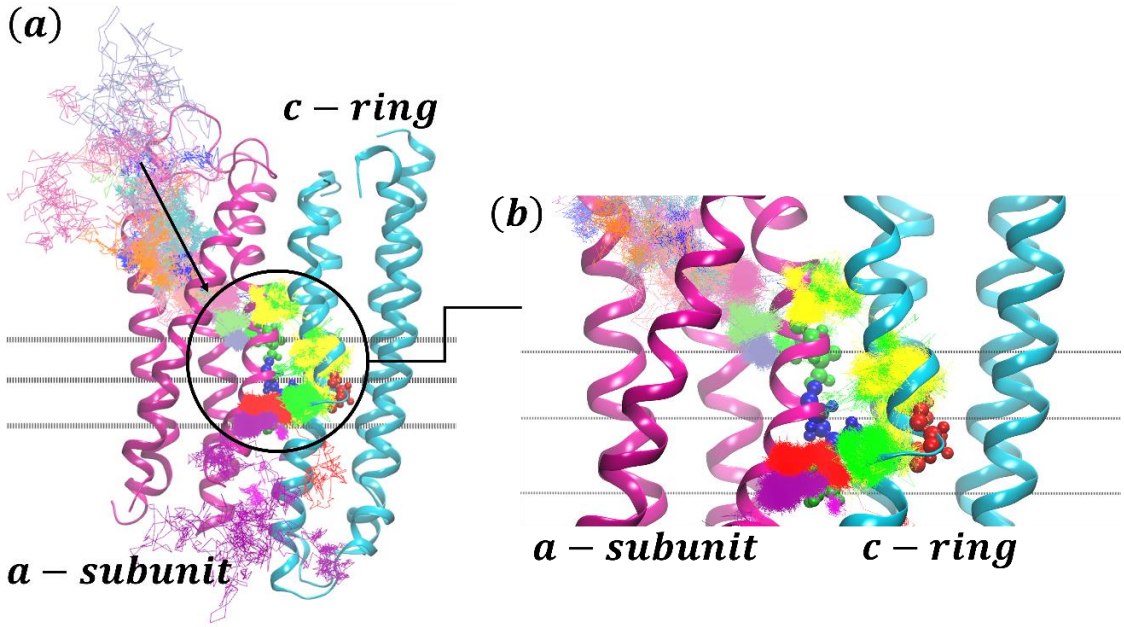

Figure 5.2 Water trajectories within ac-interface for wild type ac_{12}complex. (a) Some of the water molecules' trajectories within the proximity to the proposed inlet and outlet half-channels are represented. The black arrow indicates the possible position of the inlet half-channel. (b) View at the proton binding site. Black horizontal lines are in the plane of the terminal residue of the inlet half-channel (top line), outlet half-channel (bottom line), and in the plane of aArg210 (middle line).

Protein cavities are an excellent place for water molecules to nest in, but sometimes they will spend some time in one region and move to another. This may be due to the diffusive movement of water within the protein. To investigate how long water is nested within the particular areas of the a-subunit, we extracted the list of all of the waters that are within 3.2 Å of the particular residue, identified the residues and calculated the time they spend in contact. aSer206 and aArg210, the two residues directly involved in proton transfer (as reported by Schulten's group [10]), are in contact with a water molecule for 239 and 210 nanoseconds, respectively. Additionally, aTyr216 (184 ns), aAla217 (179 ns), aGlu219 (152 ns), and aLeu220 (187ns) all participate in a hydrogen-bond or are in contact with water. The total simulation time is 300 ns. It is important here to note

that all of the residues mentioned are reported to be sensitive to the NEM and Ag^+ probes as was experimentally confirmed before. This result furthermore supports our hypothesis that water mediates and promotes the proton transfer from the mitochondrial inner-membrane space and proton binding site, as well as from the binding site to the mitochondrial matrix. Moreover, we calculated how much time these residues are in a stable hydrogen-bond (results presented in Table 5.1). Namely, the time in contact represents the total time a water molecule spends within 3.2 Å from the residue.

Table 5.1 Contact and hydrogen-bond times

Residue	In contact with water (ns)	Time in hydrogen-bond (ns)
aArg210	210 (70%)	0
aSer206	239 (80%)	0
aTyr216	184 (61%)	33
aAla217	179 (60%)	90
aGlu219	152 (51%)	0
aLeu220	187 (62%)	0

The time of contact with water includes the time of how long they are in hydrogen-bond and the time water is in contact with residue but not in hydrogen-bond. Note: Reported times are for one water in contact with given residue.

Aside from creating hydrogen-bonds with protein residues, the hydrogen-bonding between water molecules occurs and thus creates the hydrogen-bond network, which we believe is utilized to promote proton transport. Further, we investigated hydrogen-bonds along the a-subunit; results are reported in Table 5.2. The hydrogen-bonds between residues and water were investigated utilizing the HBonds Plugin in VMD with the following parameters, a $D-A$ distance 3.0 Å and the angle $D-H\cdots A$ less cutoff 20 degrees.

Table 5.2 Polar residues along the a-subunit involved in hydrogen-bonds with water molecules

Residue	**Time (ns)**	**Spatial position**
aMet215	84 (28%)	inlet half-channel
aAla217	87 (29%)	
aTyr216	234 (78%)	
aLeu220	111 (37%)	
aGln252	93 (31%)	
aSer202	96 (32%)	outlet half-channel
aLys203	300 (100%)	
aTyr263	270 (90%)	
aSer199	300 (100%)	

All of the residues listed are experimentally proven to be sensitive to the Ag^{+} probe.

Our results are in agreement with experimental results reported by Fillingame's group [55, 119, 120, 133, 138, 139]. This furthermore supports our hypothesis that water is involved in proton transfer along the half-channels.

Now when we know which amino acids are communicating with water, we need to identify which amino acids are communicating between themselves. We utilized the Wordom package to identify the protein structure network paths over the $300\,ns$ trajectories. The program searches for the shortest non-covalent communication paths along the trajectory and gives the best representative from each communication cluster. The results of the residue-residue communication network are represented in Figure 5.3. There is a clear indication for the existence of the inlet half-channel involving aTMH4 and aTMH 4 and the water-filled area in between them. As we expected, the path is not directly down from the inner-membrane space to the proton binding site; instead, it seems somewhat similar to a random walk.

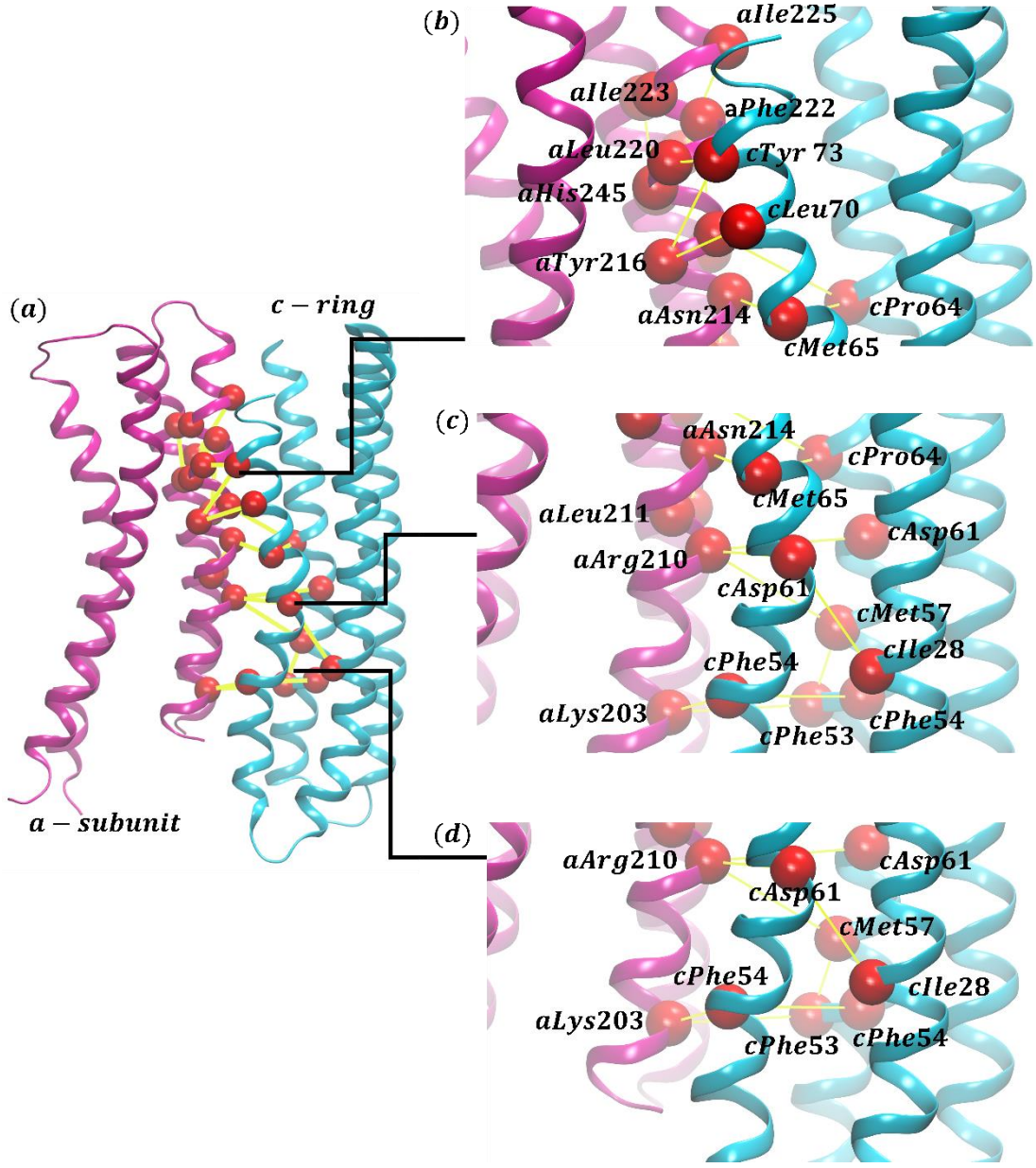

Figure 5.3 Amino acid - amino acid communication paths for wild type ac_{12} complex. (a) Side view of *ac*-interface. Communication paths along the (b) presumed inlet half-channel, (c) at the proton binding site, and (c) presumed outlet half-channel.

We note not only that residues within the a-subunit are part of the communication network, but some of the residues on the c-subunits (parallel to the a subunit) are as well. The two c-subunits represented in Figure 5.3 and involved in the protein structure network are the subunits that are being protonated or deprotonated at the same time during the proton transfer. Along the inlet half-channel, we can follow the communication network paths and propose a global path protons are most likely to take. As we expected at the proton binding site, the following communication takes place $aArg210 \Rightarrow cAsp61$ and $aAsn214 \Rightarrow cMet65$. Here we propose that the inlet half-channel involves the following amino acids: $aIle223 \Rightarrow aHis245 \Rightarrow aLeu220 \Rightarrow cTyr73 \Rightarrow aTyr216 \Rightarrow cLeu70 \Rightarrow cMet65 \Rightarrow aAsn215$. Methionine and tyrosine are part of this communication path even though they are amphipathic (they are both hydrophilic and hydrophobic) amino acids, but because of their location at the surface of the c-helix, they are classified as polar. Isoleucine and leucine are buried within the protein but at the location of the aqueous pool. The proximity of water to these residues creating hydrogen-bonding network promotes proton transfer. One can argue that proton transfer along the half-channels is the combination of structured diffusion and wire hopping. Additionally, we propose the outlet hall-channel along the following residues $cAsp61 \Rightarrow aArg210 \Rightarrow cMet57 \Rightarrow cPhe53 \Rightarrow aPhe54 \Rightarrow aLys203$. Again, water accumulated along this path will assist in proton translocation along this half-channel. To summarize, protons from the mitochondrial inner-membrane space take the proposed path along the inlet half-channel to the binding sites. At the binding site, a detailed sequence of events is outlined by Schulten's group [10]. After completing almost a full revolution, it dissociates from the cAsp61 and takes the outlet half-channel path to the mitochondrial matrix.

5.2 T8993C Mutant

The T8993C is the mutation in mtDNA on gene Atp6. This mutation causes the replacement of leucine at position 207 with proline on the a-subunit. From the reported experimental work [26, 27, 192, 247, 248], we know that this particular mutation will affect the synthesis of ATP in a way that it will slow down to less than 25%. Additionally, it will slow down the proton translocation by 30%. This particular mutation is reported to be involved with MILS. Further, in the text, we will refer to this mutant as L207P.

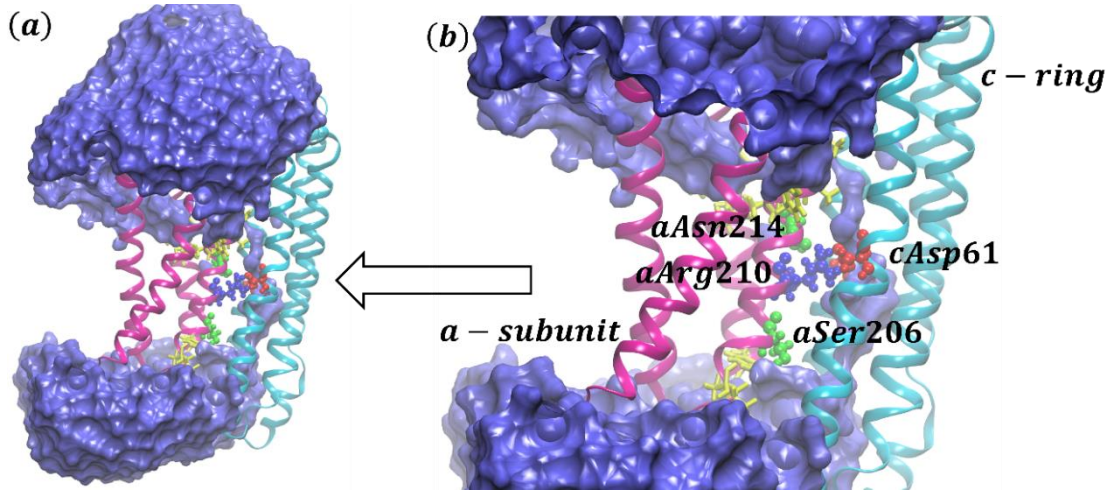

Figure 5.4 The L207P mutant after 300 nanoseconds MD simulation. (a) The representation of water accumulation within the a-subunit and ac-interface after MD simulation. Only the a-subunit and two of the c-subunits at the interface with the a-subunit are represented in order to simplify the figure. Water is shown in Surf representation and within 12 Å from the a-subunit. (b) The zoom in at the proton binding site. Critical residues directly involved in proton transfer are represented in CPK, and in addition, the residues identified by Fillingame and Steed [207] are shown in yellow licorice.

After analyzing and visualizing the trajectories produced by the 300 nanosecond all-atom production runs, we selected the most populated trajectory frame representative and visualized it in VMD (Figure 5.4). We note water accumulation in between the two c-subunits; for the proper working $F_{O,}$ water in this region was absent. Further investigation into the source of these water molecules revealed that most of it nested in that region during the equilibration phase of the MD simulation. Additionally, we investigated whether some of these waters will cross the lines bounding the proton binding site. The lines bounding the proton binding site are in the horizontal plane comprised of aAsn214 and aSer206.

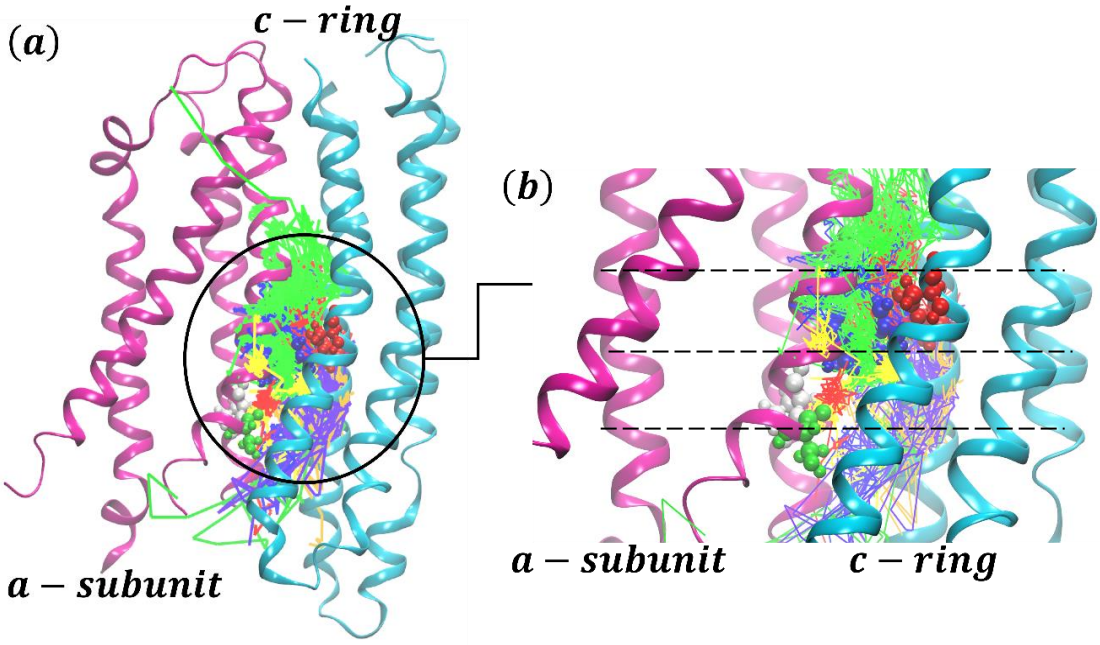

Figure 5.5 Water trajectories within ac-interface for the L207P mutant. (a) Some of the water molecules' trajectories within the proximity to the proposed inlet and outlet half-channels are represented. (b) View at the proton binding site. Black horizontal lines are in the plane of the terminal residue of the inlet half-channel (top line), outlet half-channel (bottom line), and in the plane of aArg210 (middle line).

A total of 30 water molecules moved to span the distance between the horizontal planes centered on aArg210, aAsn214, and aSer206. The trajectories for some of these events are represented in Figure 5.5. Once these crossing events occur, water is merely residing there. Analyzing the contacts between this water and amino acids nearby, we determined that cAsp61 on both c-subunits are in contact with water for $243\ ns$ and $161\ ns$ (81% and 53%), respectively. The residue that is longest in contact is the one at the position to get protonated (visible in Figure 5.5 and represented in red CPK). Additionally, aArg210 is in constant contact with water during the entire simulation time, and cGly69 is solvated for 67% of the simulation time. All of the three residues hosted by the c-subunit are involved in hydrogen-bonds for about 30% of the simulation time. During the same time, aArg210 is in a hydrogen-bond with water as well.

Table 5.3 The L207P mutant hydrogen-bonds with water molecules

Residue	**Time (ns)**	**Spatial position**
aMet215	75 (25%)	inlet half-channel
aAla217	96 (32%)	
aTyr216	120 (40%)	
aLeu220	0	
aGln252	132 (44%)	
aSer202	234 (78%)	outlet half-channel
aLys203	300 (100%)	
aTyr263	258 (86%)	
aSer199	300 (100%)	

All of the residues listed are experimentally proven to be sensitive to the Ag^{+} probe.

In an attempt to identify the positions of the half-channels, we first analyzed the hydrogen-bonding network along the polar residues within the a-subunit. The results

observed are reported in Table 5.3. Comparing the hydrogen-bonding with the wild-type, we note that the residues identified to participate in the proton transfer along the inlet half-channel spend less or no time in stable hydrogen-bonds. At the same time, the residues along the outlet half-channel are not affected even though the mutation is at position 207 (one residue away from the terminal residue of the half-channel).

Referring to Figure 5.4, one can speculate that the proton pathway is changed and consequently, the position of the inlet half-channel. Based on water accumulation, one can claim that instead of taking the 'standard' route in between the TMH of the a-subunit, the Grotthuss mechanism will promote transport along the ac-interface to the proton binding site on the c-subunit. Further investigation of the PSN paths is required in order to determine the possible routes of proton translocation.

The Wordom results are shown in Figure 5.6. Interestingly, all of the communication between residues is happening at the active binding site and around the area of the outlet half-channel. Zooming in to the area above the proton binding site (Figure 5.6b), two possible communication paths are observed:

1. $cPro64 \Rightarrow aAsn214 \Rightarrow aArg210 \Rightarrow cAsp61$
2. $aLeu211 \Rightarrow aGln252 \Rightarrow aAsn214 \Rightarrow aArg210 \Rightarrow cAsp61$

All of the a-subunit members of either communication path experimentally showed sensitivity to the Ag^+ probe and are solvated through the simulation run. Here we hypothesize that the protons are transported from the inner-membrane space to either cPro64 or aGln252 via the Grotthuss mechanism and after that via the combination of Grotthuss and proton wire mechanism.

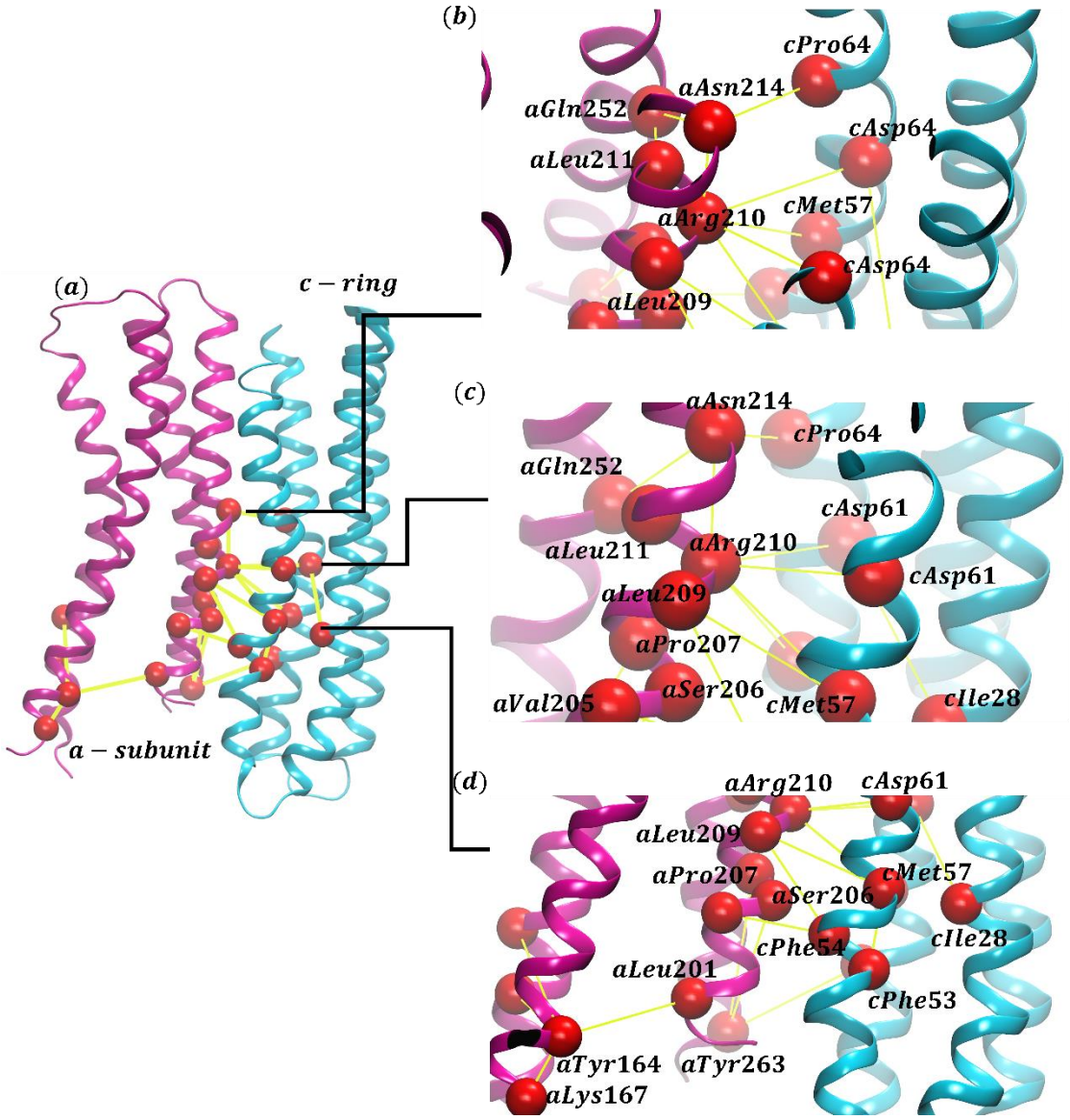

Figure 5.6 The L207P mutant amino acid - amino acid communication paths. (a) Side view of *ac*-interface. Communication paths along the (b) presumed inlet half-channel, (c) at the proton binding site, and (c) presumed outlet half-channel.

At the proton binding site, the communication path looks as expected $aAsn214 \Rightarrow aArg210 \Rightarrow cAsp61$. Interestingly, the communication path $aArg210 \Rightarrow cMet57 \Rightarrow aLeu209 \Rightarrow cPhe54 \Rightarrow aPro207 \Rightarrow aTyr263$ may suggest an alternative route in which the protons are transported along the pathway without protonating cAsp61. This may account for the 30% proton transfer decrease reported experimentally [26].

5.3 T8993G Mutant

The T8993G mutation occurs on the mtAtp6 gene and results in replacing the leucine at position 207 with positively charged arginine (we will refer to this mutant as L207R). The presence of another positively charged amino acid only three residues away from the critical aArg210 is expected to affect the proton translocation through the half-channels. Previously, it has been experimentally determined that the ability of the ATP synthase to extract the energy from the proton translocation decreases to only five percent of its full capacity [26]. This mutation, when the mutation load is 90% and higher, causes MILS [193, 249].

The MD simulations revealed two possible water paths within the vicinity of the proton binding region (*cf.* Figure 5.7). One branch of the water path spans between aAsn214 and aSer206, including the cAsp61. Another branch is observed to span the distance between aAsn214 and aSer206 along the cavity in between TMHs of subunit a. Further investigation of the effect of this accumulated water has on the residues involved in proton

transfer was carried out utilizing the PSN path calculations and hydrogen-bonding network formation.

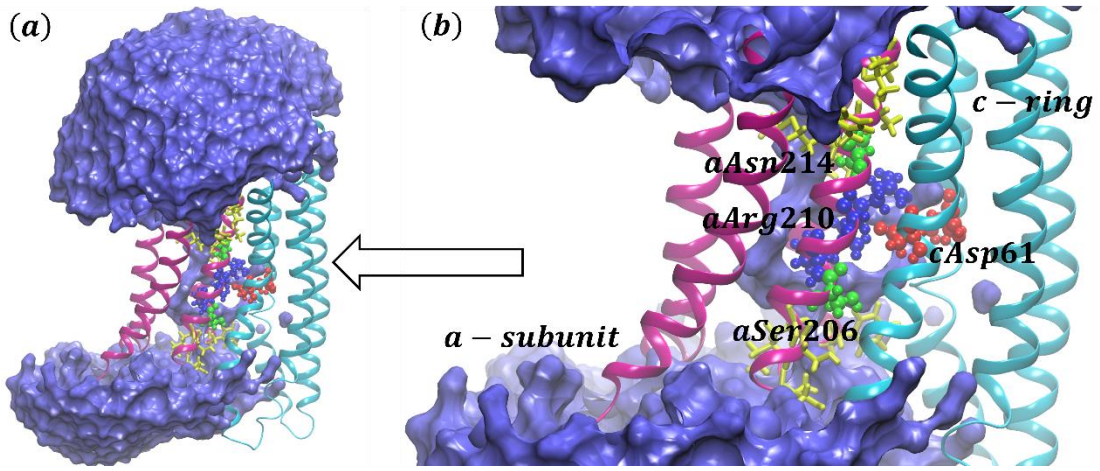

Figure 5.7 The L207R mutant after 300 nanoseconds MD simulation. (a) The representation of water accumulation within the a-subunit and ac-interface after MD simulation. Only the a-subunit and two of the c-subunits at the interface with the a-subunit are represented in order to simplify the figure. Water is shown in Surf representation and within 12 Å from the a-subunit. (b) The zoom in at the proton binding site. Critical residues directly involved in proton transfer are represented in CPK, and in addition, the residues identified by Fillingame and Steed [207] are shown in yellow licorice.

Visualizing the trajectory of some of the water molecules in the proton binding region (the region bounded by aAsn214, aArg210, aSer206, and two cAsp61 residues on the c-ring), we note that most of them are crossing the planes created by the critical aArg 210 and terminal residues of the inlet and outlet half-channels (Figure 5.8). To keep images informative enough but not extremely busy, we represented trajectories for only some of the waters in this region. As we expected, water crossed the boundaries.

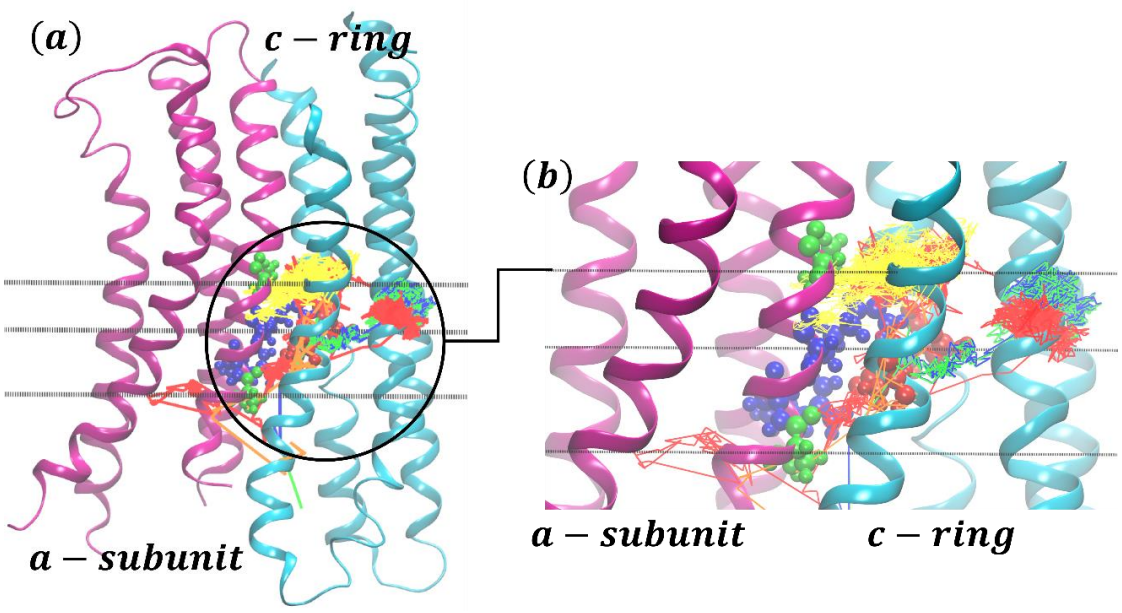

Figure 5.8 Water trajectories within the ac-interface for the L207R mutant. (a) Some of the water molecules' trajectories within the proximity to the proposed inlet and outlet half-channels are represented. (b) View at the proton binding site. Black horizontal lines are in the plane of the terminal residue of the inlet half-channel (top line), outlet half-channel (bottom line), and in the plane of *a*Arg210 (middle line).

Further analysis of the contact between water and the protein revealed that *a*Arg210, *a*Arg207, *a*Gln252, *a*Ile255, and both *c*Asp61 are in contact with water for the majority of the simulation time (>70%). The hydrogen-bond analysis revealed the results reported in Table 5.4. The time in hydrogen-bond for the residues identified as the leading indicators of the position of half-channels is considerably reduced. This indicates breakage in the hydrogen-bonding network and consequently altered paths that the protons will take. Merely through an examination of Figure 5.7, one can argue that proton pathways are altered in both the inlet and outlet half-channels. Further investigation involving the PSN pathways provided some insight into this.

Table 5.4 The L207R mutant hydrogen-bonds with water molecules.

Residue	Time (ns)	Spatial position
aMet215	108 (36%)	inlet half-channel
aAla217	0	
aTyr216	15 (5%)	
aLeu220	0	
aGln252	144 (48%)	
aSer202	36 (12%)	outlet half-channel
aLys203	21 (7%)	
aTyr263	111 (37%)	
aSer199	111 (37%)	

All of the residues listed are experimentally proven to be sensitive to the Ag^+ probe.

The PSN pathway calculations (Figure 5.9) revealed one short path along the possible position of the inlet half-channel $aAsp146 \Rightarrow cTyr73 \Rightarrow aTyr216$. Additionally, there is a cluster of communications centered around aArg210 involving cAsp61, aAsn214, aArg207, aGln252, and aPhe256 (Figure 5.9c). All members of this cluster are the residues previously identified as sensitive to the Ag^+ probe. This cluster may be involved in a water-mediated proton transfer via the $aAsn214 \Rightarrow aArg210 \Rightarrow aArg207 \Rightarrow aLeu259$ path away from the proton binding site.

The central motivating assumption for this work was that that half-channels are 'water wires' that translocate protons via hydrogen-bond networks, and that channels can be adversely affected by specific mitochondrial mutations. We believe that the results presented here support our hypothesis.

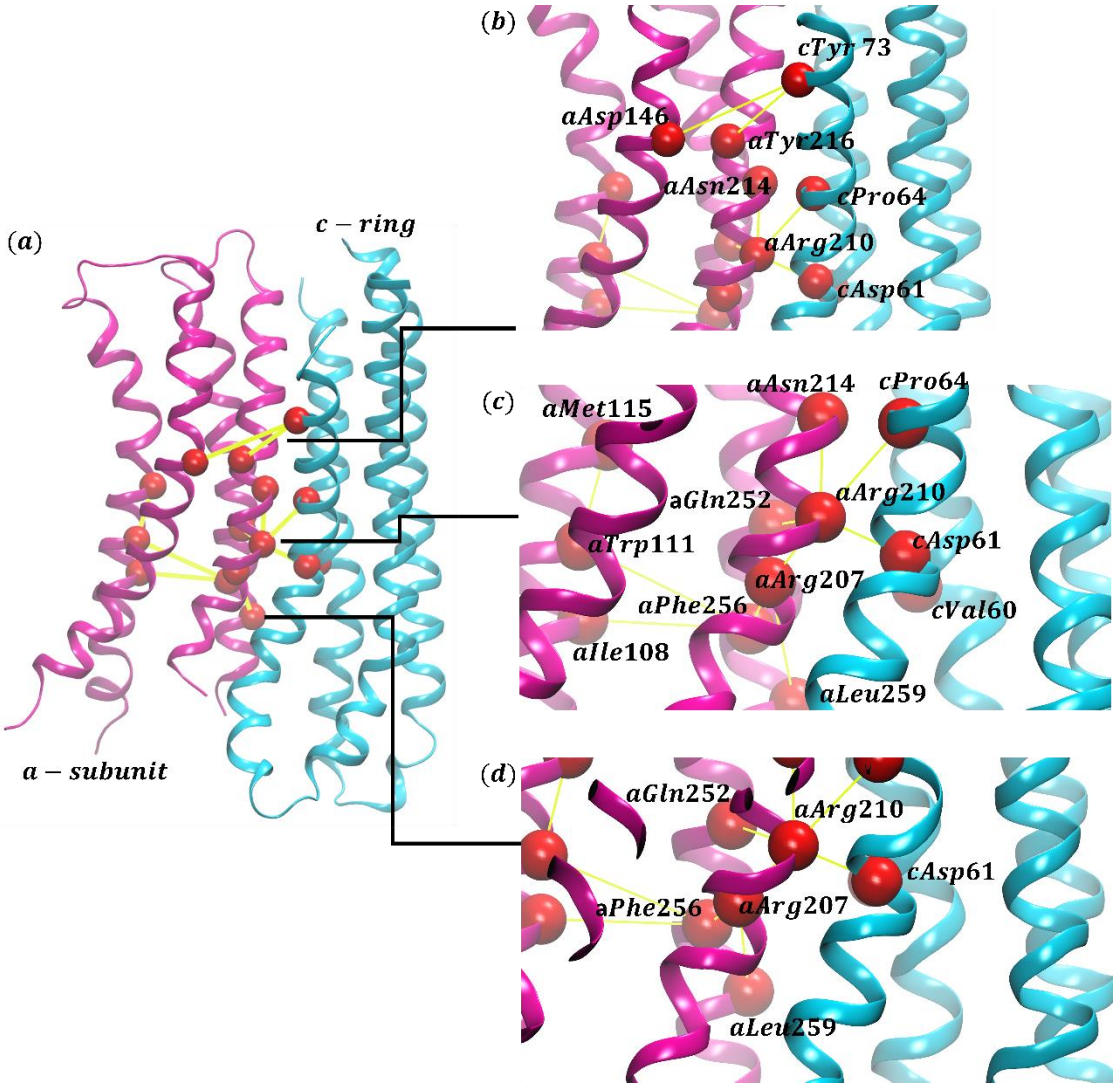

Figure 5.9 The L207R mutant amino acid - amino acid communication paths. (a) Side view of *ac*-interface. Communication paths along the (b) presumed inlet half-channel, (c) at the proton binding site, and (c) presumed outlet half-channel.

5.4 Conclusions and Future Directions

The two mutations presented in this work, T8993C and T8993G, are known to cause (when the mutation load is higher than 90%) a devastating disease (MILS) that affects newborns and reduces their life span to a couple of years. The two mutations are located in the mtAtp6 gene responsible for encoding the a-subunit of the ATP synthase. The mutations are manifested in replacing leucine (L) at position 207 with proline (P), T8993C, or arginine (R), 8993G. L207R is severely defective in ATP synthesis while L207P has a much less severe impairment.

Because of this, there is a compelling need for a detailed understanding of the proton transport mechanism in the F_O portion of the ATP synthase. Over the past couple of decades, researchers investigated ATP synthase both experimentally and theoretically, and provided much insight into the mechanisms at which this molecular machine operates. The accumulation of protons in the mitochondrial inner membrane creates an electrochemical gradient, which is used to power the ATP synthase in the direction of synthesizing the ATP. Proton transfer across the inner-membrane powers the rotational motion of F_O which is transmitted via the gamma-shaft to the F_1 part of the ATP synthase.

To date, we know that protons are transferred via the inlet half-channel to the proton binding site on the c-ring causing its rotation away from the ac-interface. After a nearly full revolution, the proton dissociates and via the outlet half-channel is transferred to the mitochondrial matrix. From previously published work [10], we know the exact sequence of events happening during the protonation and deprotonation of c-subunits, but we did not

have enough knowledge about exact proton paths before protonation and after the dissociation from the proton binding site. Extensive experimental studies by the Fillingame group revealed the polar amino acids within the a-subunit (the 'Fillingame pocket') sensitive to the $Ag^{+}$and NEM probes [55, 76, 118, 119, 122, 138, 139, 206]. The group additionally observed water accumulation in this region.

In this study, we utilized MD simulations, and by combining the hydrogen-bonding network with the protein structure network pathways, we were able to depict the possible pathways along which water mediates the proton transfer. Furthermore, we studied the water channel formation and revealed how T8993C and T8993G mutations affected the proton translocating channels.

The results revealed that water accumulated within the 'Fillingame pocket' and furthermore possible positions of the half-channels (Figure 5.10). During the $300ns$ of the production MD simulations, the average number of water molecules in the 'Fillingame pocket' remained constant, with approximately 20 molecules present at all times. The investigation of the hydrogen-bonding network and PSN paths revealed possible positions of the inlet and outlet half-channels. The wild-type inlet half channel is proposed in the following direction:

$$aIle223 \Rightarrow aHis245 \Rightarrow aLeu220 \Rightarrow cTyr73 \Rightarrow aTyr216 \Rightarrow cLeu70 \Rightarrow cMet65 \Rightarrow aAsn215\,,$$

while the outlet half-channel takes place along the $cAsp61 \Rightarrow aArg210 \Rightarrow cMet57 \Rightarrow cPhe53 \Rightarrow aPhe54 \Rightarrow aLys203$ pathway.

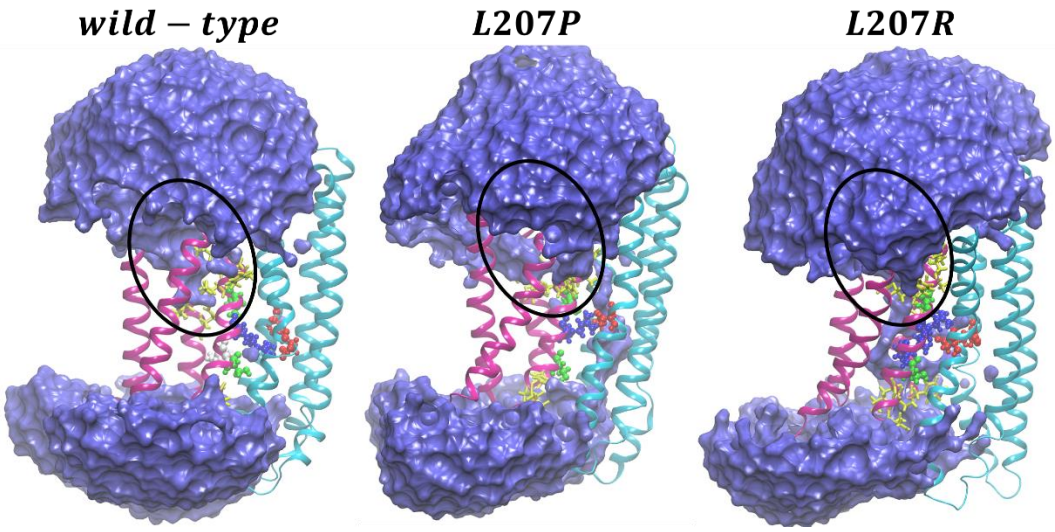

Figure 5.10 The wild-type, L207P, and L207R mutant after 300 nanoseconds MD simulation. The representation of water accumulation within the a-subunit and ac-interface after MD simulation. Only the a-subunit and two of the c-subunits at the interface with the a-subunit are represented in order to simplify the figure. Water is shown in Surf representation and within 12 Å from the a-subunit. Critical residues directly involved in proton transfer are represented in CPK, and in addition, the residues identified by Fillingame and Steed [207] are shown in yellow licorice.

The two paths are in agreement with Fillingame's experimental findings. We propose that the water accumulation in the vicinity of these two paths promotes the proton transfer via a hydrogen-bonding network. Additionally, we believe that protons are translocated by utilizing both mechanisms previously explained, structural diffusion and proton wire.

As expected, the two mutations affected the hydrogen-bonding network and PSN paths. We report the sequence of amino acids participating in the formation of half-channels for the L207P and L207R mutants.

For L207P:

$$\text{Inlet half-channel} \begin{cases} cPro64 \Rightarrow aAsn214 \Rightarrow aArg210 \Rightarrow cAsp61 \\ aLeu211 \Rightarrow aGln252 \Rightarrow aAsn214 \Rightarrow aArg210 \Rightarrow cAsp61 \end{cases}$$

Outlet: $aArg210 \Rightarrow cMet57 \Rightarrow aLeu209 \Rightarrow cPhe54 \Rightarrow aPro207 \Rightarrow aTyr263$

And for L207R:

Inlet: $aAsp146 \Rightarrow cTyr73 \Rightarrow aTyr216$

Outlet: $aAsn214 \Rightarrow aArg210 \Rightarrow aArg207 \Rightarrow aLeu259$

In conclusion, this study has revealed, for the first time, key differences between normal and mutation-impaired pathways for proton translocation in the F_O portion of the ATP synthase. Our results reveal the role of water in creating hydrogen bond networks that enable proton transport: (1) via the input half-channel toward the amino acid residues that enable proton binding to the c-ring; and (2) via the exit half-channel, from the c-ring toward the matrix. In addition, for the L207P and L207R mutations studied, we have discovered a protonic 'short circuit' created by spurious water molecules influenced by the altered electrostatic properties of the mutant amino acids. This short circuit largely bypasses the c-ring and, especially for the L207R mutant, prevents the protons from properly binding to the c-ring.

Our work thus highlights the role of water as a mediating factor during proton translocation, and how this process can become impaired by mutations and thereby hinder ATP production. It is quite extraordinary how a simple point mutation, in which one amino acid is replaced by another, can have devastating consequences on someone's life. This study reveals a clear and compelling mechanism on how and why this happens. Future studies will include: (1) a detailed analysis of the actual proton transfer process; (2) a mechanistic study of normal and mutated ATP synthase rotation; and/or (3) a study of

whether certain compensating mutations or small molecules can improve ATP production in the mutated enzyme complexes. Combined with experimental studies, our findings may ultimately help guide the development of targeted drug and gene therapies.

Bibliography

1. Oster, G. and Wang, H. Y., *Reverse Engineering a Protein: The Mechanochemistry of Atp Synthase.* Biochimica et Biophysica Acta - Bioenergetics, 2000. **1458**(2-3): p. 482-510.

2. Kornberg, A. , *For the Love of Enzymes*. Odyssey of a Biochemist, 1989, Harvard University Press: Cambridge, MA.

3. Cole, L. A., *Chapter 10: Adenosine Triphosphate Energetics*, in *Biology of Life: Biochemistry, Physiology and Philosophy*, 2016, Academic Press: San Diego. p. 65-77.

4. Pickart, C. M. and Jencks, W. P., *Energetics of the Calcium-Transporting Atpase* Journal of Biological Chemistry, 1984. **259**(3): p. 1629-1643.

5. Brooks, G. A., *Mammalian Fuel Utilization During Sustained Exercise.* Comparative Biochemistry and Physiology B-Biochemistry & Molecular Biology, 1998. **120**(1): p. 89-107.

6. Donovan, C. M. and Brooks, G. A., *Muscular Efficiency During Steady-Rate Excercise .2. Effects of Walking Speed and Work Rate.* Journal of Applied Physiology, 1977. **43**(3): p. 431-439.

7. Gaesser, G. A. and Brooks, G. A., *Muscular Efficiency During Steady-Rate Excercise - Effects of Speed and Work Rate.* Journal of Applied Physiology, 1975. **38**(6): p. 1132-1139.

8. Oster, G., Wang, H., and Grabe, M., *How Fo-Atpase Generates Rotary Torque.* Transactions of the Royal Society of London Series B-Biological Sciences, 2000. **355**(1396): p. 523-528.

9. Fillingame, R. H., *Getting to the Bottom of the F_1-Atpase.* Nature Structural and Molecular Biology, 2000. **7**(11): p. 1002-1004.

10. Aksimentiev, A., Balabin, I. A., Fillingame, R. H., and Schulten, K., *Insights into the Molecular Mechanism of Rotation in the Fo Sector of Atp Synthase.* Biophysical Journal, 2004. **86**(3): p. 1332-1344.

11. Junge, W., Lill, H., and Engelbrecht, S., *Atp Synthase: An Electrochemical Transducer with Rotatory Mechanics.* Trends in Biochemical Sciences, 1997. **22**(11): p. 420-423.

12. Junge, W. and Nelson, N., *Atp Synthase*, in *Annual Review of Biochemistry, Vol 84*, 2015, Annual Reviews: Palo Alto. p. 631-657.

13. Xing, J. H., Liao, J. C., and Oster, G., *Making Atp.* Proceedings of the National Academy of Sciences of the United States of America, 2005. **102**(46): p. 16539-16546.

14. Bergman, J., *Atp: The Perfect Energy Currency for the Cell* Creation Research Society Quarterly, 1999. **36**(1): p. 2-9.

15. Schon, E. A., *Mitochondrial Genetics and Disease.* Trends in Biochemical Sciences, 2000. **25**(11): p. 555-560.

16. Schon, E. A., DiMauro, S., and Hirano, M., *Human Mitochondrial DNA: Roles of Inherited and Somatic Mutations.* Nature Reviews Genetics, 2012. **13**(12): p. 878-890.

17. Elston, T., Wang, H., and Oster, G., *Energy Transduction in Atp Synthase.* Nature, 1998. **391**(6666): p. 510-513.

18. Oster, G., Wang, H., and Grabe, M., *How F-O-Atpase Generates Rotary Torque.* Philosophical Transactions of the Royal Society of London Series B-Biological Sciences, 2000. **355**(1396): p. 523-528.

19. Oster, G. and Wang, H. Y., *Rotary Protein Motors.* Trends in Cell Biology, 2003. **13**(3): p. 114-121.

20. Wang, H. Y. and Oster, G., *Energy Transduction in the F-1 Motor of Atp Synthase.* Nature, 1998. **396**(6708): p. 279-282.

21. Dimroth, P., *Operation of the F-0 Motor of the Atp Synthase.* Biochimica et Biophysica Acta - Bioenergetics, 2000. **1458**(2-3): p. 374-386.

22. Dimroth, P., von Ballmoos, C., and Meier, T., *Catalytic and Mechanical Cycles in F-Atp Synthases - Fourth in the Cycles Review Series.* EMBO Reports, 2006. **7**(3): p. 276-282.

23. Junge, W., Lill, H., and Engelbrecht, S., *Atp Synthase: An Electrochemical Transducer with Rotatory Mechanics.* Trends Biochem Sci, 1997. **22**(11): p. 420-423.

24. Weber, J. and Senior, A. E., *Atp Synthesis Driven by Proton Transport in F1f0-Atp Synthase.* FEBS Letters, 2003. **545**(1): p. 61-70.

25. Xing, J. H., Wang, H. Y., von Ballmoos, C., Dimroth, P., and Oster, G., *Torque Generation by the F-O Motor of the Sodium Atpase.* Biophysical Journal, 2004. **87**(4): p. 2148-2163.

26. Solaini, G., Harris, D. A., Lenaz, G., Sgarbi, G., and Baracca, A., *The Study of the Pathogenic Mechanism of Mitochondrial Diseases Provides Information on Basic Bioenergetics.* Biochimica et Biophysica Acta - Bioenergetics, 2008. **1777**(7-8): p. 941-945.

27. Cortes-Hernandez, P., Vazquez-Memije, M. E., and Garcia, J. J., *Atp6 Homoplasmic Mutations Inhibit and Destabilize the Human F1f0-Atp Synthase without Preventing Enzyme Assembly and Oligomerization.* Journal of Biological Chemistry, 2007. **282**(2): p. 1051-1058.

28. Carrozzo, R., Tessa, A., Vazquez-Memije, M. E., Piemonte, F., Patrono, C., *et al.*, *The T9176g Mtdna Mutation Severely Affects Atp Production and Results in Leigh Syndrome.* Neurology, 2001. **56**(5): p. 687-690.

29. Vazquez-Memije, M. E., Shanske, S., Santorelli, F. M., Kranz-Eble, P., DeVivo, D. C., *et al.*, *Comparative Biochemical Studies of Atpases in Cells from Patients with the T8993g or T8993c Mitochondrial DNA Mutations.* Journal of Inherited Metabolic Disease, 1998. **21**(8): p. 829-836.

30. Reece, J., Urry, L., Cain, M., Wasserman, S., Minorsky, P., *et al.*, *Campbell Biology (9th Edition)*, 2010, Benjamin Cummings: San Francisco.

31. Alberts, B., Bray, D., Hopkins, K., Johnson, A., Lewis, J., Raff, M., Roberts, K., Walter, P., *Essential Cell Biology*. 2nd ed, 2004, Gerland Science: New York

32. Know, L. , *Mitochondria and the Future of Medicine the Key of Understanding Disease, Chronic Illness, Aging, and Life Itself*, 2018, Chelsea Green Publishing: White River Junction, Vermont.

33. Kuhlbrandt, W., *Structure and Function of Mitochondrial Membrane Protein Complexes.* Bmc Biology, 2015. **13**: p. 11.

34. Ardail, D., Privat, J. P., Egretcharlier, M., Levrat, C., Lerme, F., *et al.*, *Mitochondrial Contact Sites - Lipid-Composition and Dynamics.* Journal of Biological Chemistry, 1990. **265**(31): p. 18797-18802.

35. Simbeni, R., Pon, L., Zinser, E., Paltauf, F., and Daum, G., *Mitochondrial-Membrane Contact Sites of Yeast - Characterization of Lipid Components and Possible Involment in Intramitochondrial Translocation of Phospholilipds* Journal of Biological Chemistry, 1991. **266**(16): p. 10047-10049.

36. Blanco, A. and Blanco, G., *Chapter 9 - Biological Oxidations: Bioenergetics*, in *Medical Biochemistry*, 2017, Academic Press: San Diego. p. 177-204.

37. Kadenbach, B., *Introduction to Mitochondrial Oxidative Phosphorylation*, in *Mitochondrial Oxidative Phosphorylation: Nuclear-Encoded Genes, Enzyme Regulation, and Pathophysiology*, 2012. p. 1-11.

38. Aerts, L. and Morais, V. A., *Chapter 2 - Electron Transport Chain*, in *Parkinson's Disease*, 2017, Academic Press: San Diego. p. 41-75.

39. Nijtmans, L. G. J., Ugalde, C., van den Heuvel, L. P., and Smeitink, J. A. M., *Function and Dysfunction of the Oxidative Phosphorylation System*, in *Mitochondrial Function and Biogenesis*, 2004, Springer Berlin Heidelberg: Berlin, Heidelberg. p. 149-176.

40. Nicholls D. G., Ferguson S. J. , *Bioenergetics 3* 2001, Academic Press: London.

41. Nicholls, D. G., *Mitochondrial Membrane Potential and Aging.* Aging Cell, 2004. **3**(1): p. 35-40.

42. Guo, H. and Rubinstein, J. L., *Cryo-Em of Atp Synthases.* Current Opinion in Structural Biology, 2018. **52**: p. 71-79.

43. Boyer, P. D., *The Atp Synthase - a Splendid Molecular Machine.* Annual Review of Biochemistry, 1997. **66**: p. 717-749.

44. Kagawa, Y. and Racker, E., *Partial Resolution of the Enzymes Catalyzing Oxidative Phosphorylation. 8. Properties of a Factor Conferring Oligomycin Sensitivity on Mitochondrial Adenosine Triphosphatase.* Journal of Biological Chemistry, 1966. **241**(10): p. 2461-2466.

45. Racker, E., *A Reconstituted System of Oxidative Phosphorylation.* Biochemical and Biophysical Research Communications, 1963. **14**(1): p. 75-&.

46. Racker, E., *A Mitochondrial Factor Conferring Oligomycin Sensitivity on Soluble Mitochondrial Atpase.* Biochemical and Biophysical Research Communications, 1963. **10**: p. 435-439.

47. Symersky, J., Osowski, D., Walters, D. E., and Mueller, D. M., *Oligomycin Frames a Common Drug-Binding Site in the Atp Synthase.* Proceedings of the National Academy of Sciences of the United States of America, 2012. **109**(35): p. 13961-13965.

48. Boyer, P. D., *Energy, Life, and Atp.* Bioscience Reports, 1998. **18**(3): p. 97-117.

49. Abrahams, J. P., Leslie, A. G. W., Lutter, R., and Walker, J. E., *Structure at 2.8-Angstrom Resolution of F1-Atpase from Bovine Heart-Mitochondria* Nature, 1994. **370**(6491): p. 621-628.

50. Duncan, T. M., Bulygin, V. V., Zhou, Y., Hutcheon, M. L., and Cross, R. L., *Rotation of Subunits During Catalysis by Escherichia Coli F1-Atpase* Proceedings of the National Academy of Sciences of the United States of America, 1995. **92**(24): p. 10964-10968.

51. Sabbert, D., Engelbrecht, S., and Junge, W., *Intersubunit Rotation in Active F-Atpase.* Nature, 1996. **381**(6583): p. 623-625.

52. Noji, H., Yasuda, R., Yoshida, M., and Kinosita, K., *Direct Observation of the Rotation of F-1-Atpase.* Nature, 1997. **386**(6622): p. 299-302.

53. Collinson, I. R., Runswick, M. J., Fearnley, I. M., Skehel, J. M., van Raaij, M. J., *et al., F O Membrane Domain of Atp Synthase from Bovine Heart Mitochondria: Purification, Subunit Composition, and Reconstitution with F 1 -Atpase.* Biochemistry, 1994. **33**(25): p. 7971-7978.

54. Devenish, R. J., Prescott, M., and Rodgers, A. J. W., *The Structure and Function of Mitochondrial F1f0-Atp Synthases*, in *International Review of Cell and Molecular Biology, Vol 267*, 2008. p. 1-58.

55. Fillingame, Robert H. and Steed, P. Ryan, *Half Channels Mediating H+ Transport and the Mechanism of Gating in the Fo Sector of Escherichia Coli F1fo Atp Synthase.* Biochimica et Biophysica Acta - Bioenergetics, 2014. **1837**(7): p. 1063-1068.

56. Girvin, M. E., Rastogi, V. K., Abildgaard, F., Markley, J. L., and Fillingame, R. H., *Solution Structure of the Transmembrane H+-Transporting Subunit C of the F1fo Atp Synthase†.* Biochemistry, 1998. **37**(25): p. 8817-8824.

57. Rastogi, V. K. and Girvin, M. E., *Structural Changes Linked to Proton Translocation by Subunit C of the Atp Synthase.* Nature, 1999. **402**(6759): p. 263-268.

58. Watt, Ian N., Montgomery, Martin G., Runswick, Michael J., Leslie, Andrew G. W., and Walker, John E., *Bioenergetic Cost of Making an Adenosine Triphosphate Molecule in Animal Mitochondria.* Proceedings of the National Academy of Sciences of the United States of America, 2010.

59. Stock, D., Leslie, A. G. W., and Walker, J. E., *Molecular Architecture of the Rotary Motor in Atp Synthase.* Science, 1999. **286**(5445): p. 1700-1705.

60. Meier, T., Polzer, P., Diederichs, K., Welte, W., and Dimroth, P., *Structure of the Rotor Ring of F-Type Na+-Atpase from Ilyobacter Tartaricus.* Science, 2005. **308**(5722): p. 659-662.

61. Matthies, D., Preiss, L., Klyszejko, A. L., Muller, D. J., Cook, G. M., *et al., The C13 Ring from a Thermoalkaliphilic Atp Synthase Reveals an Extended Diameter Due to a Special Structural Region.* Journal of Molecular Biology, 2009. **388**(3): p. 611-618.

62. Vollmar, M., Schlieper, D., Winn, M., Büchner, C., and Groth, G., *Structure of the C14 Rotor Ring of the Proton Translocating Chloroplast Atp Synthase.* Journal of Biological Chemistry, 2009. **284**(27): p. 18228.

63. Pogoryelov, D., Yu, J., Meier, T., Vonck, J., Dimroth, P., *et al.*, *The C15 Ring of the Spirulina Platensis F-Atp Synthase: F1/F0 Symmetry Mismatch Is Not Obligatory.* EMBO Reports, 2005. **6**(11): p. 1040-1044.

64. Pogoryelov, D., Yildiz, Ö., Faraldo-Gómez, J. D., and Meier, T., *High-Resolution Structure of the Rotor Ring of a Proton-Dependent Atp Synthase.* Nature Structural &Amp; Molecular Biology, 2009. **16**: p. 1068.

65. Arechaga, I. and Jones, P. C., *The Rotor in the Membrane of the Atp Synthase and Relatives.* FEBS Letters, 2001. **494**(1-2): p. 1-5.

66. Menz, R. I., Walker, J. E., and Leslie, A. G. W., *Structure of Bovine Mitochondrial Fl-Atpase with Nucleotide Bound to All Three Catalytic Sites: Implications for the Mechanism of Rotary Catalysis.* Cell, 2001. **106**(3): p. 331-341.

67. Stock, D., Gibbons, C., Arechaga, I., Leslie, A. G., and Walker, J. E., *The Rotary Mechanism of Atp Synthase.* Current Opinion in Structural Biology, 2000. **10**(6): p. 672-679.

68. Tsunoda, S. P., Aggeler, R., Yoshida, M., and Capaldi, R. A., *Rotation of the C Subunit Oligomer in Fully Functional F1fo Atp Synthase.* Proceedings of the National Academy of Sciences of the United States of America, 2001. **98**(3): p. 898-902.

69. Yoshida, M., Muneyuki, E., and Hisabori, T., *Atp Synthase - a Marvellous Rotary Engine of the Cell.* Nature Reviews Molecular Cell Biology, 2001. **2**(9): p. 669-677.

70. Xu, T., Pagadala, V., and Mueller, D. M., *Understanding Structure, Function, and Mutations in the Mitochondrial Atp Synthase.* Microbial Cell, 2015. **2**(4): p. 105-125.

71. Jones, P. C. and Fillingame, R. H., *Genetic Fusions of Subunit C in the F-0 Sector of H+-Transporting Atp Synthase - Functional Dimers and Trimers and*

Determination of Stoichiometry by Cross-Linking Analysis. Journal of Biological Chemistry, 1998. **273**(45): p. 29701-29705.

72. Birkenhager, R., Hoppert, M., Deckershebestreit, G., Mayer, F., and Altendorf, K., *The Fo Complex of the Escherichia Coli Atp Synthase Investigation by Electron Spectroscopic Imaging and Immunoelectron Microscop.* European Journal of Biochemistry, 1995. **230**(1): p. 58-67.

73. Takeyasu, K., Omote, H., Nettikadan, S., Tokumasu, F., IwamotoKihara, A., *et al.*, *Molecular Imaging of Escherichia Coli F0f1-Atpase in Reconstituted Membranes Using Atomic Force Microscopy.* FEBS Letters, 1996. **392**(2): p. 110-113.

74. Singh, S., Turina, P., Bustamante, C. J., Keller, D. J., and Capaldi, R., *Topographical Structure of Membrane-Bound Escherichia Coli F1f0 Atp Synthase in Aqueous Buffer.* FEBS Letters, 1996. **397**(1): p. 30-34.

75. Jones, P. C., Jiang, W. P., and Fillingame, R. H., *Arrangement of the Multicopy H+-Translocating Subunit C in the Membrane Sector of the Escherichia Coli F1f0 Atp Synthase.* Journal of Biological Chemistry, 1998. **273**(27): p. 17178-17185.

76. Jiang, W. P. and Fillingame, R. H., *Interacting Helical Faces of Subunits a and C in the F1f0 Atp Synthase of Escherichia Coli Defined by Disulfide Cross-Linking.* Proceedings of the National Academy of Sciences of the United States of America, 1998. **95**(12): p. 6607-6612.

77. Takeda, M., Chen, W. J., Saltzgaber, J., and Douglas, M. G., *Nuclear Genes Encoding the Yeast Mitochondrial Atpase Complex. Analysis of Atp1 Coding the F1-Atpase A-Subunit and Its Assembly.* Journal of Biological Chemistry, 1986. **261**(32): p. 15126-15133.

78. Takeda, M., Vassarotti, A., and Douglas, M. G., *Nuclear Genes Coding the Yeast Mitochondrial Adenosine Triphosphatase Complex. Primary Sequence Analysis of Atp2 Encoding the F1-Atpase B-Subunit Precursor.* Journal of Biological Chemistry, 1985. **260**(29): p. 15458-15465.

79. Paul, M. F., Ackermann, S., Yue, J., Arselin, G., Velours, J., *et al.*, *Cloning of the Yeast Atp3 Gene Coding for the Γ-Subunit of F1 and Characterization of Atp3 Mutants.* Journal of Biological Chemistry, 1994. **269**(42): p. 26158-26164.

80. Giraud, M. F. and Velours, J., *Atp Synthase of Yeast Mitochondria: Isolation of the F1δ Subunit, Sequence and Disruption of the Structural Gene.* European Journal of Biochemistry, 1994. **222**(3): p. 851-859.

81. Guelin, E., Chevallier, J., Rigoulet, M., Guerin, B., and Velours, J., *Atp Synthase of Yeast Mitochondria. Isolation and Disruption of the Atpε Gene.* Journal of Biological Chemistry, 1993. **268**(1): p. 161-167.

82. Macino, G. and Tzagoloff, A., *Assembly of the Mitochondrial Membrane System: Sequence Analysis of a Yeast Mitochondrial Atpase Gene Containing the Oli-2 and Oli-4 Loci.* Cell, 1980. **20**(2): p. 507-517.

83. Velours, J., Durrens, P., Aigle, M., and GuÉRin, B., *Atp4, the Structural Gene for Yeast F 0 F 1 Atpase Subunit 4.* European Journal of Biochemistry, 1988. **170**(3): p. 637-642.

84. Hensgens, L. A. M., Grivell, L. A., Borst, P., and Bos, J. L., *Nucleotide Sequence of the Mitochondrial Structural Gene for Subunit 9 of Yeast Atpase Complex.* Proceedings of the National Academy of Sciences of the United States of America, 1979. **76**(4): p. 1663-1667.

85. Macino, G. and Tzagoloff, A., *Assembly of the Mitochondrial Membrane System. The DNA Sequence of a Mitochondrial Atpase Gene in Saccharomyces Cerevisiae.* Journal of Biological Chemistry, 1979. **254**(11): p. 4617-4623.

86. Macreadie, I. G., Novitski, C. E., Maxwell, R. J., John, U., Ooi, B. G., *et al.*, *Biogenesis of Mitochondria: The Mitochondrial Gene (Aap1) Coding for Mitochondrial Atpase Subunit 8 in Saccharomyces Cerevisiae.* Nucleic Acids Research, 1983. **11**(13): p. 4435-4451.

87. Uh, M., Jones, D., and Mueller, D. M., *The Gene Coding for the Yeast Oligomycin Sensitivity-Conferring Protein.* Journal of Biological Chemistry, 1990. **265**(31): p. 19047-19052.

88. Norais, N., Prome, D., and Velours, J., *Atp Synthase of Yeast Mitochondria.* Journal of Biological Chemistry, 1991. **266**(25): p. 16541-16549.

89. Arnold, I., Bauer, M. F., Brunner, M., Neupert, W., and Stuart, R. A., *Yeast Mitochondrial F1f0-Atpase: The Novel Subunit E Is Identical to Tim11.* FEBS Letters, 1997. **411**(2-3): p. 195-200.

90. Spannagel, C., Vaillier, J., Arselin, G., Graves, P. V., and Velours, J., *The Subunit F of Mitochondrial Yeast Atp Synthase - Characterization of the Protein and Disruption of the Structural Gene Atp17.* European Journal of Biochemistry, 1997. **247**(3): p. 1111-1117.

91. Boyle, G. M., Roucou, X., Nagley, P., Devenish, R. J., and Prescott, M., *Identification of Subunit G of Yeast Mitochondrial F1f0-Atp Synthase, a Protein Required for Maximal Activity of Cytochrome C Oxidase.* European Journal of Biochemistry, 1999. **262**(2): p. 315-323.

92. Arselin, G., Vaillier, J., Graves, P. V., and Velours, J., *Atp Synthase of Yeast Mitochondria. Isolation of the Subunit H and Disruption of the Atp14 Gene.* Journal of Biological Chemistry, 1996. **271**(34): p. 20284-20290.

93. Arnold, I., Pfeiffer, K., Neupert, W., Stuart, R. A., and Schägger, H., *Atp Synthase of Yeast Mitochondria: Isolation of Subunit J and Disruption of the Atp18 Gene.* Journal of Biological Chemistry, 1999. **274**(1): p. 36-40.

94. Vaillier, J., Arselin, G., Graves, P. V., Camougrand, N., and Velours, J., *Isolation of Supernumerary Yeast Atp Synthase Subunits E and I: Characterization of Subunit I and Disruption of Its Structural Gene Atp18.* Journal of Biological Chemistry, 1999. **274**(1): p. 543-548.

95. Arnold, I., Pfeiffer, K., Neupert, W., Stuart, R. A., and Schägger, H., *Yeast Mitochondrial F1f0-Atp Synthase Exists as a Dimer: Identification of Three Dimer-Specific Subunits.* EMBO Journal, 1998. **17**(24): p. 7170-7178.

96. Ichikawa, N., Yoshida, Y., Hashimoto, T., Ogasawara, N., Yoshikawa, H., *et al.*, *Activation of Atp Hydrolysis by an Uncoupler in Mutant Mitochondria Lacking an Intrinsic Atpase Inhibitor in Yeast.* Journal of Biological Chemistry, 1990. **265**(11): p. 6274-6278.

97. Akashi, A., Yoshida, Y., Nakagoshi, H., Kuroki, K., Hashimoto, T., *et al.*, *Molecular-Cloning and Expression of a Gene for a Factor Which Stabilizes*

Formation of Inhibitor-Mitochondrial Atpase Complex from Saccharomyces-Cerevisiae. Journal of Biochemistry, 1988. **104**(4): p. 526-530.

98. Yoshida, Y., Sato, T., Hashimoto, T., Ichikawa, N., Nakai, S., *et al.*, *Isolation of a Gene for a Regulatory 15-Kda Subunit of Mitochondrial F1f0-Atpase and Construction of Mutant Yeast Lacking the Protein.* European Journal of Biochemistry, 1990. **192**(1): p. 49-53.

99. Hong, S. and Pedersen, P. L., *Atp Synthase of Yeast: Structural Insight into the Different Inhibitory Potencies of Two Regulatory Peptides and Identification of a New Potential Regulator.* Archives of Biochemistry and Biophysics, 2002. **405**(1): p. 38-43.

100. Walker, J. E., Fearnley, I. M., Gay, N. J., Gibson, B. W., Northrop, F. D., *et al.*, *Primary Structure and Subunit Stoichiometry of F1-Atpase from Bovine Mitochondria.* Journal of Molecular Biology, 1985. **184**(4): p. 677-701.

101. Fearnley, I. M. and Walker, J. E., *Two Overlapping Genes in Bovine Mitochondrial DNA Encode Membrane Components of Atp Synthase.* EMBO Journal, 1986. **5**(8): p. 2003-2008.

102. Sebald, W. and Hoppe, J., *On the Structure and Genetics of the Proteolipid Subunit of the Atp Synthase Complex*, in *Current Topics in Bioenergetics*. 1981. p. 1-64.

103. Walker, J. E., Runswick, M. J., and Poulter, L., *Atp Synthase from Bovine Mitochondria. The Characterization and Sequence Analysis of Two Membrane-Associated Sub-Units and of the Corresponding Cdnas.* Journal of Molecular Biology, 1987. **197**(1): p. 89-100.

104. Walker, J. E., Gay, N. J., Powell, S. J., Kostina, M., and Dyer, M. R., *Atp Synthase from Bovine Mitochondria: Sequences of Imported Precursors of Oligomycin Sensitivity Conferral Protein, Factor 6, and Adenosinetriphosphatase Inhibitor Protein.* Biochemistry, 1987. **26**(26): p. 8613-8619.

105. Walker, J. E., Lutter, R., Dupuis, A., and Runswick, M. J., *Identification of the Subunits of F1fo-Atpase from Bovine Heart Mitochondria.* Biochemistry, 1991. **30**(22): p. 5369-5378.

106. Fronzes, R., Chaignepain, S., Bathany, K., Giraud, M. F., Arselin, G., *et al.*, *Topological and Functional Study of Subunit H of the F1fo Atp Synthase Complex in Yeast Saccharomyces Cerevisiae.* Biochemistry, 2003. **42**(41): p. 12038-12049.

107. Gregory, R. and Hess, B., *The Sulphydryl Content of Yeast Mitochondrial F1-Atpase and the Stoichiometry of Subunits.* FEBS Letters, 1981. **129**(2): p. 210-214.

108. Hekman, C., Tomich, J. M., and Hatefi, Y., *Mitochondrial Atp Synthase Complex: Membrane Topography and Stoichiometry of the F0 Subunits.* Journal of Biological Chemistry, 1991. **266**(21): p. 13564-13571.

109. Muraguchi, M., Yoshihara, Y., Tunemitu, T., Tani, I., and Higuti, T., *Stoichiometry of Chargerin Ii (A6l) in the H+-Atp Synthase of Rat Liver Mitochondria.* Biochemical and Biophysical Research Communications, 1990. **168**(1): p. 226-231.

110. Okada, Y., Hashimoto, T., Yoshida, Y., and Tagawa, K., *Existence of Stoichiometric Amounts of an Intrinsic Atpase Inhibitor and Two Stabilizing Factors with Mitochondrial Atp Synthase in Yeast.* Journal of Biochemistry, 1986. **99**(1): p. 251-256.

111. Paumard, P., Vaillier, J., Napias, C., Arselin, G., Brèthes, D., *et al.*, *Environmental Study of Subunit I, a F(O) Component of the Yeast Atp Synthase.* Biochemistry, 2000. **39**(14): p. 4199-4205.

112. Stephens, A. N., Khan, M. A., Roucou, X., Nagley, P., and Devenish, R. J., *The Molecular Neighborhood of Subunit 8 of Yeast Mitochondrial F1f0-Atp Synthase Probed by Cysteine Scanning Mutagenesis and Chemical Modification.* Journal of Biological Chemistry, 2003. **278**(20): p. 17867-17875.

113. Stutterheim, E., Henneke, M. A. C., and Berden, J. A., *Subunit Composition of Mitochondrial F1-Atpase Isolated from Saccharomyces Carlsbergensis.* Biochimica et Biophysica Acta - Bioenergetics, 1981. **634**(C): p. 271-278.

114. Todd, R. D., Griesenbeck, T. A., and Douglas, M. G., *The Yeast Mitochondrial Adenosine Triphosphatase Complex. Subunit Stoichiometry and Physical Characterization.* Journal of Biological Chemistry, 1980. **255**(11): p. 5461-5467.

115. Arakaki, N., Ueyama, Y., Hirose, M., Himeda, T., Shibata, H., *et al.*, *Stoichiometry of Subunit E in Rat Liver Mitochondrial H+-Atp Synthase and Membrane Topology of Its Putative Ca2+-Dependent Regulatory Region.* Biochimica et Biophysica Acta - Bioenergetics, 2001. **1504**(2-3): p. 220-228.

116. Fillingame, R. H., *Subunit C of F1f0 Atp Synthase: Structure and Role in Transmembrane Energy Transduction.* Biochimica et Biophysica Acta - Bioenergetics, 1992. **1101**(2): p. 240-243.

117. Vincent, O. D., Schwem, B. E., Steed, P. R., Jiang, W., and Fillingame, R. H., *Fluidity of Structure and Swiveling of Helices in the Subunit C Ring of Escherichia Coli Atp Synthase as Revealed by Cysteine-Cysteine Cross-Linking.* Journal of Biological Chemistry, 2007. **282**(46): p. 33788-33794.

118. Dong, H. and Fillingame, R. H., *Chemical Reactivities of Cysteine Substitutions in Subunit a of Atp Synthase Define Residues Gating H+ Transport from Each Side of the Membrane.* Journal of Biological Chemistry, 2010. **285**(51): p. 39811-39818.

119. Fillingame, R. H., Angevine, C. M., and Dmitriev, O. Y., *Mechanics of Coupling Proton Movements to C-Ring Rotation in Atp Synthase.* FEBS Letters, 2003. **555**(1): p. 29-34.

120. Angevine, Christine M. and Fillingame, Robert H., *Aqueous Access Channels in Subunit a of Rotary Atp Synthase.* Journal of Biological Chemistry, 2003. **278**(8): p. 6066-6074.

121. Schwem, B. E. and Fillingame, R. H., *Cross-Linking between Helices within Subunit a of Escherichia Coli Atp Synthase Defines the Transmembrane Packing of a Four-Helix Bundle.* Journal of Biological Chemistry, 2006. **281**(49): p. 37861-37867.

122. Steed, P. R. and Fillingame, R. H., *Subunit a Facilitates Aqueous Access to a Membrane-Embedded Region of Subunit C in Escherichia Coli F1f0 Atp Synthase.* Journal of Biological Chemistry, 2008. **283**(18): p. 12365-12372.

123. Iino, R. and Noji, H., *Operation Mechanism of Fof1-Adenosine Triphosphate Synthase Revealed by Its Structure and Dynamics.* IUBMB Life, 2013. **65**(3): p. 238-246.

124. Vik, S. B. and Antonio, B. J., *A Mechanism of Proton Translocation by F1f0 Atp Synthases Suggested by Double Mutants of the a Subunit.* Journal of Biological Chemistry, 1994. **269**(48): p. 30364-30369.

125. Vik, S. B. and Ishmukhametov, R. R., *Structure and Function of Subunit a of the Atp Synthase of Escherichia Coli.* Journal of Bioenergetics and Biomembranes, 2005. **37**(6): p. 445-449.

126. Vik, S. B., Long, J. C., Wada, T., and Zhang, D., *A Model for the Structure of Subunit a of the Escherichia Coli Atp Synthase and Its Role in Proton Translocation.* Biochimica et Biophysica Acta - Bioenergetics, 2000. **1458**(2-3): p. 457-466.

127. Valiyaveetil, F. I. and Fillingame, R. H., *Transmembrane Topography of Subunit a in the Escherichia Coli F1f0 Atp Synthase.* Journal of Biological Chemistry, 1998. **273**(26): p. 16241-16247.

128. Wada, T., Long, J. C., Zhang, D., and Vik, S. B., *A Novel Labeling Approach Supports the Five-Transmembrane Model of Subunit a of the Escherichia Coli Atp Synthase.* Journal of Biological Chemistry, 1999. **274**(24): p. 17353-17357.

129. Long, J. C., Wang, S., and Vik, S. B., *Membrane Topology of Subunit a of the F1f0 Atp Synthase as Determined by Labeling of Unique Cysteine Residues.* Journal of Biological Chemistry, 1998. **273**(26): p. 16235-16240.

130. Cain, Brian D., *Mutagenic Analysis of the F0stator Subunits.* Journal of Bioenergetics and Biomembranes, 2000. **32**(4): p. 365-371.

131. Hatch, L. P., Cox, G. B., and Howitt, S. M., *The Essential Arginine Residue at Position 210 in the a Subunit of the Escherichia Coli Atp Synthase Can Be Transferred to Position 252 with Partial Retention of Activity.* Journal of Biological Chemistry, 1995. **270**(49): p. 29407-29412.

132. Valiyaveetil, F. I. and Fillingame, R. H., *On the Role of Arg-210 and Glu-219 of Subunit Alpha in Proton Translocation by the Escherichia Coli F0f1-Atp Synthase.* Journal of Biological Chemistry, 1997. **272**(51): p. 32635-32641.

133. Fillingame, R. H., Angevine, C. M., and Dmitriev, O. Y., *Coupling Proton Movements to C-Ring Rotation in F1f0 Atp Synthase: Aqueous Access Channels*

and Helix Rotations at the a-C Interface. Biochimica et Biophysica Acta - Bioenergetics, 2002. **1555**(1-3): p. 29-36.

134. Symersky, J., Pagadala, V., Osowski, D., Krah, A., Meier, T., *et al.*, *Structure of the C(10) Ring of the Yeast Mitochondrial Atp Synthase in the Open Conformation.* Nature Structural & Molecular Biology, 2012. **19**(5): p. 485-U440.

135. Pogoryelov, D., Krah, A., Langer, J. D., Yildiz, O., Faraldo-Gomez, J. D., *et al.*, *Microscopic Rotary Mechanism of Ion Translocation in the F-0 Complex of Atp Synthases.* Nature Chemical Biology, 2010. **6**(12): p. 891-899.

136. Mitome, N., Ono, S., Sato, H., Suzuki, T., Sone, N., *et al.*, *Essential Arginine Residue of the F-0-a Subunit in F0f1-Atp Synthase Has a Role to Prevent the Proton Shortcut without C-Ring Rotation in the F-0 Proton Channel.* Biochemical Journal, 2010. **430**: p. 171-177.

137. Humphrey, W., Dalke, A., and Schulten, K., *Vmd: Visual Molecular Dynamics.* Journal of Molecular Graphics 1996. **14**(1): p. 33-38.

138. Fillingame, R. H., Jiang, W., and Dmitriev, O. Y., *Coupling H+ Transport to Rotary Catalysis in F-Type Atp Synthases: Structure and Organization of the Transmembrane Rotary Motor.* Journal of Experimental Biology, 2000. **203**(1): p. 9-17.

139. Angevine, C. M., Herold, K. A. G., and Fillingame, R. H., *Aqueous Access Pathways in Subunit a of Rotary Atp Synthase Extend to Both Sides of the Membrane.* Proceedings of the National Academy of Sciences of the United States of America, 2003. **100**(23): p. 13179-13183.

140. Anderson, S., Bankier, A. T., Barrell, B. G., Debruijn, M. H. L., Coulson, A. R., *et al.*, *Sequence and Organization of the Human Mitochondrial Genome.* Nature, 1981. **290**(5806): p. 457-465.

141. Lloyd, R. E. and McGeehan, J. E., *Structural Analysis of Mitochondrial Mutations Reveals a Role for Bigenomic Protein Interactions in Human Disease.* PLoS ONE, 2013. **8**(7): p. e69003.

142. Holt, I. J., Harding, A. E., Petty, R. K., and Morgan-Hughes, J. A., *A New Mitochondrial Disease Associated with Mitochondrial DNA Heteroplasmy.* American Journal of Human Genetics, 1990. **46**(3): p. 428–433.

143. Moslemi, A. R., Darin, N., Tulinius, M., Oldfors, A., and Holme, E., *Two New Mutations in the Mtatp6 Gene Associated with Leigh Syndrome.* Neuropediatrics, 2005. **36**(5): p. 314-318.

144. Childs, A. M., Hutchin, T., Pysden, K., Highet, L., Bamford, J., *et al.*, *Variable Phenotype Including Leigh Syndrome with a 9185t > C Mutation in the Mtatp6 Gene.* Neuropediatrics, 2007. **38**(6): p. 313-316.

145. Castagna, A. E., Addis, J., McInnes, R. R., Clarke, J. T. R., Ashby, P., *et al.*, *Late Onset Leigh Syndrome and Ataxia Due to a T to C Mutation at Bp 9,185 of Mitochondrial DNA.* American Journal of Medical Genetics Part A, 2007. **143A**(8): p. 808-816.

146. Verity, C. M., Winstone, A. M., Stellitano, L., Krishnakumar, D., Will, R., *et al.*, *The Clinical Presentation of Mitochondrial Diseases in Children with Progressive Intellectual and Neurological Deterioration: A National, Prospective, Population-Based Study.* Developmental Medicine and Child Neurology, 2010. **52**(5): p. 434-440.

147. Gigarel, N., Hesters, L., Samuels, D. C., Monnot, S., Burlet, P., *et al.*, *Poor Correlations in the Levels of Pathogenic Mitochondrial DNA Mutations in Polar Bodies Versus Oocytes and Blastomeres in Humans.* American Journal of Human Genetics, 2011. **88**(4): p. 494-498.

148. Pereira, L., Soares, P., Radivojac, P., Li, B. A., and Samuels, D. C., *Comparing Phylogeny and the Predicted Pathogenicity of Protein Variations Reveals Equal Purifying Selection across the Global Human Mtdna Diversity.* American Journal of Human Genetics, 2011. **88**(4): p. 433-439.

149. Pfeffer, G., Blakely, E. L., Alston, C. L., Hassani, A., Boggild, M., *et al.*, *Adult-Onset Spinocerebellar Ataxia Syndromes Due to Mtatp6 Mutations.* Journal of Neurology Neurosurgery and Psychiatry, 2012. **83**(9): p. 883-886.

150. Aure, K., Dubourg, O., Jardel, C., Clarysse, L., Sternberg, D., *et al.*, *Episodic Weakness Due to Mitochondrial DNA Mt-Atp6/8 Mutations.* Neurology, 2013. **81**(21): p. 1810-1818.

151. Saneto, R. P. and Singh, K. K., *Illness-Induced Exacerbation of Leigh Syndrome in a Patient with the Mtatp6 Mutation, M. 9185 T > C.* Mitochondrion, 2010. **10**(5): p. 567-572.

152. Carrozzo, R., Murray, J., Capuano, O., Tessa, A., Chichierchia, G., *et al.*, *A Novel Mtdna Mutation in the Atpase6 Gene Studied by E-Coli Modeling.* Neurological Sciences, 2000. **21**(5): p. S983-S984.

153. Carrozzo, R., Murray, J., Santorelli, F. M., and Capaldi, R. A., *The T9176g Mutation of Human Mtdna Gives a Fully Assembled but Inactive Atp Synthase When Modeled in Escherichia Coli.* FEBS Letters, 2000. **486**(3): p. 297-299.

154. Alvarez-Iglesias, V., Barros, F., Carracedo, A., and Salas, A., *Minisequencing Mitochondrial DNA Pathogenic Mutations.* Bmc Medical Genetics, 2008. **9**.

155. Thyagarajan, D., Shanske, S., Vazquezmemije, M., Devivo, D., and Dimauro, S., *A Novel Mitochondrial Atpase 6-Point Mutation in Familial Bilateral Striatal Necrosis.* Annals of Neurology, 1995. **38**(3): p. 468-472.

156. Campos, Y., Martin, M. A., Rubio, J. C., Solana, L. G., GarciaBenayas, C., *et al.*, *Leigh Syndrome Associated with the T9176c Mutation in the Atpase 6 Gene of Mitochondrial DNA.* Neurology, 1997. **49**(2): p. 595-597.

157. Dionisi-Vici, C., Seneca, S., Zeviani, M., Fariello, G., Rimoldi, M., *et al.*, *Fulminant Leigh Syndrome and Sudden Unexpected Death in a Family with the T9176c Mutation of the Mitochondrial Atpase 6 Gene.* Journal of Inherited Metabolic Disease, 1998. **21**(1): p. 2-8.

158. Makino, M., Horai, S., Goto, Y., and Nonaka, I., *Confirmation That a T-to-C Mutation at 9176 in Mitochondrial DNA Is an Additional Candidate Mutation for Leigh's Syndrome.* Neuromuscular Disorders, 1998. **8**(3-4): p. 149-151.

159. Rubio-Gozalbo, M. E., Dijkman, K. P., van den Heuvel, L. P., Sengers, R. C. A., Wendel, U., *et al.*, *Clinical Differences in Patients with Mitochondriocytopathies*

Due to Nuclear Versus Mitochondrial DNA Mutations. Human Mutation, 2000. **15**(6): p. 522-532.

160. Mishmar, D. and Zhidkov, I., *Evolution and Disease Converge in the Mitochondrion.* Biochimica et Biophysica Acta - Bioenergetics, 2010. **1797**(6-7): p. 1099-1104.

161. Nakano, K., Ohsawa, I., Yamagata, K., Nakayama, T., Sasaki, K., *et al.*, *Continuous Culture of Novel Mitochondrial Cells Lacking Nuclei.* Mitochondrion, 2003. **3**(1): p. 21-27.

162. Dobrowolski, S. F., Gray, J., Miller, T., and Sears, M., *Identifying Sequence Variants in the Human Mitochondrial Genome Using High-Resolution Melt (Hrm) Profiling.* Human Mutation, 2009. **30**(6): p. 891-898.

163. Nishigaki, Y., Ueno, H., Coku, J., Koga, Y., Fujii, T., *et al.*, *Extensive Screening System Using Suspension Array Technology to Detect Mitochondrial DNA Point Mutations.* Mitochondrion, 2010. **10**(3): p. 300-308.

164. Kucharczyk, R., Salin, B., and di Rago, J. P., *Introducing the Human Leigh Syndrome Mutation T9176g into Saccharomyces Cerevisiae Mitochondrial DNA Leads to Severe Defects in the Incorporation of Atp6p into the Atp Synthase and in the Mitochondrial Morphology.* Human Molecular Genetics, 2009. **18**(15): p. 2889-2898.

165. Kucharczyk, R., Ezkurdia, N., Couplan, E., Procaccio, V., Ackerman, S. H., *et al.*, *Consequences of the Pathogenic T9176c Mutation of Human Mitochondrial DNA on Yeast Mitochondrial Atp Synthase.* Biochimica et Biophysica Acta - Bioenergetics, 2010. **1797**(6-7): p. 1105-1112.

166. Kucharczyk, R., Dautant, A., Godard, F., Tribouillard-Tanvier, D., and di Rago, J. P., *Functional Investigation of an Universally Conserved Leucine Residue in Subunit a of Atp Synthase Targeted by the Pathogenic M.9176 T > G Mutation.* Biochimica et Biophysica Acta - Bioenergetics, 2019. **1860**(1): p. 52-59.

167. Shidara, Y., Yamagata, K., Kanamori, T., Nakano, K., Kwong, J. Q., *et al.*, *Positive Contribution of Pathogenic Mutations in the Mitochondrial Genome to the Promotion of Cancer by Prevention from Apoptosis.* Cancer Research, 2005. **65**(5): p. 1655-1663.

168. Verny, C., Guegen, N., Desquiret, V., Chevrollier, A., Prundean, A., *et al.*, *Hereditary Spastic Paraplegia-Like Disorder Due to a Mitochondrial Atp6 Gene Point Mutation.* Mitochondrion, 2011. **11**(1): p. 70-75.

169. Ronchi, D., Bordoni, A., Cosi, A., Rizzuti, M., Fassone, E., *et al.*, *Unusual Adult-Onset Leigh Syndrome Presentation Due to the Mitochondrial M.9176t > C Mutation.* Biochemical and Biophysical Research Communications, 2011. **412**(2): p. 245-248.

170. Ciafaloni, E., Santorelli, F. M., Shanske, S., Deonna, T., Roulet, E., *et al.*, *Maternally Inherited Leigh Syndrome.* Journal of Pediatrics, 1993. **122**(3): p. 419-422.

171. de Vries, D. Daniëlle, van Engelen, Baziel G. M., Gabreëls, Fons J. M., Ruitenbeek, Wim, and van Oost, Bernard A., *A Second Missense Mutation in the Mitochondrial Atpase 6 Gene in Leigh's Syndrome.* Annals of Neurology, 1993. **34**(3): p. 410-412.

172. Santorelli, F. M., Shanske, S., Macaya, A., Devivo, D. C., and Dimauro, S., *The Mutation at Nt-8993 of Mitochondrial-DNA Is a Common-Cause of Leighs Syndrome.* Annals of Neurology, 1993. **34**(6): p. 827-834.

173. Santorelli, F. M., Shanske, S., Jain, K. D., Tick, D., Schon, E. A., *et al.*, *A T-C Mutation at Nt-8993 of Mitochondrial-DNA in a Child with Leigh-Syndrome.* Neurology, 1994. **44**(5): p. 972-974.

174. Pallotti, F., Baracca, A., Hernandez-Rosa, E., Walker, W. F., Solaini, G., *et al.*, *Biochemical Analysis of Respiratory Function in Cybrid Cell Lines Harbouring Mitochondrial DNA Mutations.* Biochemical Journal, 2004. **384**: p. 287-293.

175. Morava, E., Rodenburg, R. J., Hol, F., de Vries, M., Janssen, A., *et al.*, *Clinical and Biochemical Characteristics in Patients with a High Mutant Load of the Mitochondrial T8993g/C Mutations.* American Journal of Medical Genetics Part A, 2006. **140A**(8): p. 863-868.

176. Rantamaki, M. T., Soini, H. K., Finnila, S. M., Majamaa, K., and Udd, B., *Adult-Onset Ataxia and Polyneuropathy Caused by Mitochondrial 8993t -> C Mutation.* Annals of Neurology, 2005. **58**(2): p. 337-340.

177. Harding, A. E., Holt, I. J., Sweeney, M. G., Brockington, M., and Davis, M. B., *Prenatal Diagnosis of Mitochondrial Dna8993 T----G Disease.* American Journal of Human Genetics, 1992. **50**(3): p. 629-633.

178. Pastores, G. M., Santorelli, F. M., Shanske, S., Gelb, B. D., Fyfe, B., *et al.*, *Leigh-Syndrome and Hypertrophic Cardiomyopathy in an Infant with a Mitochondrial-DNA Point Mutation (T8993g).* American Journal of Medical Genetics, 1994. **50**(3): p. 265-271.

179. Shoffner, J. M., Fernhoff, P. M., Krawiecki, N. S., Caplan, D. B., Holt, P. J., *et al.*, *Subacute Necrotizing Encephalopathy - Oxidative-Phosphorylation Defects and the Atpase 6 Point Mutation.* Neurology, 1992. **42**(11): p. 2168-2174.

180. Baracca, A., Sgarbi, G., Mattiazzi, M., Casalena, G., Pagnotta, E., *et al.*, *Biochemical Phenotypes Associated with the Mitochondrial Atp6 Gene Mutations at Nt8993.* Biochimica et Biophysica Acta - Bioenergetics, 2007. **1767**(7): p. 913-919.

181. Mak, S. C., Chi, C. S., Liu, C. Y., Pang, C. Y., and Wei, Y. H., *Leigh Syndrome Associated with Mitochondrial DNA 8993 T->G Mutation and Ragged-Red Fibers.* Pediatric Neurology, 1996. **15**(1): p. 72-75.

182. Lenaz, G., Baracca, A., Carelli, V., D'Aurelio, M., Sgarbi, G., *et al.*, *Bioenergetics of Mitochondrial Diseases Associated with Mtdna Mutations.* Biochimica et Biophysica Acta - Bioenergetics, 2004. **1658**(1-2): p. 89-94.

183. Wallace, D. C., Singh, G., Lott, M. T., Hodge, J. A., Schurr, T. G., *et al.*, *Mitochondrial DNA Mutation Associated with Leber's Hereditary Optic Neuropathy.* Science, 1988. **242**(4884): p. 1427-1430.

184. Carelli, V., *Chapter 4 Leber's Hereditary Optic Neuropathy*, in *Blue Books of Practical Neurology*, 2002, Butterworth-Heinemann: Oxford, UK. p. 115-142.

185. Howell, N., Bindoff, L. A., McCullough, D. A., Kubacka, I., Poulton, J., *et al.*, *Leber Hereditary Optic Neuropathy: Identification of the Same Mitochondrial Nd1 Mutation in Six Pedigrees.* American Journal of Human Genetics, 1991. **49**(5): p. 939-950.

186. Carelli, V., Ghelli, A., Ratta, M., Bacchilega, E., Sangiorgi, S., *et al.*, *Leber's Hereditary Optic Neuropathy: Biochemical Effect of 11778/Nd4 and 3460/Nd1 Mutations and Correlation with the Mitochondrial Genotype.* Neurology, 1997. **48**(6): p. 1623-1632.

187. Majander, A., Huoponen, K., Savontaus, M. L., Nikoskelainen, E. K., and Wikstrom, M. , *Electron Transfer Properties of Nadh: Ubiquinone Reductase in the Nd1/3460 and the Nd4/11778 Mutations of the Leber Hereditary Optic Neuroretinopathy (Lhon).* FEBS Letters, 1991. **292**(1): p. 289-292.

188. Carelli, V., Ghelli, A., Bucchi, L., Montagna, P., De Negri, A., *et al.*, *Biochemical Features of Mtdna 14484 (Nd6/M64v) Point Mutation Associated with Leber's Hereditary Optic Neuropathy.* Annals of Neurology, 1999. **45**(3): p. 320-328.

189. Cock, H. R., Cooper, J. M., and Schapira, A. H. V., *The 14484 Nd6 Mtdna Mutation in Leber Hereditary Optic Neuropathy Does Not Affect Fibroblast Complex I Activity [1]*. American Journal of Human Genetics, 1995. **57**(6): p. 1501-1502.

190. Tatuch, Y., Christodoulou, J., Feigenbaum, A., Clarke, J. T., Wherret, J., *et al.*, *Heteroplasmic Mtdna Mutation (T----G) at 8993 Can Cause Leigh Disease When the Percentage of Abnormal Mtdna Is High.* American Journal of Human Genetics, 1992. **50**(4): p. 852-858.

191. Vazquez-Memije, M. E., Shanske, S., Santorelli, F. M., Kranz-Eble, P., DeVivo, D. C., *et al.*, *Comparative Biochemical Studies of Atpases in Cells from Patients with the T8993g or T8993c Mitochondrial DNA Mutations.* Journal of Inherited Metabolic Disease, 1998. **21**(8): p. 829-836.

192. Sgarbi, G., Baracca, A., Lenaz, G., Valentino, L. M., Carelli, V., *et al.*, *Inefficient Coupling between Proton Transport and Atp Synthesis May Be the Pathogenic Mechanism for Narp and Leigh Syndrome Resulting from the T8993g Mutation in Mtdna.* Biochemical Journal, 2006. **395**: p. 493-500.

193. DiMauro, Salvatore and Schon, Eric A., *Mitochondrial Respiratory-Chain Diseases.* New England Journal of Medicine, 2003. **348**(26): p. 2656-2668.

194. Uittenbogaard, M., Brantner, C. A., Fang, Z. S., Wong, L. J. C., Gropman, A., *et al.*, *Novel Insights into the Functional Metabolic Impact of an Apparent De Novo M.8993t > G Variant in the Mt-Atp6 Gene Associated with Maternally Inherited*

Form of Leigh Syndrome. Molecular Genetics and Metabolism, 2018. **124**(1): p. 71-81.

195. Baracca, A., Barogi, S., Carelli, V., Lenaz, G., and Solaini, G., *Catalytic Activities of Mitochondrial Atp Synthase in Patients with Mitochondrial DNA T8993g Mutation in the Atpase 6 Gene Encoding Subunit A.* Journal of Biological Chemistry, 2000. **275**(6): p. 4177-4182.

196. Howitt, S. M., Rodgers, A. J. W., Hatch, L. P., Gibson, F., and Cox, G. B., *The Coupling of the Relative Movement of the a and C Subunits of the F-0 to the Conformational Changes in the F-1-Atpase.* Journal of Bioenergetics and Biomembranes, 1996. **28**(5): p. 415-420.

197. Hartzog, P. E., Gardner, J. L., and Cain, B. D., *Modeling the Leigh Syndrome Nt8993 T -> C Mutation in Escherichia Coli F1f0 Atp Synthase.* International Journal of Biochemistry & Cell Biology, 1999. **31**(7): p. 769-776.

198. Hartzog, P. E. and Cain, B. D., *The Aleu207-->Arg Mutation in F1f0-Atp Synthase from Escherichia Coli. A Model for Human Mitochondrial Disease.* Journal of Biological Chemistry, 1993. **268**(17): p. 12250-12252.

199. García, J. J., Ogilvie, I., Robinson, B. H., and Capaldi, R. A., *Structure, Functioning, and Assembly of the Atp Synthase in Cells from Patients with the T8993g Mitochondrial DNA Mutation. Comparison with the Enzyme in Rho Cells Completely Lacking Mtdna.* Journal of Biological Chemistry, 2000. **275**(15): p. 11075-11081.

200. Preiss, L., Yildiz, O., Hicks, D. B., Krulwich, T. A., and Meier, T., *A New Type of Proton Coordination in an F1fo-Atp Synthase Rotor Ring.* PLoS Biology, 2010. **8**(8).

201. Karplus, M. and Gao, Y. Q., *Biomolecular Motors: The F1-Atpase Paradigm.* Current Opinion in Structural Biology, 2004. **14**(2): p. 250-259.

202. Bustamante, C., Keller, D., and Oster, G., *The Physics of Molecular Motors.* Accounts of Chemical Research, 2001. **34**(6): p. 412-420.

203. Mitchell, P, *David Keilinís Respiratory Chain Concept and Its Chemiosmotic Consequences.* Science, 1979. **206**: p. 1148-1159.

204. Mitchell, P. and Moyle, J., *Estimation of Membrane Potential and Ph Difference across Cristae Membrane of Rat Liver Mitochondria.* European Journal of Biochemistry, 1969. **7**(4): p. 471-484.

205. MacKerell, AD, Brooks, JB, Brooks III, CL, Nilsson, L, Roux, B, *et al.*, *Charmm: The Energy Function and Its Parameterization with an Overview of the Program (1998) the Encyclopedia of Computational Chemistry.* von Ragué Schleyer, P. John Wiley & Sons: Chichester, UK: p. 271-277.

206. Steed, P. R. and Fillingame, R. H., *Aqueous Accessibility to the Transmembrane Regions of Subunit C of the Escherichia Coli F1f0 Atp Synthase.* Journal of Biological Chemistry, 2009. **284**(35): p. 23243-23250.

207. Fillingame, R. H. and Steed, P. R., *Half Channels Mediating H Transport and the Mechanism of Gating in the F-O Sector of Escherichia Coli F1fo Atp Synthase.* Biochimica et Biophysica Acta - Bioenergetics, 2014. **1837**(7): p. 1063-1068.

208. Wraight, C. A., *Chance and Design—Proton Transfer in Water, Channels and Bioenergetic Proteins.* Biochimica et Biophysica Acta - Bioenergetics, 2006. **1757**(8): p. 886-912.

209. Agmon, Noam, *The Grotthuss Mechanism.* Chemical Physics Letters, 1995. **244**(5): p. 456-462.

210. Day, Tyler JF, Schmitt, Udo W, and Voth, Gregory A, *The Mechanism of Hydrated Proton Transport in Water.* Journal of the American Chemical Society, 2000. **122**(48): p. 12027-12028.

211. Kornyshev, A. A., Kuznetsov, A. M., Spohr, E., and Ulstrup, J., *Kinetics of Proton Transport in Water.* Journal of Physical Chemistry B, 2003. **107**(15): p. 3351-3366.

212. Lapid, H., Agmon, N., Petersen, M. K., and Voth, G. A., *A Bond-Order Analysis of the Mechanism for Hydrated Proton Mobility in Liquid Water.* Journal of chemical physics, 2005. **122**(1): p. 014506.

213. Marx, D., Tuckerman, M. E., Hutter, J., and Parrinello, M., *The Nature of the Hydrated Excess Proton in Water.* Nature, 1999. **397**(6720): p. 601.

214. Ohmine, I. and Saito, S., *Water Dynamics: Fluctuation, Relaxation, and Chemical Reactions in Hydrogen Bond Network Rearrangement.* Accounts of Chemical Research, 1999. **32**(9): p. 741-749.

215. McRee, D. E., *Computational Techniques*, in *Practical Protein Crystallography (Second Edition)*, 1999, Academic Press: San Diego. p. 91-271.

216. Israelachvili, J. N., *8 - Special Interactions: Hydrogen-Bonding and Hydrophobic and Hydrophilic Interactions*, in *Intermolecular and Surface Forces (Third Edition)*, 2011, Academic Press: San Diego. p. 151-167.

217. del Sol, A., Fujihashi, H., Amoros, D., and Nussinov, R., *Residues Crucial for Maintaining Short Paths in Network Communication Mediate Signaling in Proteins.* Molecular Systems Biology, 2006. **2**: p. 12.

218. Vishveshwara, S., Ghosh, A., and Hansia, P., *Intra and Inter-Molecular Communications through Protein Structure Network.* Current Protein & Peptide Science, 2009. **10**(2): p. 146-160.

219. Brinda, K. V. and Vishveshwara, S., *A Network Representation of Protein Structures: Implications for Protein Stability.* Biophysical Journal, 2005. **89**(6): p. 4159-4170.

220. Kanna, N. and Vishveshwara, S., *Identification of Side-Chain Clusters in Protein Structures by a Graph Spectral Method.* Journal of Molecular Biology, 1999. **292**(2): p. 441-464.

221. Seeber, M., Cecchini, M., Rao, F., Settanni, G., and Caflisch, A., *Wordom: A Program for Efficient Analysis of Molecular Dynamics Simulations.* Bioinformatics, 2007. **23**(19): p. 2625-2627.

222. Seeber, M., Felline, A., Raimondi, F., Muff, S., Friedman, R., *et al.*, *Wordom: A User-Friendly Program for the Analysis of Molecular Structures, Trajectories, and Free Energy Surfaces.* Journal of Computational Chemistry, 2011. **32**(6): p. 1183-1194.

223. Tirion, M. M., *Large Amplitude Elastic Motions in Proteins from a Single-Parameter, Atomic Analysis.* Physical Review Letters, 1996. **77**(9): p. 1905.

224. Ghosh, A. and Vishveshwara, S., *A Study of Communication Pathways in Methionyl-Trna Synthetase by Molecular Dynamics Simulations and Structure Network Analysis.* Proceedings of the National Academy of Sciences of the United States of America, 2007. **104**(40): p. 15711-15716.

225. Dijkstra, Edsger W, *A Note on Two Problems in Connexion with Graphs.* Numerische Mathematik, 1959. **1**(1): p. 269-271.

226. Raimondi, F., Felline, A., Seeber, M., Mariani, S., and Fanelli, F., *A Mixed Protein Structure Network and Elastic Network Model Approach to Predict the Structural Communication in Biomolecular Systems: The Pdz2 Domain from Tyrosine Phosphatase 1e as a Case Study.* Journal of Chemical Theory and Computation, 2013. **9**(5): p. 2504-2518.

227. Seeber, M., Felline, A., Raimondi, F., Mariani, S., and Fanelli, F., *Webpsn: A Web Server for High-Throughput Investigation of Structural Communication in Biomacromolecules.* Bioinformatics, 2015. **31**(5): p. 779-781.

228. Phillips, J. C., Braun, R., Wang, W., Gumbart, J., Tajkhorshid, E., *et al.*, *Scalable Molecular Dynamics with Namd.* Journal of Computational Chemistry, 2005. **26**(16): p. 1781.

229. Board, J. A., Hakura, Z. S., Elliott, W. D., and Rankin, W. T., *Scalable Variants of Multipole-Based Algorithms for Molecular Dynamics Applications*. Proceedings of the Seventh Siam Conference on Parallel Processing for Scientific Computing, 1995, Siam: Philadelphia. 295-300.

230. Verlet, L., *Computer "Experiments" on Classical Fluids. I. Thermodynamical Properties of Lennard-Jones Molecules.* Physical Review, 1967. **159**(1): p. 98-103.

231. Frenkel, D. and Smit, B., *Understanding Molecular Simulation: From Algorithms to Applications*, 2001, Academic Press: London.

232. Grubmüller, H., Heller, H., Windemuth, A., and Schulten, K., *Generalized Verlet Algorithm for Efficient Molecular Dynamics Simulations with Long-Range Interactions.* Molecular Simulation, 1991. **6**(1-3): p. 121-142.

233. Heller, H., Grubmuller, H., and Schulten, K., *Molecular Dynamics Simulation on a Parallel Computer.* Molecular Simulation, 1990. **5**(3-4): p. 133-165.

234. Tuckerman, MBBJM, Berne, Bruce J, and Martyna, Glenn J, *Reversible Multiple Time Scale Molecular Dynamics.* The Journal of Chemical Physics, 1992. **97**(3): p. 1990-2001.

235. Ewald, P, *The Calculations of Optical and Electrostatic Lattice Potentials.* Annalen der Physik, 1921. **369 (3)**: p. 253-287.

236. Bergdorf, M., Peter, C., and Hünenberger, P. H., *Influence of Cut-Off Truncation and Artificial Periodicity of Electrostatic Interactions in Molecular Simulations of Solvated Ions: A Continuum Electrostatics Study.* The Journal of Chemical Physics, 2003. **119**(17): p. 9129-9144.

237. de Leeuw, Simon W, Perram, John William, and Smith, Edgar Roderick, *Simulation of Electrostatic Systems in Periodic Boundary Conditions. I. Lattice Sums and Dielectric Constants.* Proceedings of the Royal Society of London A: Mathematical and Physical Sciences, 1980. **373**(1752): p. 27-56.

238. Feller, S. E., Pastor, R. W., Rojnuckarin, A., Bogusz, S., and Brooks, B. R., *Effect of Electrostatic Force Truncation on Interfacial and Transport Properties of Water.* The Journal of Physical Chemistry, 1996. **100**(42): p. 17011-17020.

239. Kastenholz, M. A. and Hünenberger, P. H., *Influence of Artificial Periodicity and Ionic Strength in Molecular Dynamics Simulations of Charged Biomolecules Employing Lattice-Sum Methods.* Journal of Physical Chemistry B, 2004. **108**(2): p. 774-788.

240. Loncharich, R. J. and Brooks, B. R., *The Effects of Truncating Long-Range Forces on Protein Dynamics.* Proteins: Structure, Function, and Bioinformatics, 1989. **6**(1): p. 32-45.

241. Skeel, R. D., Tezcan, I., and Hardy, D. J., *Multiple Grid Methods for Classical Molecular Dynamics.* Journal of Computational Chemistry, 2002. **23**(6): p. 673-684.

242. Phillips, James C., Braun, Rosemary, Wang, Wei, Gumbart, James, Tajkhorshid, Emad, *et al.*, *Scalable Molecular Dynamics with Namd.* Journal of Computational Chemistry, 2005. **26**(16): p. 1781-1802.

243. Darden, T., York, D., and Pedersen, L., *Particle Mesh Ewald - an N.Log(N) Method for Ewald Sums in Large Systems.* Journal of Chemical Physics, 1993. **98**(12): p. 10089-10092.

244. Ryckaert, J. P., Ciccotti, G., and Berendsen, H. J. C., *Numerical-Integration of Cartesian Equations of Motion of a System with Constraints - Molecular-Dynamics of N-Alkanes.* Journal of Computational Physics, 1977. **23**(3): p. 327-341.

245. Feller, S. E., Zhang, Y. H., Pastor, R. W., and Brooks, B. R., *Constant-Pressure Molecular-Dynamics Simulation - the Langevin Piston Method.* Journal of Chemical Physics, 1995. **103**(11): p. 4613-4621.

246. Martyna, G. J., Tobias, D. J., and Klein, M. L., *Constant-Pressure Molecular-Dynamics Algorithms.* Journal of Chemical Physics, 1994. **101**(5): p. 4177-4189.

247. Sgarbi, G, Casalena, G. A. , Baracca, A. , Lenaz, G. , DiMauro, S. *, et al., Human Narp Mitochondrial Mutation Metabolism Corrected with A-Ketoglutarate/Aspartate: A Potential New Therapy.* Archives of Neurology, 2009. **66**(8): p. 951-957.

248. Vázquez-Memije, M. E., Shanske, S., Santorelli, F. M., Kranz-Eble, P., DeVivo, D. C., *et al., Comparative Biochemical Studies of Atpases in Cells from Patients with the T8993g or T8993c Mitochondrial DNA Mutations.* Journal of Inherited Metabolic Disease, 1998. **21**(8): p. 829-836.

249. DiMauro, S. and De Vivo, D. C., *Genetic Heterogeneity in Leigh Syndrome.* Annals of Neurology, 1996. **40**(1): p. 5-7.